MARTIN-LUTHER-UNIVERSITÄT
HALLE-WITTENBERG

CONTRIBUTIONS TO ANALYTICAL, CONSISTENT MODELLING OF BOREHOLE HEAT EXCHANGERS AND GROUND HEAT COLLECTORS

Dissertation
zur Erlangung des
Doktorgrades der Naturwissenschaften (Dr. rer. nat.)

der
Naturwissenschaftlichen Fakultät III
Agrar- und Ernährungswissenschaften,
Geowissenschaften und Informatik
der Martin-Luther-Universität Halle-Wittenberg

vorgelegt von
Frau Van de Ven, Adinda

Gutachter:
Prof. Dr. rer. nat. Peter Bayer
Prof. Dr.-Ing Roland Koenigsdorff
Assistant Prof. Dr. Johannes Miocic

Tag der Verteidigung: 23. September 2025

„Caminante, no hay camino, se hace camino al andar. “

(„Wanderer, es gibt keinen Weg, der Weg entsteht beim Gehen. “)

(“Traveller, there is no road, you make your own path as you walk.”)

— Antonio Machado, *Proverbios y Cantares*, in *Campos de Castilla* (1912)

Abstract

Shallow geothermal systems coupled with heat pumps can play a significant role in the decarbonisation of the heating sector by providing a more efficient and sustainable alternative to air-source heat pumps, especially due to their lower power consumption and benefits such as reliable performance in colder climates and the avoidance of noise pollution. However, their major drawback, the higher investment costs compared to air-source heat pumps, often hinders their installation. In addition, the low level of awareness, the lack of expertise with such systems, and the absence of appropriate, easy-to-use modelling approaches that enable a neutral comparison represent a further barrier. While this thesis focuses on the latter aspect, it simultaneously contributes to reducing initial costs by employing optimised and user-friendly modelling methods.

The afore-addressed neutrality – achieved through an overarching, consistent methodology – and user-friendliness – resulting from analytical approaches – are characteristic features of the analytical, consistent modelling methodology for shallow geothermal closed-loop systems presented and applied in this thesis. This methodology breaks-down the computational domain into two sections, to which different modelling approaches are applied. The first section comprises of the source system itself (including the installation situation) and is represented by analytical resistance models and, where required, extended by capacity models. In contrast, the second section includes the surrounding subsurface and surface influences, if applicable. The latter is modelled via extensions of the instantaneous point source. Further relevant thermal effects are to be captured by approximate solutions as a complementary approach. In addition, variable heat loads and thermal interference in source fields are represented by temporal and spatial superposition, respectively.

The potential of the overarching analytical, consistent modelling methodology is exemplified by three applications. The first application analyses the applicability of the infinite moving line source combined with analytical resistance models to finite grouted borehole heat exchangers embedded in a soil completely exposed to groundwater flow. As a result, the use of a correction function is recommended in order to avoid an underestimation of the temperature change at the borehole wall. Furthermore, the applicability of analytical resistance models, as well as the infinite moving line source to finite boreholes of at least 30 m and Péclet numbers greater than 0.05, is demonstrated.

The second example illustrates how a continuous finite plane source solution with an isothermal boundary condition, in a semi-infinite solid, can be derived from an instantaneous point source. This approach serves to model the subsurface around a planar trench collector, whereas the thermal behaviour within the collector itself is represented by a corresponding

collector resistance. In addition, a solution is presented that also accounts for seasonal variation of the spatially averaged temperature across an extended vertical range.

Finally, the last example presents a complementary solution for the freezing and thawing of the subsurface around ground heat collectors, which complies with the consistent modelling methodology. Alongside the theoretical framework, the method is implemented in practice for a horizontal pipe and a trench collector. The strengths and weaknesses of the freezing approach are revealed through comparison with numerical simulations, which show good accuracy in temperature prediction. At the same time, the comparison highlights areas where there is still potential for optimisation, particularly regarding the determination of the maximum extent of the frozen ground for the planar trench collector.

Through the three extensive examples elaborated in this thesis, the potential offered by the presented analytical, consistent modelling methodology is demonstrated, while simultaneously emphasising that further aspects – such as modelling other source systems and incorporating additional thermal effects – still require investigation.

Zusammenfassung

Erdgekoppelte Wärmepumpen können als erneuerbares Heizsystem einen wesentlichen Beitrag zur sogenannten Wärmewende leisten. Außerdem sind sie aufgrund ihres geringeren Stromverbrauches und somit ihrer höheren Effizienz nachhaltiger als Luft-Wärmepumpen. Ein weiterer Vorteil von erdgekoppelten Wärmepumpen ist die fehlende Lärmbelästigung, welche bei Luft-Wärmepumpen immer wieder thematisiert wird. Dennoch können erdgekoppelte Wärmepumpen in puncto Investitionskosten nicht mit den Luft-Wärmepumpen mithalten, was häufig dazu führt, dass diese Systeme nicht verbaut werden. Hinzu kommen Aspekte wie die geringere Bekanntheit, die nicht-vorhandene Expertise im Umgang mit solchen Systemen, sowie fehlende, einfache Modellansätze, welche einen neutralen Vergleich unterschiedlicher Systeme ermöglichen. Diese Arbeit knüpft an den zuletzt genannten Punkt an und trägt gleichzeitig dazu bei, die Anfangskosten durch effizientere Planung und die Wahl des am besten geeigneten Quellensystems zu reduzieren.

Die benannten benutzerfreundlichen und neutral vergleichbaren Modellansätze werden mithilfe einer übergeordneten, analytischen Modellierungsmethodik für geschlossene oberflächennahe Geothermiesysteme geschaffen. Diese Methodik zerlegt das Rechengebiet in zwei Teile, auf die unterschiedliche Modellansätze angewandt werden. Das erste Gebiet entspricht dem Quellensystem und seiner Einbausituation, welche durch analytische Widerstandsmodelle abgebildet werden, ggfs. erweitert um Kapazitäten. Das zweite Gebiet berücksichtigt das thermische Verhalten im umgebenden Erdreich und kann auch, anhand Erweiterungen der momentanen Punktquelle, Erdreichoberflächeneinflüsse berücksichtigen. Zusätzliche relevante thermische Effekte, welche nicht anhand der vorherigen Ansätze abbildbar sind, werden über Näherungslösungen ergänzt. Darüber hinaus werden variable Entzugsleistungen über zeitliche Superposition dargestellt, während die Wechselwirkung zwischen den Quellen in einem Feld über die örtliche Superposition geschieht.

Das Potenzial der übergeordneten Methodik wird anhand dreier konkreter Beispiele in dieser Arbeit aufgezeigt. Die erste Anwendung behandelt eine verfüllte Erdwärmesonde im strömenden Grundwasser, die durch die Kombination einer unendlichen, bewegten Linienquelle mit dem etablierten Bohrlochwiderstandsmodell abgebildet wird. Aus den Untersuchungen heraus wird eine Korrekturfunktion der unendlichen, bewegten Linienquelle empfohlen, um eine Unterdimensionierung zu verhindern. Des Weiteren wurde nachgewiesen, dass analytische Widerstandsmodelle sowie die unendliche, bewegte Linienquelle für endliche Erdwärmesonden mit einer Länge von mindestens 30 m und einer Péclet-Zahl größer als 0,05 geeignet sind.

Das zweite Anwendungsbeispiel der übergeordneten Methodik zeigt die Herleitung einer analytischen Lösung der endlichen Flächenquelle mit isothermer Randbedingung im halb-unendlichen Untergrund. Dieses analytische Modell wird zur thermischen Simulation des Erdreichs um einen plattenförmigen Grabenkollektor herum genutzt. Die Wärmeübertragung innerhalb des Kollektors wird über einen Kollektorwiderstand bestimmt. Zusätzlich wird eine örtliche Mittelung der saisonalen Temperaturschwankungen im Untergrund über die Einbautiefe des Kollektors erarbeitet.

Abschließend, in einer dritten Studie wird eine Näherungslösung für die Berücksichtigung des Einfrierens und Auftauens des Erdreiches um Erdwärmekollektoren herum konform der definierten übergeordneten Modellierungsmethodik vorgestellt. Neben einer allgemeinen Formulierung der Vorgehensweise wird der Ansatz konkret für ein horizontales Rohr und einen plattenförmigen Grabenkollektor implementiert. Über Vergleiche mit numerischen Simulationen werden die Stärken und Schwächen des analytischen Ansatzes aufgedeckt. So wird deutlich, dass die Temperaturberechnung für beide Kollektorgeometrien gute Ergebnisse aufweist, während bei der Bestimmung der maximalen Ausdehnung des gefrorenen Erdreichs beim Grabenkollektor noch Optimierungspotential vorhanden ist.

Die drei umfassenden Beispiele in dieser Arbeit zeigen das Potenzial der übergeordneten, analytischen, konsistenten Modellbildungsmethodik. Dennoch gilt es zu betonen, dass weitere Aspekte – wie die Modellierung anderer Quellensysteme (z. B. geothermisch aktivierte Bauteilsysteme) und die Berücksichtigung zusätzlicher thermischer Effekte – zu ergänzen sind, um das Potenzial der Methodik in vollem Umfang zu nutzen.

Nomenclature

General symbols

A	m²	Area
c_p	J/(kg·K)	Specific heat capacity
c_v	MJ/(m³·K)	Volumetric heat capacity
D	m	Diameter
d	m	Thickness in *y*-direction
Fo	-	Dimensionless time, Fourier number
Fr	m² or m	Amount of frozen soil representative of the model´s scale. In m² for the 2D model, and in m for the 3D model.
g	-	Dimensionless temperature response of the line source
H	m	Height in *z*-direction
h	W/(m²·K)	Heat transfer coefficient
I_0	-	Modified Bessel function of the first kind
K_0	-	Modified Bessel function of the second kind
L	m	Length in *x*-direction
Nu	-	Nusselt number
Pe	-	Péclet number
Pr	-	Prandtl number
$\dot{Q}$	W	Heat extraction or injection rate
$\dot{q}$	W/m² or W/m	Specific heat extraction or injection rate
R	(m·K)/W or (m²·K)/W	Thermal resistance
Re	-	Reynolds number
r	m	Radius
S	-	Shape factor of the frozen ground
T	K or °C	Temperature
t	s	Time
t_0	s	Phase constant, i.e. time of the year at which the temperature at the ground surface reaches its minimum
U	m/s	Flow velocity
V	m³	Volume
$\dot{V}$	m³/h	Volume flow
W	W/m²	Source term
x, y, z	m	Cartesian coordinates

Greek symbols

α	m²/s	Thermal diffusivity
γ	(m·K)/W or (m²·K)/W	Dimensional factor
Γ	-	Generalised incomplete gamma function
Δ	-	Change in a physical quantity
δ	m	Maximum extension of the frozen ground
θ	-	Dimensionless temperature response derived from the source solutions (extensions of the instantaneous point source)
Λ	J/kg	Enthalpy
λ	W/(m·K)	Thermal conductivity
v_{Darcy}	m/s	Darcy velocity
ρ	kg/m³	Density

τ	s	Time integral variable
ϕ	-	Porosity of the subsurface
φ	rad	The angular coordinate in polar representation

Subscripts

a	Refers to the air properties
analyt	Refers to the analytical solution
am	Refers to the amplitude of the seasonal temperature oscillation
b	Refers to the borehole
c	Refers to the collector
cor	Refers to the correction or the corrected value
cw	Refers to the collector wall
eff	Refers to the effective properties of the porous medium
eq	Refers to an equivalent value of a property
fl	Refers to the fluid
fr	Refers to the frozen properties or amount
grout	Refers to the grout properties
h	Refers to the convective heat transfer
hist	Refers to the history, i.e. previous time steps
hydr	Refers to the hydraulically relevant geometry
ia	Refers to the interaction between elements
ice	Refers to the ice properties
inner	Refers to the inner circle
inst	Refers to the installation depth
lat	Refers to the latent heat or phase change
meas	Refers to the measurement data
no Fr	Refers to the simulations without frost
num	Refers to the numerical simulation
o	Refers to the source outlet
outer	Refers to the outer circle
p	Refers to the period of the seasonal temperature oscillation
pipe	Refers to the pipe property
pp	Refers to polypropylene
s	Refers to the solid matrix
sp	Refers to the temperature spread over the collector
steady	Refers to the steady-state condition
surf	Refers to the ground surface
tot	Refers to the total amount of the physical quantity
undist sub	Refers to the undisturbed subsurface state
unfr	Refers to the unfrozen properties or amount
w	Refers to the water properties
θ	Refers to a quantity related to the heat transfer component; derived from source solutions (extensions of the instantaneous point source) and calculated using dimensionless temperature responses

Superscripts

$'$	Refers to the heat source
$\bar{}$	Refers to the mean of a physical quantity
*	Refers to the dimensionless physical quantity
^{1}	Refers to a single collector element

Abbreviations

BC	Boundary condition
BHE	Borehole heat exchanger
FLS	Finite line source
FMLS	Finite moving line source
FPS	Finite plane source
GHC	Ground heat collector
GSHP	Ground source heat pump
gTABS	Geothermally activated building structures and infrastructure
IC	Initial condition
ILS	Infinite line source
IMLS	Infinite moving line source
IPS	Infinite plane source
MLS	Moving line source
RMSE	Root mean square error
TRT	Thermal response test
UPS	Uninterrupted power supply

Table of contents

Publications

This thesis is a cumulative dissertation comprising three peer-reviewed publications. Chapters 2, 3, and 4 are largely revised versions of the published papers listed below, with modifications primarily related to formatting and layout.

Chapter 2:

Van de Ven, Adinda; Koenigsdorff, Roland; Bayer, Peter (2021): Enhanced Steady-State Solution of the Infinite Moving Line Source Model for the Thermal Design of Grouted Borehole Heat Exchangers with Groundwater Advection. In: Geosciences 11 (10), S. 410. DOI: 10.3390/geosciences11100410.

Chapter 3:

Van de Ven, Adinda; Bayer, Peter; Koenigsdorff, Roland (2024): Analytical solution for the simulation of ground thermal conditions around planar trench collectors. In: Geothermics 124, S. 103123. DOI: 10.1016/j.geothermics.2024.103123.

Chapter 4:

Van de Ven, Adinda; Bayer, Peter; Koenigsdorff, Roland (2025): Analytical Modelling Approach of Ground Freezing and Thawing Around Ground Heat Collectors. In: Geothermal Energy 13 (43). DOI: 10.1186/s40517-025-00367-0.

Author contribution statement

In the three publications included in this cumulative doctoral thesis, Adinda Van de Ven is listed as the first, corresponding, and lead author, having made the most substantial contribution throughout the entire research process. Her involvement spans from conceptualisation and methodology development to data analysis, results visualisation, manuscript drafting and finalisation as well as managing the revision process. The specific author contributions for each publication, as defined by the Contributor Roles Taxonomy (CRediT) are detailed as follows:

Chapter 2:

Van de Ven et al. (2021)

Adinda Van de Ven:	Conceptualisation, Methodology, Software, Validation, Investigation, Data curation, Writing – original draft, Writing – review and editing, Visualisation, Project administration.
Roland Koenigsdorff:	Conceptualisation, Methodology, Formal analysis, Resources, Data curation, Writing – review and editing, Supervision, Funding Acquisition.
Peter Bayer:	Formal analysis, Writing – review and editing, Supervision.

Chapter 3:

Van de Ven et al. (2024)

Adinda Van de Ven:	Methodology, Software, Validation, Formal analysis, Investigation, Data curation, Writing – original draft, Visualisation, Project administration, Funding acquisition.
Peter Bayer:	Conceptualisation, Writing – review & editing, Supervision.
Roland Koenigsdorff:	Conceptualisation, Methodology, Writing – review & editing, Supervision, Project administration, Funding Acquisition.

Chapter 4:

Van de Ven et al (2025)

Adinda Van de Ven:	Conceptualisation, Methodology, Software, Validation, Formal analysis, Investigation, Data curation, Writing – original draft, Visualisation, Project administration, Funding acquisition.
Peter Bayer:	Conceptualisation, writing – review & editing, Supervision.
Roland Koenigsdorff:	Conceptualisation, Methodology, Writing – review & editing, Supervision, Project administration, Funding acquisition.

Acknowledgements

First and foremost, I would like to express my sincere gratitude to Roland Koenigsdorff – my supervisor and primary contact for all my research questions – for his support, motivation and encouragement during my overall research journey. I am deeply appreciative of all the technical and strategic discussions over the years, the growth opportunities he offered me, and for the support he provided in the final stage of my dissertation, allowing me to fully concentrate on completing my work, as well as for the occasional insertion or deletion of an ‘n’ in documents written in German.

Next, I would like to thank Peter Bayer, whose immediate enthusiasm and support for this undertaking made it possible in the first place. His consistently positive attitude served as a source of motivation and encouragement throughout this journey. I am also deeply grateful for the freedom he granted me to pursue my ideas, as well as for his invaluable advice and guidance along the way.

I would also like to extend my gratitude to Stefan Hofmann for his valuable support with mathematical topics.

I would like to take this opportunity to thank my colleagues in Biberach an der Riß, particularly Fabian Neth for the professional exchange and valuable feedback whenever I sought his input. My appreciation also goes to Daniel Buchmiller for his support with measurement techniques and his readiness to help with any Python-related questions. I am equally thankful to Andreas Köhler for his hands-on assistance with the TRT experiments, as well as to all others with whom I shared the challenges and occasional struggles of this journey.

In addition, I wish to thank my former colleague Michal Bachseitz, who supported me during the initial steps of developing the ground heat collector frost model, even though none of the initial approach remained in the end.

I would like to sincerely thank the project partners of the QEWSplus project who provided hands-on support during the installation of the investigated trench collector. In particular, I am deeply grateful to Hagen Steger and Anna Albers from KIT and Roman Zorn from EifER, not only for their feedback and assistance with geoscientific questions but also for their invaluable contributions throughout the practical implementation. Their contributions exemplify the collaborative and supportive spirit of the QEWSplus family, a group to which many dedicated individuals belong and whose collective efforts made this project such a rewarding experience.

I wish to acknowledge Olivia Zoch for her dedicated proofreading of the paper included in Chapter 2, Ryan Pearson for his dedicated proofreading of the papers included in Chapter 3, and 4, as well as Liam Whiteley for reviewing Chapter 1 and 5 with equal care. Their meticulous attention to detail has significantly enhanced the overall quality of this work.

I am extremely grateful to my parents and my sister for their constant support, no matter how far apart we are. Their faith in me helped me immensely in times of self-doubt and struggles.

Lastly, I want to express my deepest gratitude to my partner, Leander, whose unwavering support, patience, and encouragement have been a cornerstone throughout this journey. He has always believed in me, even in moments when I doubted myself, and has provided me with the strength to persevere when giving up felt like the easier option. His understanding and emotional support have been invaluable and is beyond words. I am deeply thankful for his presence every step of the way.

1 General introduction

Driven by an increasing concern of global warming, the development and utilisation of renewable energy for building heating and cooling gain importance as a part of efforts to lower greenhouse gas emissions (Cui et al., 2024). Under the European Green Deal (European Commission, 2019), several directives have been adopted – such as the Energy Performance of Buildings Directive, known as the EPBD (European Parliament and Council, 2024), the Energy Efficiency Directive, referred to as EED (European Parliament and Council, 2023a) and the Renewable Energy Directive, also called RED III (European Parliament and Council, 2023b) – leading to an increased use of heat pump systems for building heating and cooling as an alternative to fossil fuel-based heating systems. Building on this regulatory framework, heat pumps have emerged as a key low-carbon solution with two main types: air-source heat pumps, which extract heat from the outside air, and ground-source heat pumps (GSHPs), which draw heat from the ground. While both contribute to decarbonising buildings, ground-source systems are generally more efficient and environmentally favourable (Saner et al., 2010; Yu et al., 2013). Nevertheless, the significantly higher installation costs of GSHPs hinder their economic viability. One way to reduce initial investment barriers can be achieved through technical and planning optimisations. This work aims to enhance the design process by optimising system dimensioning, thereby achieving optimal performance with minimal planning effort. Furthermore, the focus is on a neutral comparison of closed-loop systems, regardless of the modelling methodology. Consequently, open-loop systems, such as geothermal energy wells, are not within the scope of this analysis.

1.1 Shallow geothermal closed-loop systems

Shallow geothermal closed-loop systems consist of closed circuits embedded in the ground and connected to a building heating distribution system, typically via a heat pump (Ahmed et al., 2022; Figueira et al., 2024). They transfer the thermal energy from the soil into the heat exchanger by conduction, i.e. no mass transport like fluid exchange occurs between the subsurface and the source system. Generally, these systems can be divided into three categories: borehole heat exchangers (BHEs), ground heat collectors (GHCs) and geothermally activated building structures and infrastructure (gTABS). Fundamentally, the three system types differ with respect to installation depth, required land area and their primary functional role within the building or infrastructure (Hou et al., 2022; Rees, 2016b; Verein Deutscher Ingenieure e. V., 2019).

BHEs are vertically drilled boreholes typically ranging from 50 to 400 metres in depth, containing either, for example, a single U-pipe, double U-pipes or a coaxial pipe as the heat exchanger (Reuß et al., 2020; Rivera et al., 2015b), as depicted in Fig. 1-1. Due to their large

borehole lengths, they require little surface area and are less affected by seasonal temperature fluctuations at the ground surface.

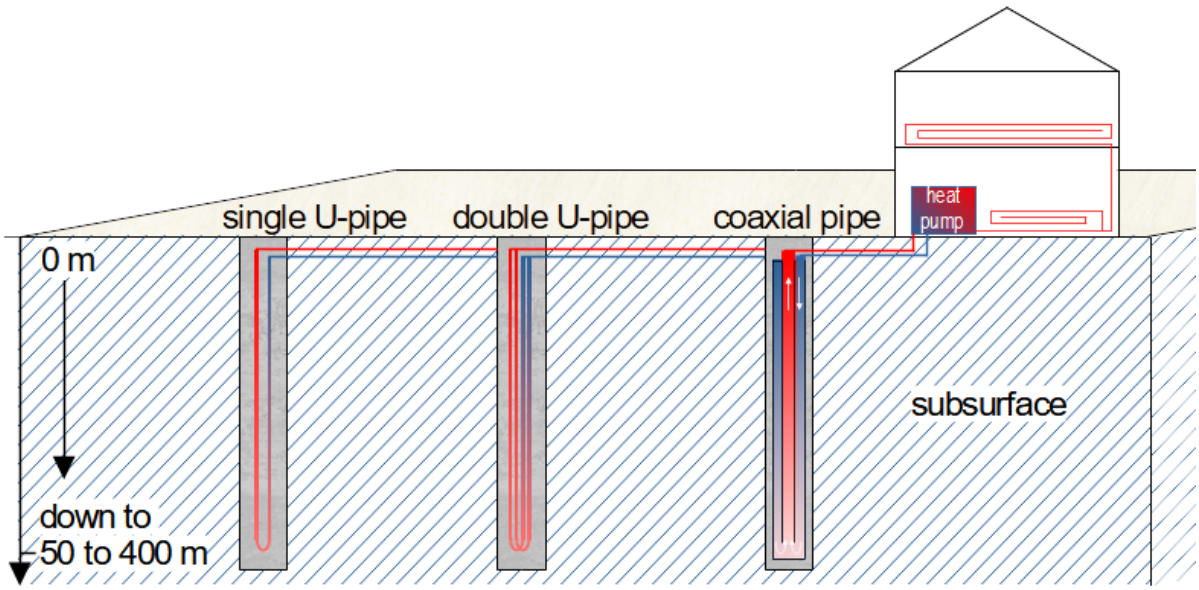

Fig. 1-1: Various types of borehole heat exchangers.

In contrast, GHCs need larger land areas than BHEs. However, their installation costs are comparatively lower (Figueira et al., 2024). Further, as the installation depth of GHCs are only down to approximately 10 metres, they are highly affected to seasonal temperature variations at the ground surface. As a result, these systems operate at lower temperatures in the heating season, often leading to freezing of the subsurface around the collector (Koenigsdorff, 2011). Furthermore, GHCs exhibit a broad variety of geometrical configurations, ranging from simple horizontal pipes and slinky-type heat exchangers to geothermal baskets, capillary tube mats, and trench collectors, which can be installed either vertically and horizontally within the trench. Three variants are illustrated in Fig. 1-2.

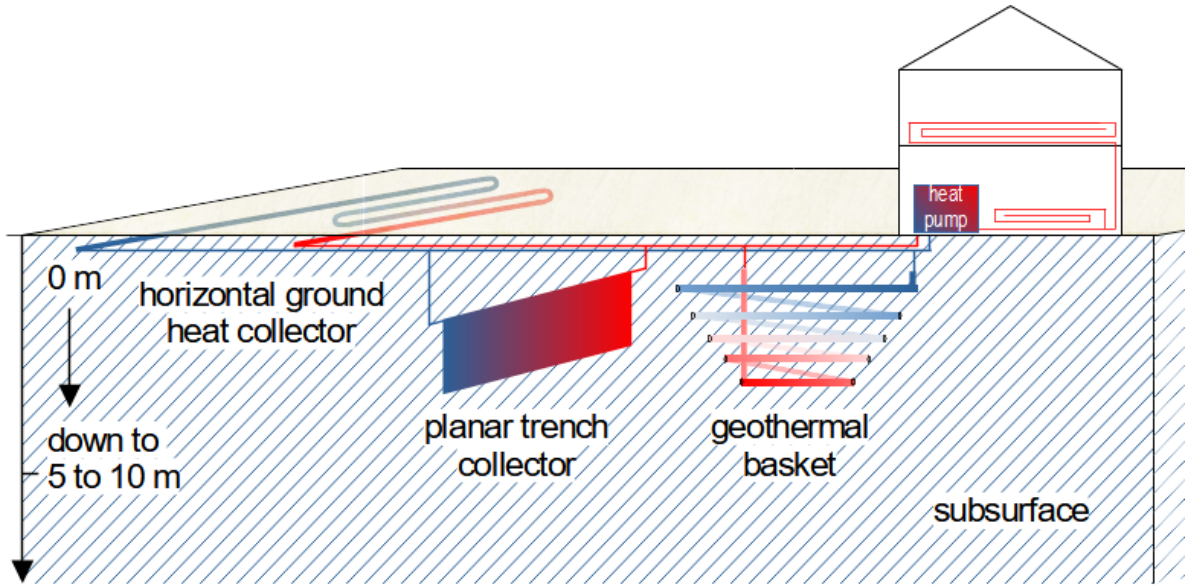

Fig. 1-2: Various types of ground heat collectors.

In comparison to the two previous systems, gTABS do not require extra space, as their primary function forms an integral part of the building's structure or infrastructure, while additionally fulfilling a thermal role (Helsen, 2016). As a consequence, the thermal performance is constrained by structural demands and additional building services requirements associated with the respective building or constructive component. Fig. 1-3 illustrates three potential variants of these systems. While gTABS represent an important component of closed-loop shallow geothermal systems – particularly due to their simultaneous fulfilment of thermal and structural functions – they are not explicitly addressed within the scope of this work. Nevertheless, their importance in the overall context of geothermal source system technologies is recognised.

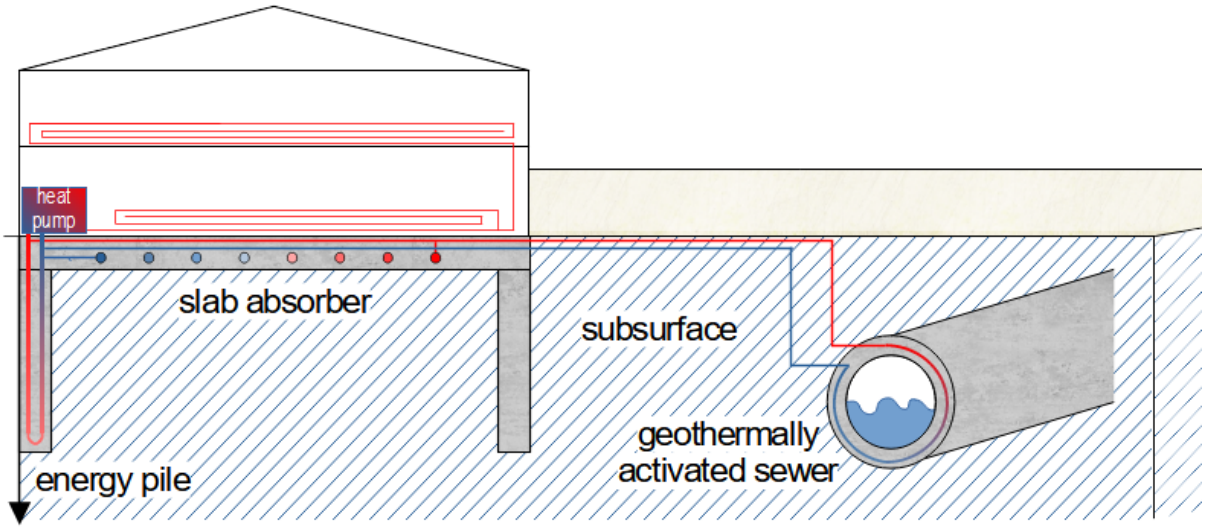

Fig. 1-3: Various types of geothermally activated building structures and infrastructure.

1.2 Shallow geothermal closed-loop models

For the design of shallow closed-loop geothermal systems, a variety of design approaches exist – ranging from simple rules of thumb or performance data based on the manufacturer's practical experience and through user-friendly analytical models, to highly complex, yet precise, numerical simulations. However, despite the availability of various design methods, the consideration in feasibility studies remains limited and often not all shallow geothermal source systems are included in this planning phase. This is primarily due to the relatively low level of awareness and expertise regarding such systems within the field, as well as the lack of appropriate modelling frameworks that are neutrally comparable and easy to use. Moreover, when multiple models are employed, differing uncertainties and errors associated with the chosen modelling approach are mostly neglected, as they are inherently challenging to quantify accurately (Karrer et al., 2020). Therefore, a standardised, analytical and consistent modelling methodology is defined in Chapter 1.2.3 to enable a fair and unbiased comparison of geothermal source systems, while providing user-friendly design models. This approach supports the identification of the most suitable geothermal solution for the specific site under consideration and thus functions as a valuable decision support tool in the design phase. In the following chapters, a comprehensive overview of existing numerical and analytical modelling approaches for BHEs and GHCs – including their advantages and disadvantages – is provided to identify current gaps and limitations. This serves as a foundation for the subsequent presentation of the consistent modelling framework.

1.2.1 Numerical models

Numerical models, if correctly formulated, excel at accurately simulating physical phenomena. This benefit comes along with two main drawbacks: they are complex, memory-intense and have long computational times. As many numerical models are developed and presented for scientific investigations, this section presents only a small selection of numerical models, chosen to illustrate different purposes, applications, and – where applicable – limitations.

Among geothermal source models, those for BHEs are the most prevalent. In general, the models can be classified into two categories according to their primary focus: either on long-term behaviour or on short-term dynamic effects (Lamarche and Beauchamp, 2007a). One of the earliest numerical models for BHE design and its long-term behaviour is proposed by Eskilson (1987). Although based on the analytical finite line source model, Eskilson (1987) developed the so-called *g*-functions, which describe the dimensionless temperature response, but derived the solution numerically. On the other hand, in the same period as Eskilson´s (1987) work, Hellström (1991) introduced the duct storage model, also known as DST-model. This model focusses on cold and heat storage in the ground for short-term analysis and was later integrated into TRNSYS (Hellström et al., 1996). Yavuzturk et al. (1999) proposed a

conceptually simple, two-dimensional, finite volume model to analyse the thermal behaviour for BHEs over short-term periods. The model was designed to predict the thermal response of the heat exchanger on shorter time scales of up to one month, as well as to simulate its short-term performance under in situ conductivity test conditions. As computational capabilities improved, an increasing number of models have been developed that capture both the short-term and long-term behaviour of shallow geothermal source systems. Rees and He (2013), for example, implemented a dynamic three-dimensional numerical model in Fortran 90, which incorporates ground, grout, pipes and fluid within a finite volume framework. The model allows both short and long timescale analysis (Rees and He, 2013). Whereas earlier studies, such as those by Yavuzturk et al. (1999) and Rees and He (2013), relied on fully custom-developed numerical models, the use of commercial and open-source software solutions for numerical simulations has since become standard in the field resulting in a substantial number of numerical models. Rivera et al. (2015a), for instance, employed FEFLOW for their numerical model. As this model was used to verify their developed analytical model, groundwater advection and land surface effects are both considered (Rivera et al., 2015a). In Barbieri et al. (2022) MODFLOW-USG is used to evaluate thermal response tests. Furthermore, COMSOL Multiphysics was utilised by Ozudogru et al. (2014), who combined a one-dimensional pipe model with a three-dimensional environmental domain.

While research on GHCs is more recent and less extensive compared to BHEs, a substantial number of numerical models have nonetheless been developed to address the wide geometric variety inherent to this field. Ramming (2007) was among the few researchers who implemented their own numerical model for ground heat collectors. The two-dimensional model was implemented in Fortran 90 and set up as a TRNSYS module, allowing the uncomplicated use of further TRNSYS modules, e.g. for weather data or heat pump models (Ramming, 2007). Notably, Ramming (2007) also accounted for phase change processes in the soil. Wu et al. (2010) utilised the commercial software ANSYS Fluent for their model, whereas Fujii et al. (2012) used FEFLOW. Both analysed slinky ground heat exchangers (Fujii et al., 2012; Wu et al., 2010). Go et al. (2016) and Yang et al. (2020), on the other hand, modelled a spiral-coil-loop heat exchanger in COMSOL Multiphysics. Ground freezing can be modelled with a variety of numerical tools, yet many proposed numerical GHC models exclude it – despite its importance to system performance. In contrast, artificial ground freezing is systematically integrated into simulations in the field of mining and construction, where it plays a critical role in ensuring subsurface stability by preventing groundwater seepage (Alzoubi et al., 2019; Zhou and Meschke, 2013). As these applications place a high demand on accurately modelling ground freezing, they can provide valuable insights and serve as a reference for incorporating ground freezing in geothermal simulations. The work of Fontaine et al. (2011) also examined ground freezing to investigate the stability of the subsurface and the building

foundation, while additionally considering heating energy availability rather than limiting the scope solely to stability. Furthermore, Gan (2013) modelled ground freezing around horizontal ground heat exchangers as well as Hüsing et al. (2016). The latter developed a TRNSYS model, which they claim to offer improvements over the models proposed by Giardina (1995), Ramming (2007) and Glück (2009). Bottarelli et al. (2015) added a phase change material (a mixture of water and micro-encapsulated paraffin) to the backfilling material of their trench. In their numerical model, both the phase transition of the paraffin and the groundwater is considered by an equivalent solid, which represents the thermal properties of both materials (Bottarelli et al., 2015). Finally, Hirsch et al. (2019) utilised DELPHIN to set up their ground heat exchanger model. This model considers both ground freezing and moisture transport (Hirsch et al., 2019).

1.2.2 Analytical models

In contrast to numerical models, the strength of analytical models lies in their computational speed. This is fundamentally tied to a simplified representation of the physics and geometry, achieved by focusing on the essential aspects of the intended outcome.

BHEs are generally modelled using line or cylinder sources. The infinite line source (ILS) model, developed by Kelvin (Kelvin, 1890), represents the system as an infinite line within an infinite, homogeneous medium, which extracts or injects heat through heat conduction (Christodoulides et al., 2020). In the standard evaluation procedure for thermal response tests (TRTs) this model is used to determine thermal parameters of the BHE and the surrounding subsurface (Gehlin, 2002; Verein Deutscher Ingenieure e. V., 2020).

While the ILS model does not account for the finite length effects and therefore does not reach a steady state, the finite line source (FLS) model incorporates for these boundary effects. The FLS even considers the ground surface, for example by applying an isothermal boundary condition (Eskilson, 1987). Eskilson (1987) first proposed this analytical solution for BHEs, but used a numerical approach to determine the *g*-functions (Lamarche and Beauchamp, 2007a). Over the years, several computational optimisations of the analytical FLS model have been developed (Cimmino, 2018, 2021; Lamarche and Beauchamp, 2007a; Zeng et al., 2002). Beyond these optimisations, various extensions to the FLS model have been developed during the last decades to enhance its applicability, e.g. Bandos et al. (2009) added the geothermal temperature gradient and a time-dependent surface temperature, in Abdelaziz et al. (2014) multilayers are considered and Rivera et al. (2016) introduced an extension to represent various surface boundaries. Moving sources as in Sutton et al. (2003) and Molina-Giraldo et al. (2011) enable the integration of groundwater advection in the subsurface.

Cylinder sources provide access to a wider range of modelling options as line sources. They can not only vary in length (infinite or finite), but also with respect to the capacity of the

borehole, the cylinder inside boundary and the thermophysical properties within the cylinder compared to the surrounding subsurface (Man et al., 2010; Verein Deutscher Ingenieure e. V., 2020; Zhou et al., 2022). With sufficiently long operating time and identical borehole and subsurface parameters, both the line source and the cylinder source models deliver similar results (Lamarche and Beauchamp, 2007a; Verein Deutscher Ingenieure e. V., 2020). Further, cylinder sources are likewise applied to model spiral-shaped GHCs (Christodoulides et al., 2020).

Solutions addressing line or cylinder sources in composite media are comparatively less common in the literature. Jaeger (1944) laid the theoretical foundation for these solutions. More than forty years later, Hellström (1991) introduced solutions for a single, double and triple U-pipe in a composite circular region by superposing multiple eccentric pipes. Beyond this, Li and Lai (2012) proposed thermal response functions for energy piles and BHEs, derived from this theoretical framework. Urchueguía et al. (2023) likewise developed a methodology to estimate ground and grout thermal parameters based on the composite media theory. In Lamarche and Beauchamp (2007b) a cylinder source in a composite region is presented to analyse the short-time behaviour of BHEs.

The analytical buried electrical cable method was first developed by Carslaw and Jaeger (1959) and applied to BHEs by Young (2004), whereby the analogy between both systems was used. This model, analogous to the composite media model proposed by Lamarche and Beauchamp (2007b), enables the representation of the short-time behaviour of BHEs as well.

Bandyopadhyay et al. (2008) developed an analytical model to represent the short-term behaviour of BHEs by considering the thermal capacity of the circulating fluid. This is achieved by modelling an equivalent single core of the U-tube in grouted boreholes, with the solution obtained using the Gaver-Stehfest numerical inversion algorithm. Since the circulated fluid in the model is represented as a solid, Javed et al. (2009) referred to the approach as the analytical virtual solid model.

GHCs differ fundamentally from BHEs as they are buried at a shallow depth and thus, may freeze their surrounding ground, which enhances performance due to additional heat extraction through phase change processes in the subsurface (Verein Deutscher Ingenieure e. V., 2019). Furthermore, these systems exhibit a wide geometric diversity, leading to a broad spectrum of analytical models. Despite not capturing the phase change, analytical models for GHCs based on the extensions of the instantaneous point source are frequently applied. Claesson and Dunand (1983), for instance, proposed different variants of horizontal line source solutions, e.g. for infinite and finite lengths, for steady-state situations and periodical heat extraction, for line sources above a ground water flow or directly within moving groundwater etc. The next major development was made by Fontaine et al. (2011) as they extend the

steady-state model of Claesson and Dunand (1983) for the unsteady case. Lamarche (2019), in turn, improved the simulation of the finite line source in terms of computational efficiency and account for seasonal temperature variations at different heights using the assumption of Kusuda and Achenbach (1965).

Another collector design that is frequently studied in the literature is the so-called slinky-coil collector. The analytical model used to represent this kind of collector is the ring source model (Larwa et al., 2019; Li et al., 2012a; Xiong et al., 2015). Xiong et al. (2015) further incorporated the influence of the ground surface temperature variation by superimposing its effect through a numerical model. In addition to slinky coils, the ring source is frequently employed as a modelling approach for geothermal baskets (Jeon et al., 2018; Witte et al., 2022) or horizontal spiral heat exchangers (Wang et al., 2016). Goodness of fit between experimental results and numerical simulations has been reported by Jeon et al. (2018) and Witte et al. (2022), respectively. Furthermore, Wang et al. (2016) consider annual variation of the local ground surface temperature and validate their model using both numerical simulations and field test data.

In their study of a planar ground heat collector, Bortoloni and Bottarelli (2015) didn´t employ a source model directly, but applied the same heat transfer per unit trench length corresponding to slinky-coil configurations, as tabulated in the Italian regulations. A comparison of their equivalent slinky-coil approach and 2D numerical simulations revealed a good accuracy of the design minimum temperature (Bortoloni and Bottarelli, 2015).

The analytical model of Ramming (2007) for horizontal ground heat collectors initially describes the heat flow from the surface and deeper subsurface layers separately and subsequently superposes them. In addition, the cooling of the area surrounding the collector pipes caused by the operation of the heat pump operation is taken into account, as well as seasonal temperature variations by employing the assumption of Kusuda and Achenbach (1965). Furthermore, Ramming (2007) selects the boundary condition depending on whether ground freezing occurs: if no freezing takes place, a first-type (Dirichlet) boundary condition is applied; once freezing sets in around the pipes, a second-type (Neumann) boundary condition is used. Finally, the geometry of the frozen region is adapted once the freezing fronts of adjacent pipes merge.

Since not all of the aforementioned models accurately represent heat transfer within the source system itself, analytical resistance models are often used to complement them. In literature, various methods are proposed to describe borehole resistances. The multipole method, proposed by Claesson and Bennet (1987) and Bennet et al. (1987), is a widely used approach for modelling BHE resistances. According to Lamarche et al. (2010), this method performed best in their comprehensive comparative study. An additional analytical framework for

determining BHE resistances was given by Hellström (1991), referred to as the line-source formula. Furthermore, Hellström (1991) purposed a formula to extrapolate the 2D approach to a real 3D borehole configuration by applying an equivalent borehole resistance. Lamarche et al. (2010) examined further alternative borehole resistance approaches based on experimental and numerical studies, concluding that the multipole method and the equivalent borehole resistance model are most suitable.

A fundamental methodology frequently used in analytical modelling of shallow geothermal source systems is the superposition principle. This principle can be used for both spatial superposition of several heat sources and temporal superposition of varying heat loads. The latter was already applied by Eskilson (1987) for dimensioning purposes, where the heat load was decomposed into three components: a mean extraction rate, a periodic component and a short-term extraction pulse. Spatial superposition is used to represent the interaction of multiple interfering sources, as demonstrated by Cimmino (2021) for borehole fields and by Miocic et al. (2024) for applications on even larger spatial scales.

1.2.3 Consistent modelling methodology

In order to promote ground-coupled heat pumps and enable the early identification of the most suitable solution for a given location, an analytical, consistent modelling methodology for closed-loop geothermal source systems is defined. This ensures a neutral comparison of such systems, independent of the individual modelling approach used. Furthermore, analytical models are user-friendly and excel in computational speed and efficiency when compared to numerical models. Given the variety of existing analytical modelling methods, each with its own strengths and limitations, the following consistent modelling methodology is proposed, broadly following the structured approach described in Van de Ven et al. (2018).

The computational domain is divided into two distinct regions:

- the source system itself, including the installation situation (see Fig. 1-4 a), and
- the surrounding subsurface, including surface influences (see Fig. 1-4 b).

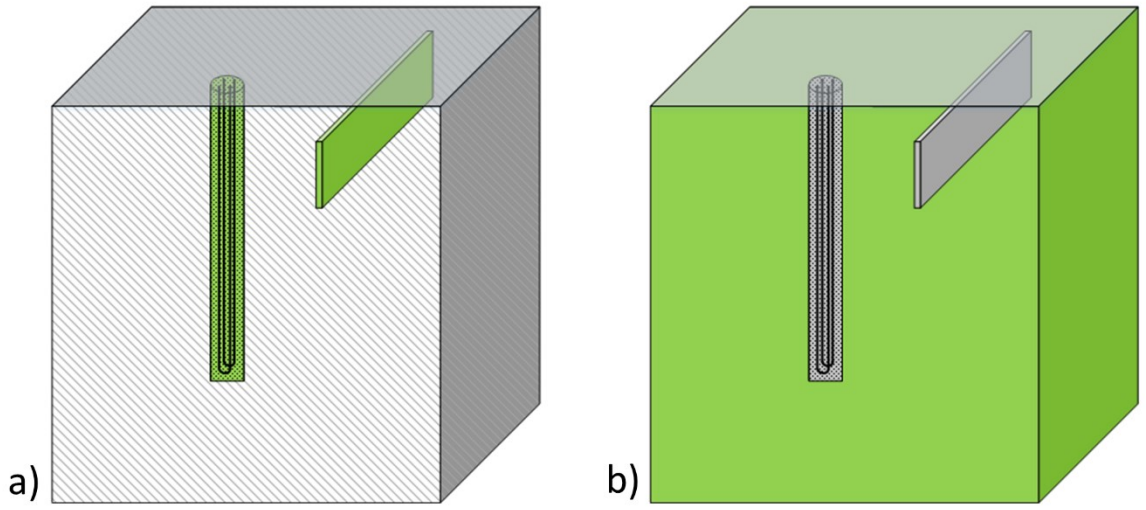

Fig. 1-4: Division of the computational domain in a) the source system itself, incl. the installation situation and b) the surrounding subsurface, incl. surface influences. (Karrer et al., 2020)

Within the domain of the source system itself, including the installation situation (see green areas in Fig. 1-4 a), heat transfer is represented using analytical thermal resistance models, and, if applicable, extended by capacity models. The borehole resistance R_b of a BHE is a typical example of such an analytical, stationary thermal resistance model. In contrast, the surrounding subsurface (see green area in Fig. 1-4 b) is modelled by extensions of the instantaneous point source, which align with the fundamental solution of potential theory (Carslaw and Jaeger, 1959). These extensions may not only be of geometrical nature (line, plane, ring, etc.), but may also relate to boundary conditions, e.g. by using the method of image, or to heat transfer processes, e.g. the representation of convection by moving sources. Additional relevant heat transfer processes, which cannot be captured by extensions of the instantaneous point source model alone, may be accounted for through approximate solutions as a complementary approach. As source solutions generally account for a constant heat injection or extraction rate, time-dependent heat loads are represented by temporal superposition of these solutions; whereas the consideration of neighbouring sources and their interference is captured by spatial superposition.

1.3 Research questions and objectives

The overarching purpose of this research is to enhance the understanding and design of shallow geothermal closed-loop systems as a sustainable energy source and a contribution to achieving greenhouse gas neutrality in the building sector. One key aspect to achieve this is the proper understanding of the operating characteristics of different geothermal heat exchanger systems, and the availability of appropriate methods for the design process. To identify the most suitable geothermal source system for a given application and site, a

consistent modelling approach is needed for different systems under consideration, without prioritising any particular system by the model itself.

This modelling framework requires a general structure applicable to all geothermal closed-loop source systems. Furthermore, the framework should lower the hurdle for design engineers to consider multiple systems in the initial decision-making process and allow for a seamless transition into the design phase, while adhering to a consistent, easy-to-use model. Therefore, analytical models are preferred because they are simpler and require less detailed description of physical processes in the subsurface and their modelling compared to numerical simulations. Additionally, they provide the benefit of shorter calculation times, which is particularly advantageous given that time pressure is daily reality in the construction industry.

In order contribute to the overarching purpose, three specific objectives have been formulated to tackle critical analytical modelling gaps that currently hinder the optimal design and operation of these systems. The three objectives of this thesis are closely interlinked, as they collectively aim to tackle key challenges in the design and operation of shallow geothermal closed-loop systems. While Objective 1 focuses on understanding the thermal behaviour of borehole heat exchangers under groundwater flow conditions, Objectives 2 and 3 expand the analysis to ground heat collectors, with an emphasis on thermal performance under seasonal temperature variations and specific physical phenomena such as freezing and thawing.

Objective 1: Borehole heat exchangers

The first objective focuses on analysing the influence of groundwater advection on BHEs, with particular attention to the role of backfilling in modifying thermal behaviour. Groundwater flow is a well-established factor in the thermal performance of BHEs (Diao et al., 2004; Zhang et al., 2020), and several models exist to account for its effects (Lazzari et al., 2010; Molina-Giraldo et al., 2011; Sutton et al., 2003). However, in many regions, backfilling is a mandatory requirement, sealing the borehole and preventing groundwater flow within it. This results in distinct thermal characteristics that remain insufficiently explored. By addressing this gap, Objective 1 provides insights into how backfilling influences the thermal performance of BHEs under real conditions. This topic is examined in detail in Chapter 2.

Objective 2: Planar ground heat collectors

The second objective investigates the heat transfer characteristics of planar trench collectors, which represent an alternative design to traditional geometries, such as linear-loops or slinky-coils (Congedo et al., 2012; Lamarche, 2019; Xiong et al., 2015). While planar collectors exhibit distinct characteristics, their potential benefits compared to other ground heat collector geometries remain insufficiently explored (Hou et al., 2022). This lack of research is particularly evident in the context of user-friendly tools for analysing thermal performance during the design

phase. Furthermore, the shallow installation depth of planar collectors makes them highly sensitive to seasonal temperature variations. By thoroughly analysing the heat conduction around planar collectors, an important gap in the understanding of their thermal behaviour can be bridged. Detailed findings are presented in Chapter 3.

Objective 3: Freezing and thawing effects

The third objective extends the analysis of ground heat collectors by examining the effects of freezing and thawing processes on their thermal performance. Phase change phenomena, such as latent heat effects, introduce significant complexity due to their non-linear nature (Zhou and Meschke, 2013), posing challenges for accurate modelling and analysis. These processes not only affect heat transfer dynamics but also introduce an additional parameter of interest for system design: the extent of the frozen ground (Verein Deutscher Ingenieure e. V., 2019). By addressing this parameter alongside operating temperatures, Objective 3 contributes to a more comprehensive understanding of the overall thermal performance of ground heat collectors. This topic is examined in Chapter 4.

To achieve these objectives, the models developed in this thesis comply with the overarching analytical, consistent modelling methodology outlined in Chapter 1.2.3, enabling a neutral comparison of various shallow geothermal source systems while offering design engineers the advantage of models that are easy to use. Furthermore, the consistent methodology ensures that performance differences can be attributed solely to the systems themselves, rather than to variations in modelling approaches. The methodology is not limited to the systems analysed in this thesis but serves as a representative framework for broader applications. All analytical approaches in this thesis are systematically verified through numerical simulations and, where available, validated with experimental data. The potential of these approaches is further demonstrated through exemplary applications, providing valuable insights for both research and practical design purposes.

By addressing these objectives through a consistent and validated methodological framework, this thesis contributes to a deeper understanding of shallow geothermal systems, supporting their efficient design and promoting their widespread adoption as a sustainable energy solution.

2 Analytical simulation of grouted borehole heat exchangers with groundwater advection

2.1 Chapter overview

The objective of this study is to assess the suitability of the analytical infinite moving line source (IMLS) model in determining the temperature of vertical grouted borehole heat exchangers (BHEs) for steady-state conditions when horizontal groundwater advection is present. Therefore, a numerical model of a grouted borehole is used as a virtual reality for the three analysis parts. These parts comprise the compatibility of the thermal borehole resistance model for borehole heat exchangers with groundwater advection, the applicability of the infinite moving line source model to finite boreholes and the steady-state thermal conditions at the wall of a grouted borehole. As a result of the first part, it has been discovered that established analytical methods to determine the borehole thermal resistance as a mean value over the borehole perimeter can also be applied to BHEs with groundwater advection. Furthermore, the deviation between a finite moving line source (FMLS) and the IMLS is found to be only less than 5% for BHEs of a depth of 30 m or more, and Péclet numbers Pe greater than 0.05. Finally, the accuracy of the temperature change calculated with the IMLS model at the radius of the borehole wall compared to the temperature change at a numerically simulated grouted borehole is addressed. A discrepancy of the *g*-functions resulting in a poor dimensioning of BHEs by the IMLS model is revealed, which is ascribed to the impermeable grouting material of the numerical model. A correction function has been developed and applied to the IMLS model for steady-state conditions to overcome this discrepancy and to avoid poor dimensioning of BHEs.

2.2 Introduction

Ground-source heat pump (GSHP) systems represent a valuable CO_2-emission-reducing alternative for heating and cooling of residential and commercial buildings compared to conventional systems (Aditya and Narsilio, 2020; Bayer et al., 2012; Blum et al., 2010). A typical GSHP system consists of a heat pump coupled with horizontal ground heat exchangers or, more commonly, vertical BHEs. According to Bayer et al. (2012) and Rees (2016a), the increased use of these systems in the last decades can be ascribed mainly to the refocusing of energy policy in Europe and the significant economic growth in China. Compared to air-source heat pump systems, the efficiency of GSHP systems is better and their environmental impact is lower (Saner et al., 2010; Yu et al., 2013). However, installation costs are significantly higher, which affects their economic competitiveness (Blum et al., 2010; Diao et al., 2004). For the design of cost-optimised systems, it is important to consider all relevant heat transfer effects of the ground source and to include as many geological characteristics for site-specific system tuning as possible.

One main criterion for the design of vertical BHEs is a given limit for its minimum or maximum operating temperature (Fascì et al., 2019; Reuß et al., 2020; Rivera et al., 2017; Verein Deutscher Ingenieure e. V., 2019). The operating temperatures can be calculated either by numerical simulations, which are highly flexible but are accompanied by the expense of high computational and memory demand, or by (semi-)analytical models. The latter provides compact solutions that are only valid for particular conditions and that often represent conceptual simplifications of the true settings in the field. In practice, straightforward tools such as EED (Earth Energy Designer) (Blocon AB, 2020), GLHEPro (Ground Loop Heat Exchanger Design Software) (Spitler et al., 2016), EWS (Programm EWS) (Arthur Huber, 2016), and GEO-HAND^{light} (Koenigsdorff, 2011), are widely used for the dimensioning process of BHEs (Reuß et al., 2020). Operating temperatures of BHEs in these programs are calculated by superposing the temperature change at the borehole wall and within the borehole itself, which are both due to the thermal loads (extraction or injection of heat), on undisturbed ground temperature. These two different temperature changes are commonly derived by established procedures: the temperature change at the borehole wall or further away in the subsurface is computed by extensions of the instantaneous point source model (Erol and François, 2018). A resistance model (the borehole resistance R_b, partially extended by thermal capacities) is applied to the temperature change in the borehole (Arthur Huber, 2016; Blocon AB, 2020; Carli et al., 2010; Erol and François, 2018; Koenigsdorff, 2011; Spitler et al., 2016).

The calculation of the effective thermal borehole resistance is generally based on the multipole method developed by Bennet et al. (1987). It determines the thermal borehole resistance for steady-state conditions within a grouted, sealed borehole (Javed and Spitler, 2016). Advanced multipole methods provide equations to calculate the borehole resistance based on the average temperature at the borehole wall in a composite region (Claesson and Hellström, 2011). In this way, both the cross-section perpendicular to the borehole axis with BHE pipes and the surrounding ground are modelled using heat conduction, which leads to radially symmetric heat transfer in and around the borehole. In shallow ground, a second heat transport process can play an important role, which is advection caused by groundwater flow. However, the compatibility of this analytical method for the calculation of the borehole resistance for BHEs with advection (non-radially symmetric heat transfer around the borehole) has not been examined in detail.

For BHEs, the most prevalent model for the determination of temperature change in the subsurface and at the borehole wall is the finite line source (FLS) model, which was numerically simulated by Eskilson (1987). The simulation results are saved as non-dimensional thermal response functions, so-called *g*-functions (Javed et al., 2009). The *g*-function for one single borehole depends on dimensionless time t/t_{steady}, which is defined as the ratio of the considered time t to the steady-state time t_{steady} as determined by Eskilson (1987), and the dimensionless geometry r_b/H_b (Eskilson, 1987). If a borehole field of several interacting BHEs is considered, additional parameters such as the

number and arrangement of the boreholes, and the distance between them, have an impact on the *g*-function as well. Furthermore, Eskilson (1987) introduced the analytical solution of the FLS for steady-state conditions and with an isothermal boundary condition at the surface. Using the latter for dimensioning purposes, Eskilson (1987) recommended the application of the volume conservation principle in order to define the mean temperature at the borehole wall at steady-state conditions. In contrast, Zeng et al. (2002) suggested using the integral mean temperature, which leads to nearly the same equation. Both the numerically determined transient *g*-functions of Eskilson (1987) and the analytical FLS model for steady-state conditions account for heat conduction in a homogeneous subsurface, thereby ignoring heterogeneity or advection associated with groundwater flow.

Several studies investigated analytical models, which consider both conductive and advective heat transport in the subsurface for configuring BHEs (Angelotti et al., 2018; Antelmi et al., 2020; Chiasson and O'Connell, 2011; Claesson and Hellström, 2000; Diao et al., 2004; Erol and François, 2018; Hecht-Méndez et al., 2013; Katsura et al., 2006; Kölbel, 2010; Mohammadzadeh Bina et al., 2020; Molina-Giraldo et al., 2011; Stauffer et al., 2017; Sutton et al., 2003; Zhang et al., 2020). For instance, Claesson and Hellström (2000) introduced a groundwater *g*-function, which is used to reduce the values computed by a *g*-function for heat conduction. This results in an effective *g*-function for calculating the temperature change at the borehole wall in a uniform regional groundwater flow field (Chiasson and O'Connell, 2011; Claesson and Hellström, 2000). The most common representation of groundwater flow effects is accomplished with the so-called 'moving line source' (MLS) (Sutton et al., 2003). Using the MLS model, a BHE without grouting and a specific borehole diameter completely embedded in an aquifer can be simulated to determine its temperature change (Katsura et al., 2006; Kölbel, 2010; Sutton et al., 2003). Chiasson and O'Connell (2011) investigated three analytical solutions for the heat transfer characteristics around BHEs with significant groundwater flow. The first model is the IMLS. The second one is the groundwater *g*-function as presented in Claesson and Hellström (2000) and the third model uses a mass-heat transport analogy. By evaluating thermal response test data, they yielded unrealistic values for the effective thermal conductivity using the MLS and the groundwater *g*-function solution. The mass heat transport analogy regarding thermal dispersion yields the best results, implying that thermal dispersion is important for relatively high groundwater flow rates (Chiasson and O'Connell, 2011). However, all three solutions determined borehole resistance values in the same range as the multipole method, with differences of about 6%. This indicates that the multipole method can also be applied for BHEs with advection. In Tye-Gingras and Gosselin (2014) a model is presented to determine the time-dependent ground response functions of BHE fields with groundwater advection. Therefore, a combination of the infinite cylinder source for short times and the FMLS for larger times and a significant flow velocity is used. Zhang et al. (2020) combined the multipole method according to Hellström (1991) with the FMLS solution of Molina-Giraldo et al. (2011). The models for the heat transfer inside (multipole method) and outside

the borehole (FMLS solution) are coupled by an iterative procedure (Zhang et al., 2020). The outlet temperature is iteratively defined for a known inlet temperature and the mass flow rate of the U-pipe. However, the model is only validated with the thermal response test (TRT) data of an area without groundwater flow (Zhang et al., 2020).

Previous investigations dealing with the use of the MLS to determine the temperature change in the subsurface, e.g., Antelmi et al. (2020), Carli et al. (2010), Erol and François (2018), Guo et al. (2020), Katsura et al. (2006), Molina-Giraldo et al. (2011) and Rivera et al. (2015a), mostly neglect the effect of an impermeable, grouted borehole. Instead, the BHE is treated as a linear source surrounded by homogeneous ground with constant horizontal groundwater flow velocity. In order to account for the reduced groundwater flow within the grout, Wagner et al. (2013) proposed a correction factor, which does not further resolve the heat transfer processes of the borehole and, strictly speaking, is only valid for a given geometry, borehole radius, and grout specification. Tye-Gingras and Gosselin (2014) recommended the use of the FMLS for Péclet numbers only up to 0.1 to keep the error margin of the dimensionless response function under 3%. The deviations due to the differences of the assumptions of the analytical model and a grouted borehole are significant for larger Péclet numbers and, in contrast to pure heat conduction, do not decrease with time (Tye-Gingras and Gosselin, 2014).

The objective of this study is to develop a generally valid IMLS implementation that accounts for the effect of the grout. Although the use of real measurement data would be more valuable for validation purposes, highly reliable thermal test data of a grouted borehole including hydraulic testing of the aquifer are extremely rare. Therefore, a detailed numerical model of a cross section of a grouted borehole is used as virtual reality to compare the temperature change at the borehole radius r_b, determined by the IMLS, with the temperature occurring at the grouted borehole. The analytical model assumes that the groundwater flows horizontally directly around the vertical heat source, i.e. that heat conduction and advection occur within the borehole, which differs strongly from the real situation. For the case without grouting, the numerical and analytical model agree. In addition, horizontal groundwater flow induces a non-radial temperature distribution around the borehole, it must be examined whether this affects the borehole resistance, and to what extent existing analytical methods to calculate the borehole resistance can still be used. An extra focus is placed on the validity of the infinite implementation of the MLS. Clearly, BHEs are better represented by finite lines and by including the three-dimensional effects from the ground surface and the borehole toe. The IMLS does not account for these but is a popular simplification and easier to implement for BHE simulation than the FMLS. As horizontal advection due to groundwater flow is expected to reduce the relative impact of the axial heat flow components at the top and bottom of a BHE, the IMLS may serve as a sufficient estimate, especially for dimensioning longer BHEs.

2.3 Models and methods

2.3.1 Infinite moving line source

The IMLS model can be used for problems in which either sources of heat move through a fixed medium or for cases of heat production at a fixed point past which a uniformly moving medium flows (Carslaw and Jaeger, 1959). For the sake of simplicity, the model will henceforth be presented using the formulation of a heat source, although a negative load can be used to represent a heat sink. The derivation of the IMLS model is briefly described below. Based on the differential equation formulation of Bear (1988) for an aquifer in a porous medium, Sutton et al. (2003) transformed the two-dimensional, differential energy equation using the effective (volume-weighted) thermal diffusivity α_{eff} of the porous matrix and the groundwater flow direction parallel to the axis of x:

$$\frac{\partial T}{\alpha_{\mathrm{eff}}\partial t} = \left(\frac{\partial^2 T}{\partial x^2} + \frac{\partial^2 T}{\partial y^2}\right) - \frac{U_{\mathrm{eff}}\partial T}{\alpha_{\mathrm{eff}}\partial x} \tag{2-1}$$

Herein U_{eff} is the weighted flow velocity, which is deduced from the differential equation using the Darcy velocity $\upsilon_{\mathrm{Darcy}}$, which is defined as:

$$U_{\mathrm{eff}} = \frac{\rho_w c_{p,\mathrm{w}} \upsilon_{\mathrm{Darcy}}}{\left[\phi\rho_{\mathrm{w}} c_{p,\mathrm{w}} + (1-\phi)\rho_{\mathrm{s}} c_{p,\mathrm{s}}\right]} \tag{2-2}$$

Adding the following initial and boundary conditions (IC and BC, respectively) to the differential equation (2-1) allows for the use of Green´s function to determine the impulse response (Carslaw and Jaeger, 1959):

- an initial temperature of the porous medium of zero (IC),
- a continuous source of constant strength $\dot{q}(t)$ generated at $(x', y') = (0,0)$ from $t = 0$ onwards (BC),
- a surface temperature of zero located at infinity (BC).

The transient solution of the differential equation (2-1) for the listed conditions is given by Carslaw and Jaeger (1959) and Sutton et al. (2003):

$$\Delta T = \frac{\dot{q}}{2\pi\lambda_{\mathrm{eff}}} \left\{ \frac{\mathrm{e}^{\frac{U_{\mathrm{eff}}(x-x')}{2\alpha_{\mathrm{eff}}}}}{2} \int_0^t \frac{\mathrm{e}^{-\left[\frac{(x-x')^2+(y-y')^2}{4\alpha_{\mathrm{eff}}(t-\tau)} + \frac{U_{\mathrm{eff}}^2(t-\tau)}{4\alpha_{\mathrm{eff}}}\right]}}{(t-\tau)} d\tau \right\} \tag{2-3}$$

Herein λ_{eff} represents the effective (volume-weighted) thermal conductivity and α_{eff} the corresponding thermal diffusivity of the porous medium. Sutton et al. (2003) reformulated eq. (2-3) in polar coordinates (r, φ) while using the generalised incomplete gamma function $\Gamma(a, x\,; b)$ (Chaudhry and Zubair, 2001) and the dimensionless parameters Fo (dimensionless time) and Pe (ratio of advective to diffusive heat transport component) for the temperature evaluation at the borehole wall $(r = r_{\mathrm{b}})$.

$$\Delta T = \frac{\dot{q}}{2\pi\lambda_{\mathrm{eff}}} \left\{ \frac{\mathrm{e}^{\frac{Pe}{2}\cos(\varphi)}}{2} \; \Gamma\left(0, \frac{1}{4Fo}; \frac{Pe^2}{16}\right) \right\} \tag{2-4}$$

With:

$$Pe = \frac{U_{\mathrm{eff}}\, r_{\mathrm{b}}}{\alpha_{\mathrm{eff}}} \tag{2-5}$$

$$Fo = \frac{\alpha_{\mathrm{eff}}\, t}{r_{\mathrm{b}}^2} \tag{2-6}$$

Eq. (2-4) gives the transient temperature change due to an IMLS at the borehole wall of a single BHE. The lack of radial symmetry of the thermal conditions around a BHE with groundwater advection (see Fig. 2-1) urges the use of the angular component φ, with $\varphi = 0$ representing the groundwater flow direction in the plane perpendicular to the heat source and corresponding to the point directly downstream of the BHE (see Fig. 2-1).

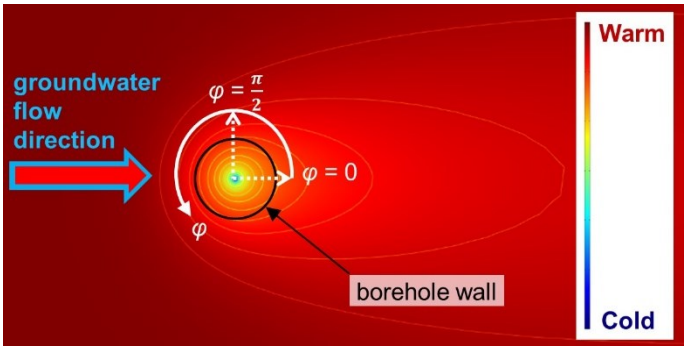

Fig. 2-1: Temperature distribution around a heat sink with groundwater advection.

Since the IMLS represents the BHE as an infinite line source, three-dimensional effects at the top and bottom of a BHE are neglected, as well as the impact of e.g. temperature fluctuations at the ground surface. Rivera et al. (2016) investigated the influence of spatially variable ground heat flux on closed-loop BHEs. They found that in cases with groundwater advection, the penetration depth of thermal ground surface effects is restricted to the downstream side of the thermal plume. They then revealed that the extraction rate of the BHE represents the most important parameter in areas close to the BHE and at greater depth (Rivera et al., 2016). Furthermore, it is assumed that the subsurface consists of a homogeneous medium without temperature-dependent thermophysical properties. Consequently, the impact of a sealing grouting material, which differs in several material properties from the surrounding subsurface, is also neglected.

For steady-state conditions the generalised incomplete gamma function disappears and the modified Bessel function of the second kind K_0 is used, so that eq. (2-4) reduces to:

$$\Delta T = \frac{\dot{q}}{2\pi\lambda_{\mathrm{eff}}} \left\{ \mathrm{e}^{\frac{Pe}{2}\cos(\varphi)} K_0\left(\frac{Pe}{2}\right) \right\} \tag{2-7}$$

Integrating eq. (2-7) over the angle φ from 0 to π and dividing the result by π yields the mean temperature at the borehole wall. The integration of eq. (2-7) over φ leads to the use of the modified Bessel function of the first kind, I_0, resulting in the following equation:

$$\Delta T = \frac{\dot{q}}{2\pi\lambda_{\mathrm{eff}}} \left\{ I_0\left(\frac{Pe}{2}\right) K_0\left(\frac{Pe}{2}\right) \right\} \tag{2-8}$$

Based on this, Sutton et al. (2003) presented a procedure to determine whether to use the transient solution or the steady-state solution of the IMLS model.

Analogous to Eskilson´s definition of a *g*-function (Eskilson, 1987), eq. (2-8) can be rewritten to obtain a groundwater *g*-function for steady-state conditions and the described simplifications of an IMLS, resulting in:

$$g_{\mathrm{steady,IMLS}}(Pe) = I_0\left(\frac{Pe}{2}\right) K_0\left(\frac{Pe}{2}\right) \tag{2-9}$$

Using this approach implies that the temperature change in the subsurface with groundwater flow is directly proportional to the heat extraction or injection and inversely proportional to $2\pi\lambda_{\mathrm{eff}}$. Furthermore, the temperature change strongly depends on Pe.

2.3.2 Finite moving line source

In order to estimate the error of ignoring axial effects, a comparison of the infinite to the finite moving line source model is carried out. The mean integral temperature over the borehole radius ($r = r_{\mathrm{b}}$), and the borehole length H of the steady-state solution of the FMLS with an isothermal boundary condition at the surface is deduced from the steady-state solution of the moving point source (Carslaw and Jaeger, 1959):

$$\Delta T(x,y,z) = \frac{\dot{q}}{4\pi\lambda_{\mathrm{eff}}\sqrt{(x-x')^2+(y-y')^2+(z-z')^2}} \, \mathrm{e}^{\frac{-U_{\mathrm{eff}}\left(\sqrt{(x-x')^2+(y-y')^2+(z-z')^2}-(x-x')\right)}{2\alpha_{\mathrm{eff}}}} \tag{2-10}$$

Integrating z' in the steady-state solution from eq. (2-10) over the length H_b and using the method of image, results in the FMLS. The steady-state solution of the FMLS in cylindrical coordinates and with an isothermal boundary condition for the mean temperature change, averaged over the angle and the length, is stated as:

$$\Delta\bar{T}(r, H_\mathrm{b}, Pe) = \frac{\dot{q}}{2\pi\lambda_\mathrm{eff}} \left\{ \frac{I_0\left(\frac{Pe}{2}\right)}{2\ H_\mathrm{b}} \int_0^{H_\mathrm{b}} \int_0^{H_\mathrm{b}} \left(\frac{\mathrm{e}^{\frac{-U_\mathrm{eff}\left(\sqrt{r^2+(z-z')^2}\right)}{2\alpha_\mathrm{eff}}}}{\sqrt{r^2+(z-z')^2}} - \frac{\mathrm{e}^{\frac{-U_\mathrm{eff}\left(\sqrt{r^2+(z+z')^2}\right)}{2\alpha_\mathrm{eff}}}}{\sqrt{r^2+(z+z')^2}} \right) dz'dz \right\} \tag{2-11}$$

The associated *g*-function is:

$$g_{\mathrm{steady,FMLS}}(r, H_\mathrm{b}, Pe) = \frac{I_0\left(\frac{Pe}{2}\right)}{2H_\mathrm{b}} \int_0^{H_\mathrm{b}} \int_0^{H_\mathrm{b}} \left(\frac{\mathrm{e}^{\frac{-U_\mathrm{eff}\left(\sqrt{r^2+(z-z')^2}\right)}{2\alpha_\mathrm{eff}}}}{\sqrt{r^2+(z-z')^2}} - \frac{\mathrm{e}^{\frac{-U_\mathrm{eff}\left(\sqrt{r^2+(z+z')^2}\right)}{2\alpha_\mathrm{eff}}}}{\sqrt{r^2+(z+z')^2}} \right) dz'dz \tag{2-12}$$

For BHEs, generally an isothermal boundary condition representing the mean ground surface temperature is used for dimensioning purposes.

2.3.3 Numerical model

In order to examine the applicability of the analytical IMLS solution for the temperature calculation at the borehole wall of grouted BHEs, a finite-element-based numerical model considering all relevant heat transfer processes in the subsurface caused by a grouted BHE is developed in COMSOL Multiphysics. Equivalent to the assumptions of the analytical model, a two-dimensional numerical model is set up, similar to that of Lazzari et al. (2010). In this way, the focus is set on the role of the grout, while keeping calculation time low. The error caused by ignoring the three-dimensional effects of a finite borehole is subsequently evaluated by comparison with the FMLS (eq. (2-11)).

The numerical model accounts for the coupled conductive and advective heat transport in a uniform porous subsurface. The porous medium is simulated, assuming a local thermal equilibrium of the fluid and the porous matrix, with volume-averaged properties of both phases, based on eq. (2-1) (Gossler et al., 2019). The groundwater flow is modelled by Darcy´s law assuming a uniform flow field with the pressure gradient as the driving force in the hydraulic potential field. Combining the heat transfer in the porous-media-interface with Darcy´s law-interface warrants the common approach of a homogenisation of the porous and fluid medium into one representative medium, i.e. no detailed model on pore-scale is necessary (COMSOL Multiphysics, 2021). This requires that homogenisation is feasible and that local effects of hydraulic parameter heterogeneity describing the ambient ground conditions can be ignored.

A grouted borehole with radius r_b and a centred heat source in the grouting material is embedded in the simulated ground and is treated independently, particularly with regard to heat transfer processes

and its boundary conditions towards the subsurface. Since the grouting of boreholes is applied to seal the borehole against the adjacent subsurface, the grouting material is modelled using heat conduction only, so that no groundwater flow occurs within the borehole itself. The model allows for different thermal properties of the grouting material in the borehole and the porous medium around the borehole. As is common in related works (e.g. Spitler et al. (2016)), the heat exchanger pipes are not modelled explicitly but represented by a concentric heat source in the grouted borehole.

For the purpose of examining the thermal borehole resistance model for BHEs with groundwater advection, the numerical model is slightly modified. The point heat source is replaced by a centred hole in the grouting material. This simplified geometry represents a coaxial BHE or the equivalent radius for a U-pipe or double U-pipe (Claesson and Dunand, 1983). The simplification of replacing the (double) U-pipe by an equivalent radius is common practice in the analytical modelling of BHEs, especially for short time analysis (Gu and O´Neal, 1998; Gu and O'Neal, 1995; Javed and Claesson, 2011; Kavanaugh, 1985; Lazzarotto and Pallard, 2019). Lamarche and Beauchamp (2007b) have shown that the results between an analytical model with equivalent radius and a detailed numerical model are in favourable agreement.

To test a broad spectrum of conditions, a parameter study consisting of 6,336 model runs is conducted, with varying subsurface and grouting material properties. Table 2-1 shows all examined parameter values and ranges, covering Darcy velocities from 2.94 cm/day up to 8.81 m/day. This range corresponds to the velocities investigated in related work (Katsura et al., 2006; Lazzari et al., 2010; Sutton et al., 2003; Wagner et al., 2013). A preparatory sensitivity analysis was conducted to define the necessary numerical simulation domain and grid geometry. As a result, a suitable domain of 70 m x 30 m was determined, along with a borehole at a 10 m distance of the groundwater inflow (see Fig. 2-2). A triangulated mesh containing 12,730 elements (Fig. 2-2) was generated with the highest resolution in the immediate vicinity of the heat source/sink (in the BHE). The element size of the mesh increases uniformly towards the borehole wall and continues to increase in the subsurface while the temperature gradient declines. The thermal boundaries are set at a constant temperature, identical to a given initial temperature, except for the downstream boundary with an outflow condition implemented to compute the temperatures here for each simulated scenario (COMSOL Multiphysics, 2019). Given this model setup with an identical setting and a homogeneous, porous subsurface with no grouting, numerically derived *g*-function values were compared with IMLS results. Relative discrepancies for the simulations with the parameter value ranges given in Table 2-1 were found to be less than 3%, with an absolute deviation of less than 0.01 K and a standard deviation of 0.00084 K.

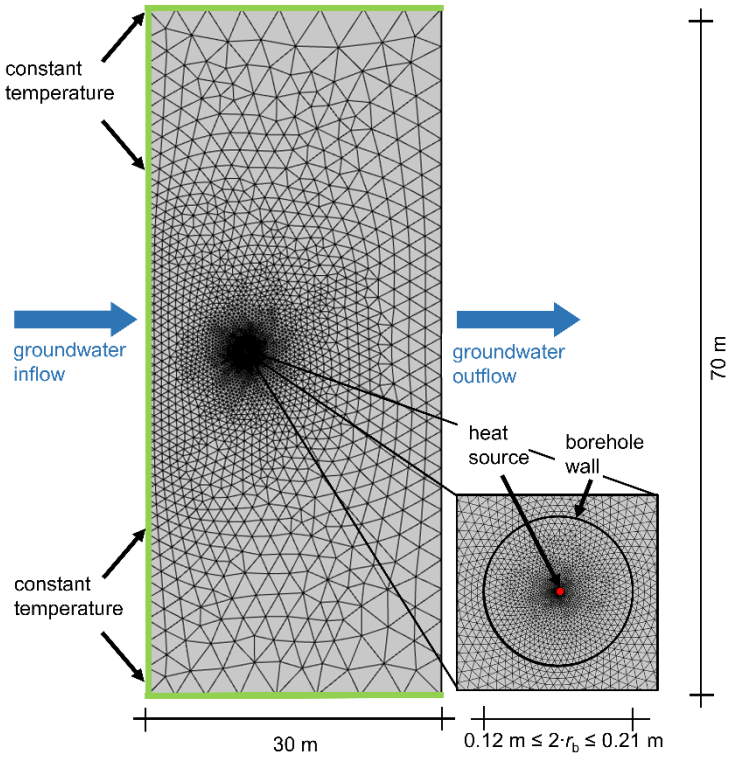

Fig. 2-2: Model domain of the numerical model and its boundary conditions.

Table 2-1: Examined parameter ranges for the comparison between the numerical model and the IMLS.

Parameter description	**Unit**	**Value range**			
Darcy velocity v_{Darcy}	cm/day	2.94	up to		881.28
Thermal conductivity of the solid phase λ_s	W/(m·K)	1.0	2.0	3.0	4.0
Porosity of the subsurface ϕ	-	0.1	0.3	0.5	
Thermal conductivity of the grouting material λ_{grout}	W/(m·K)	1.0	2.0		
Borehole radius r_b	m	0.06	0.075	0.09	0.105
→ Resulting Péclet numbers Pe	-	0.1	up to		10
Initial and boundary temperature $T_{\mathrm{undist\,sub}}$	°C	10			
Heat extraction rate $\dot{q}$	W/m	-20			

2.3.4 Correction of infinite moving line source and application to borehole heat exchanger design

As revealed in Wagner et al. (2013), Van de Ven et al. (2018) and Wagner et al. (2014), there is a deviation between the real temperature change at the wall of a grouted borehole and the corresponding temperature change calculated with the IMLS model. This deviation is ascribed to the different thermal and hydraulic properties of the grouting material and the subsurface. Since the operating temperature is often the limiting parameter for the dimensioning of BHEs, it is crucial to attain the correct temperature change of the BHE in the design process. Therefore, the aim of this

chapter is to overcome the addressed deviation by introducing a generally valid correction function f_{cor} which allows for the adjustment of the IMLS model. This follows the same idea as the correction factor presented in Wagner et al. (2013) for relating the effective Darcy velocity derived from a TRT to the “true” Darcy velocity in the surrounding ground.

The deviation between the numerical model with grouting and the analytical model without grouting is taken as correction in order to make the analytical model applicable for grouted boreholes. Consequently, the correction function here is defined as the ratio of the *g*-function of the grouted borehole as determined by the numerical model and of the *g*-function resulting from the IMLS:

$$f_{\mathrm{cor}} = \frac{g_{\mathrm{steady,num}}}{g_{\mathrm{steady,IMLS}}} \tag{2-13}$$

The values or correlations that define f_{cor} are deduced by comparison with the numerical model. Knowing f_{cor}, the mean undisturbed subsurface temperature $\bar{\bar{T}}_{\mathrm{undist\,sub}}$, as well as the borehole resistance R_{b}, the mean fluid temperature in a borehole $\bar{\bar{T}}_{\mathrm{b,fl,steady}}$ at steady-state conditions can then be calculated using Eqs. (2-9) and (2-13) as follows:

$$\bar{\bar{T}}_{\mathrm{b,fl,steady}} = \bar{\bar{T}}_{\mathrm{undist\,sub}} + \dot{q}\left(\frac{f_{\mathrm{cor}}\, g_{\mathrm{steady,IMLS}}}{2\pi\lambda_{\mathrm{eff}}} + R_{\mathrm{b}}\right) \tag{2-14}$$

A prerequisite for the presented method is that the Darcy velocity and the thermal conductivity of the subsurface are known. These can be determined by laboratory testing of material properties or by using a TRT and the method found in Wagner et al. (2013). Furthermore, an average Darcy velocity can be estimated with the use of hydrogeological maps, site-specific pumping or tracer tests.

2.4 Results and discussion

2.4.1 Compatibility of the thermal borehole resistance model for borehole heat exchangers with groundwater advection

To implement the IMLS model in design programs, it has to be assessed if the non-radially symmetric temperature distribution at the borehole wall can be averaged and then be used to determine the borehole resistance for BHEs under the influence of advection. Therefore, a steady-state simulation with groundwater flow and a 48-hour transient simulation without groundwater flow are conducted, and the numerical results are compared with the analytical solution of heat conduction in an annulus. The BHE is considered to be perfectly sealed for horizontal groundwater advection in the surrounding subsurface so that only heat conduction occurs within the grouting material of the borehole. The temperature distribution around the borehole depends on groundwater flow velocity and direction, and thus the computed borehole resistance differs depending on the observed angle. However, averaged over the borehole wall, the value of the thermal resistance is the same as without groundwater flow. An excerpt of the results is shown in Table 2-2. The maximum deviation between the thermal borehole

resistances is less than 1% and can be ascribed to the accuracy of the numerical solution. Hence, it can be concluded that the multipole method for the determination of the thermal borehole resistances is also applicable to BHEs with groundwater advection. However, it is a prerequisite that the correct temperature at the borehole wall is calculated.

Table 2-2: Comparison of thermal borehole resistance calculations by numerical and analytical models.

Borehole radius r_b	**Thermal conductivity of the grout** λ_grout	**Darcy velocity** v_Darcy	**Num. sim. with advection**	**Num. sim. without advection**		**Analytical solution**	
			Thermal borehole resistance R_b	**Thermal borehole resistance** R_b	**Percentage deviation**	**Thermal borehole resistance** R_b	**Percentage deviation**
m	**W/(m·K)**	**m/s**	**(m·K)/W**	**(m·K)/W**	**%**	**(m·K)/W**	**%**
0.060	1.0	$3.40\cdot10^{-6}$	0.2102	0.2096	-0.26	0.2104	0.09
	2.0	$3.40\cdot10^{-6}$	0.1051	0.1048	-0.26	0.1052	0.09
	1.0	$1.70\cdot10^{-5}$	0.2102	0.2096	-0.26	0.2104	0.09
	2.0	$1.70\cdot10^{-5}$	0.1051	0.1048	-0.26	0.1052	0.09
	1.0	$3.40\cdot10^{-5}$	0.2102	0.2096	-0.26	0.2104	0.09
	2.0	$3.40\cdot10^{-5}$	0.1051	0.1048	-0.26	0.1052	0.09
	1.0	$1.70\cdot10^{-4}$	0.2102	0.2096	-0.26	0.2104	0.09
	2.0	$1.70\cdot10^{-4}$	0.1051	0.1048	-0.26	0.1052	0.09
0.105	1.0	$3.40\cdot10^{-6}$	0.2991	0.2973	-0.61	0.2994	0.10
	2.0	$3.40\cdot10^{-6}$	0.1496	0.1487	-0.59	0.1497	0.10
	1.0	$1.70\cdot10^{-5}$	0.2991	0.2973	-0.61	0.2994	0.10
	2.0	$1.70\cdot10^{-5}$	0.1496	0.1487	-0.59	0.1497	0.10
	1.0	$3.40\cdot10^{-5}$	0.2991	0.2973	-0.61	0.2994	0.10
	2.0	$3.40\cdot10^{-5}$	0.1496	0.1487	-0.59	0.1497	0.10
	1.0	$1.70\cdot10^{-4}$	0.2991	0.2973	-0.61	0.2994	0.10
	2.0	$1.70\cdot10^{-4}$	0.1496	0.1487	-0.59	0.1497	0.10

2.4.2 Applicability of the infinite moving line source model to finite boreholes

The inaccuracy caused by using the IMLS instead of the FMLS and thus by neglecting the three-dimensional effects at the surface and bottom of a finite BHE is investigated by comparing both models for a broad range of parameters. Since the error between the IMLS and the FMLS decreases with borehole length, only small borehole depths from 10 m down to 50 m are examined for all parameter value combinations given in Table 2-1.

The percentage deviation of the *g*-functions of the IMLS and the FMLS with an isothermal boundary condition at the ground surface is calculated according to Eq. (2-15) and exemplarily depicted in Fig. 2-3 a for a borehole radius of 0.075 m and in Fig. 2-3 b for a borehole depth of 30 m.

$$\frac{g_{\text{steady,IMLS}} - g_{\text{steady,FMLS}}}{g_{\text{steady,FMLS}}} \tag{2-15}$$

As expected, the deviation between both models declines with increasing borehole depth and Péclet numbers as well as with decreasing borehole radius. For boreholes with a length of 30 m or more, the deviation is less than 5% for $Pe \geq 0.06$. This reveals that a small error is introduced by neglecting the three-dimensional effects at the top and the bottom of a BHE that is influenced by horizontal groundwater flow.

In Molina-Giraldo et al. (2011) the three-dimensional effects of a BHE with advection are investigated as well, but the Péclet number is expressed by setting the characteristic length to the borehole length ($H_\mathrm{b} = 50$ m) (i.e. replacing r_b by H_b in Eq. (2-5)). Translating the findings of Molina-Giraldo et al. (2011) for a BHE with a length of 50 m, the discrepancy between the finite and the infinite MLS becomes irrelevant for $Pe \geq 0.015$. The investigated range here does not cover such small Péclet numbers as in Molina-Giraldo et al. (2011), but the results are consistent. Furthermore, the IMLS model calculates (slightly) larger *g*-functions and as a result, a greater temperature change than the FMLS model. Hence, the IMLS model is the more conservative model and therefore favourable for designing BHEs of 30 m and more.

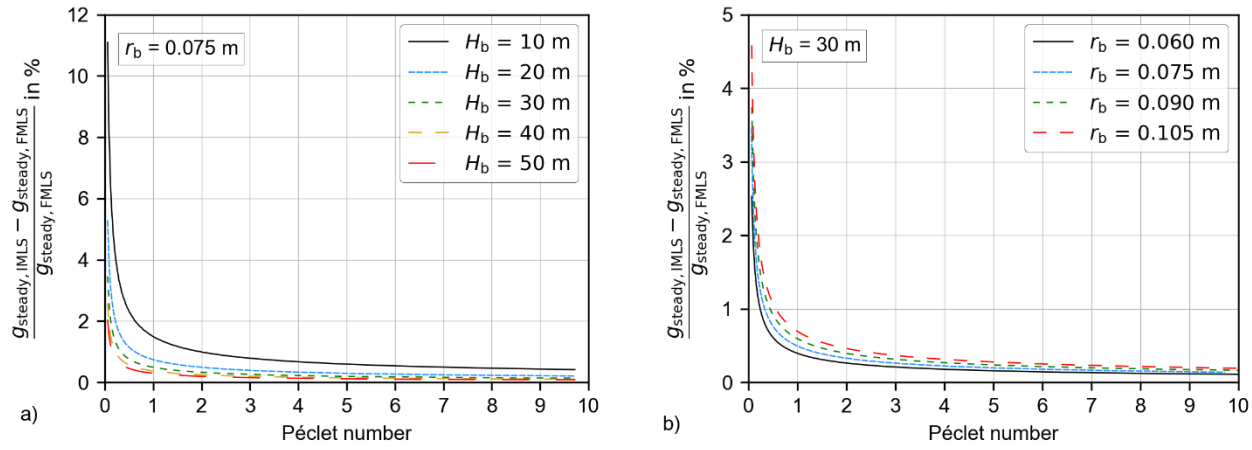

Fig. 2-3: Percentage deviation of the *g*-functions calculated with the infinite and finite MLS with an isothermal boundary condition at the ground surface a) for a borehole radius of $r_\mathrm{b} = 0.075$ m and b) a borehole length of $H_\mathrm{b} = 30$ m.

2.4.3 Steady-state thermal conditions at the wall of a grouted borehole

To characterise the deviation between the numerical simulation and the analytical IMLS solution, the steady-state thermal conditions at the outside wall of a grouted borehole are investigated. The computed discrepancy for different borehole radii depending on the Darcy velocity is shown in Fig. 2-4.

The relative error between the *g*-function of the analytical solution and the numerical simulation is calculated according to:

$$\frac{g_{\text{steady,num}} - g_{\text{steady,IMLS}}}{g_{\text{steady,num}}} \tag{2-16}$$

It is revealed that the error gradually increases with increasing Darcy velocities. This is mainly caused by the rapidly sinking *g*-function values with increasing Darcy velocity. The derived curves for different radii are not identical but have a similar shape.

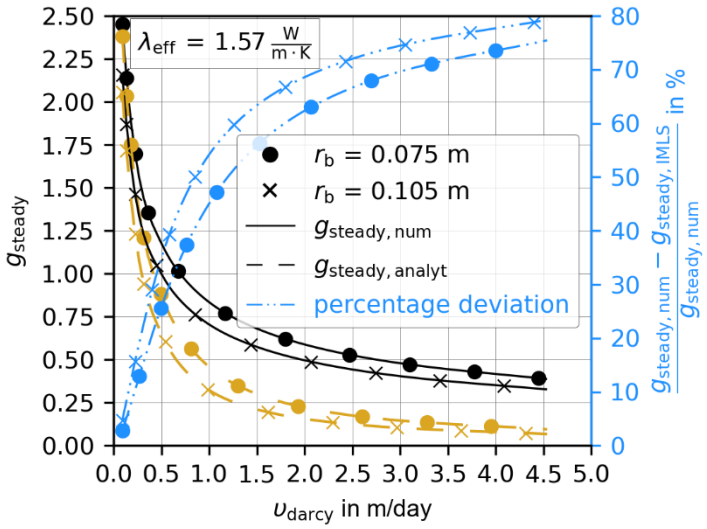

Fig. 2-4: Deviation of the *g*-functions between the numerical model with a grouted borehole and the analytical IMLS model.

Investigating the deviation between both models depending on the effective thermal conductivity λ_{eff} of the subsurface and the Darcy velocity v_{Darcy}, shows that the discrepancy decreases with higher values of λ_{eff} and lower values of v_{Darcy}, as depicted in Fig. 2-5. Both parameters have an effect of the same order of magnitude but in opposite directions, which means that, for example, the effect of a lower thermal conductivity can be compensated by a corresponding increase in Darcy velocity. Thus, the fraction, i.e. the relative role, of Darcy velocity (advection) and thermal conductivity (diffusion) is crucial. The relative role of advection and diffusion is expressed by the Péclet number according to Eq. (2-5), which also includes the borehole radius as a length scale. Therefore, the combined effect of advection and diffusion for assessing the accuracy of the analytical model can be summarised in Fig. 2-6, which confirms the rising deviation of the steady-state values of the *g*-functions for higher Péclet numbers. A high effective thermal conductivity λ_{eff} requires a greater Darcy velocity to reach the same Péclet number in comparison to lower λ_{eff}. However, this barely influences the deviation of the IMLS, as shown in Fig. 2-6. Thus, it can be concluded, that the higher the overall influence of advection, the greater the error.

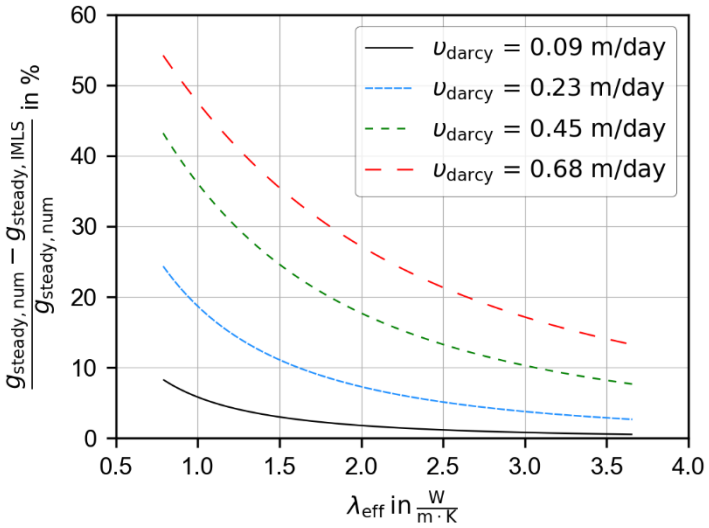

Fig. 2-5: Percentage deviation of the *g*-functions depending on the effective thermal conductivity for different Darcy velocities.

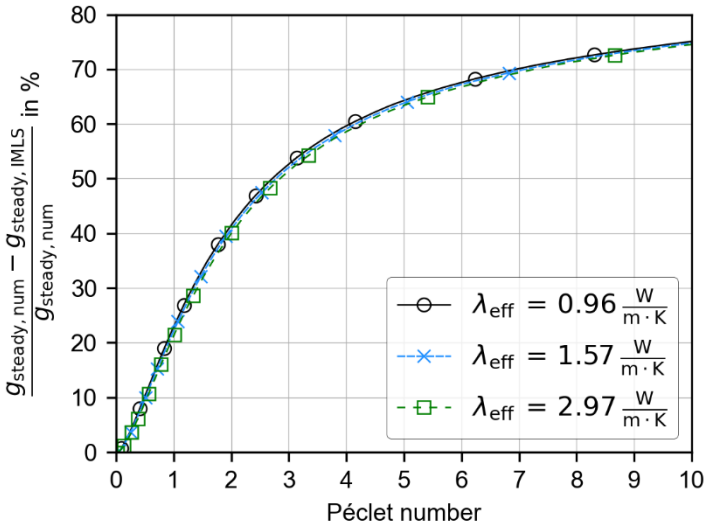

Fig. 2-6: Percentage deviation of the *g*-functions depending on the Péclet number for different effective thermal conductivities.

2.4.4 Correction function

By introducing a correction function for the groundwater *g*-function for steady-state conditions, the temperature change at the borehole wall of a grouted borehole can be determined. Therefore, the results of the analytical and numerical solutions are related by Eq. (2-13) and fitted by a second-degree polynomial as shown in Fig. 2-7. The corrected *g*-function depicted in Fig. 2-8 is generated by multiplying the correction function with the groundwater *g*-function and can then be implemented in design programs such as EED or GEO-HAND^{light} for the planning of BHEs with groundwater advection, without changing further calculation methods and without the need for a complex numerical simulation. The correction function overcomes the deficiency of neglecting the

effect of the non-permeable, grouted borehole, and thus prevents a temperature change prediction that is too low during the design phase.

Since the groundwater *g*-function for one borehole (Eq. (2-9)), as well as the model discrepancies, depend chiefly on the Péclet number; Fig. 2-7 shows the correlation of the required correction based on this parameter. By means of regression analysis, a manageable, second-degree polynomial shown in Eq. (2-17) is fitted to the simulation results, yielding a coefficient of determination of $R^2 = 0.993$. The second-degree polynomial is acceptable for practical applications and everyday use, since many uncertainties of a similar order of magnitude are involved while characterising a BHE with groundwater advection. Eq. (2-17) is only valid for Péclet numbers from $Pe = 0$ up to $Pe = 10$.

$$f_{\mathrm{cor}}(Pe) = -6.11 \cdot 10^{-3} \cdot Pe^2 + 3.68 \cdot 10^{-1} \cdot Pe + 1 \qquad \text{(2-17)}$$

$$for\ 0 \leq Pe \leq 10$$

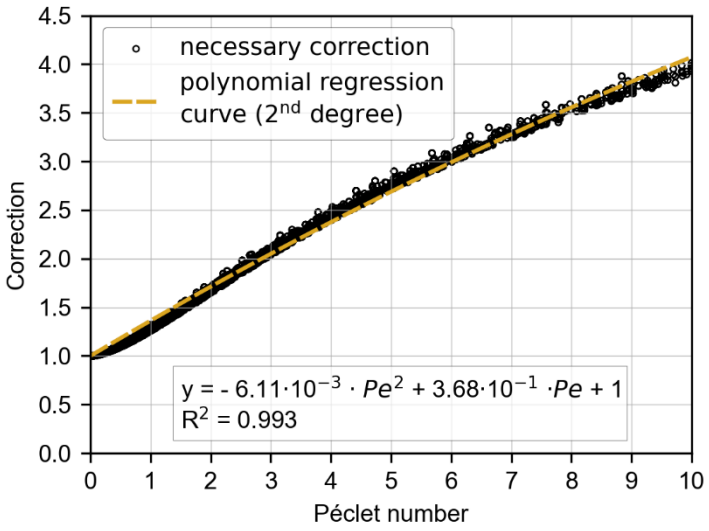

Fig. 2-7: Second-degree polynomial correction function for the IMLS for steady-state conditions.

Using a fifth-degree polynomial yields a more correct correlation reproducing the characteristic course of the simulated data. Since other parameters lead to higher uncertainties while determining the temperature of a vertical grouted borehole, a second-degree polynomial is considered adequate for practical usage.

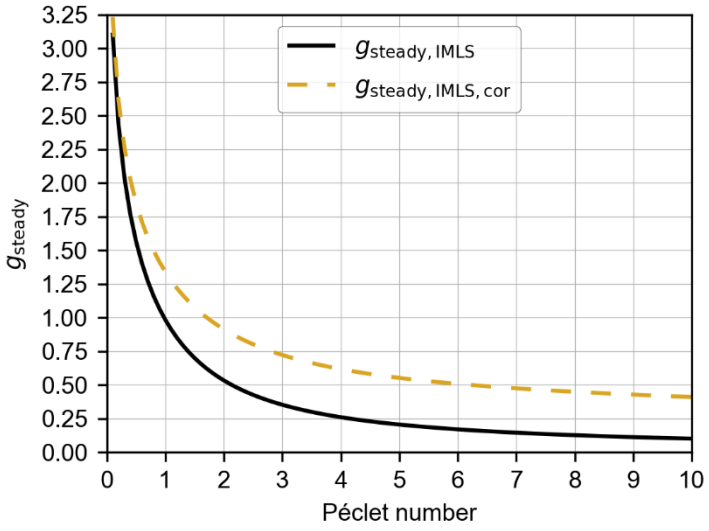

Fig. 2-8: Groundwater *g*-function values for steady-state conditions with and without correction.

2.4.5 Demonstration example

To demonstrate the impact of the proposed correction procedure on the design of a BHE, three examples for typical thermal and hydraulic property data for various geological materials as given in Sutton et al. (2003) are investigated. These are listed in Table 2-3 as 'Karst Limestone', 'Sand (Coarse)', and 'Gravel'. A fourth example, 'Gravel (modified)', is also based on the same source but for an increased borehole radius of 0.075 m and a decreased velocity leading to a Péclet number of one. The Péclet numbers are calculated according to Eq. (2-5), as in Sutton et al. (2003).

Table 2-3: Thermal and hydraulic properties of the subsurface used for the setup of demonstration examples. (Sutton et al., 2003)

Material	**Thermal conductivity** λ	**Vol. heat capacity** c_v	**Porosity** ϕ	**Darcy Velocity** v_{Darcy}	**Borehole Radius** r_b	**Péclet number** Pe
	W/(m·K)	**MJ/(m³·K)**	**-**	**m/yr**	**m**	**-**
Groundwater*	0.60	4.18				
Karst limestone*	3.40	13.40	0.275	31.63	0.054	0.09
Sand (coarse)*	0.8	1.40	0.385	23.14	0.054	0.23
Gravel*	0.8	1.40	0.310	945.50	0.054	9.17
Gravel (modified)**	0.8	1.40	0.310	74.25	0.075	1.00

* as defined in Sutton et al. (2003)

** based on Sutton et al. (2003)

Considering that in this study, the IMLS model is corrected for the effect of a grouted borehole only at steady-state conditions, an application with an almost constant heating or cooling demand is best suited. A typical example with a more or less constant cooling load is a data centre, which releases

nearly the same amount of heat all year long. The servers of the Biberach University of Applied Sciences are used in an exemplary manner for the calculation. They have a constant power consumption of 8 kW of the uninterrupted power supply (UPS), as taken from measurement data of 2017 depicted in Fig. 2-9.

The power consumption of the UPS is equivalent to the required cooling load of the data centre. The mean undisturbed subsurface temperature next to the data centre is assumed to be about 12 °C. A maximum temperature increase of the mean fluid temperature of 10 K is desired in order to guarantee a mean fluid temperature of 22 °C, which is necessary to operate the cooling device of the data centre.

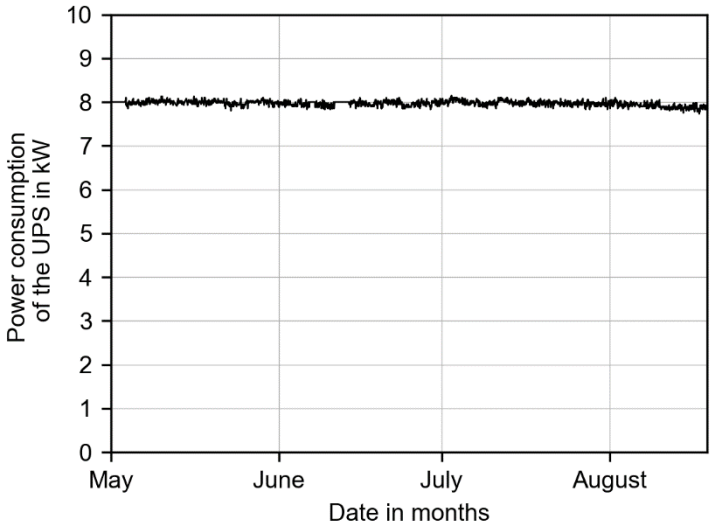

Fig. 2-9: Cooling load of the servers at Biberach University of Applied Sciences.

Using the thermal and hydraulic properties listed in Table 2-3, a heat injection rate of 8 kW, a thermal resistance of 0.08 (m·K)/W, an undisturbed subsurface temperature of 12 °C, and a maximum temperature increase of 10 K, the required borehole depths and the resulting specific heat injection rates are determined by transforming Eq. (2-14). Furthermore, the percentage deviation of the aforementioned properties calculated with and without the proposed correction in Eq. (2-17) are listed as well. The percentage deviation expresses the discrepancy between both calculations compared with the calculation using the uncorrected *g*-function.

Table 2-4: Calculation example for the four cases listed in Table 2-3.

Heat injection rate					8.00	kW	
Borehole resistance					0.08	(m·K)/W	
Maximum temperature change of the subsurface					10	K	
	Péclet number	**Model selection**	***g*-function**	**Borehole length**	**Percentage deviation of the borehole length**	**Specific heat injection rate**	**Percentage deviation of the specific heat injection rate**
	-	**-**	**-**	**m**	**%**	**W/m**	**%**
Karst limestone*	0.09	FLS	6.6	383.52	74.39	20.86	−42.66
		IMLS without correction	3.22	219.93	0.00	36.38	0.00
		IMLS with correction	3.32	224.60	2.13	35.62	−2.08
Sand (coarse)*	0.23	FLS	6.6	1,226.29	161.34	6.52	−61.74
		IMLS without correction	2.30	469.24	0.00	17.05	0.00
		IMLS with correction	2.49	501.66	6.91	15.95	−6.46
Gravel*	9.17	FLS	6.6	1,202.67	1,350.07	6.65	−93.10
		IMLS without correction	0.11	82.94	0.00	96.46	0.00
		IMLS with correction	0.42	137.10	65.31	58.35	−39.51
Gravel (modified)**	1.00	FLS	6.6	1,202.67	414.82	6.65	−80.58
		IMLS without correction	0.98	233.61	0.00	34.25	0.00
		IMLS with correction	1.34	294.67	26.14	27.15	−20.72

* as defined in Sutton et al. (2003)

** based on Sutton et al. (2003)

The calculation examples in Table 2-4 show that considering groundwater flow leads to a shorter borehole being required for a given heat demand, i.e. using the IMLS model instead of the FLS model is strongly recommended if advection is present. However, for rising Péclet numbers, the borehole depth is increasingly underestimated and thus the specific heat extraction rate is overestimated for grouted boreholes if the IMLS solution is not corrected. For a constant effective thermal conductivity but a rising Péclet number, i.e. rising contribution by groundwater flow and thus higher Darcy velocity, the percentage deviation, as well as the absolute deviation, increases rapidly for small Péclet

numbers. In the range of $Pe = 0$ to 10, the absolute deviation reaches a maximum around $Pe = 2$ for the investigated examples and then slowly decreases (Fig. 2-10). The wrong estimation without correction can also be quantified by missing borehole length. For equal borehole radii, the percentage deviation of the borehole length varies with the borehole resistance, since a greater resistance and thus a worse thermal conductivity of the grouting material leads to a larger overall borehole length. The absolute missing borehole length caused by ignoring the grouted and sealed borehole is, on the contrary, independent of the borehole resistance. The percentage deviation and the missing borehole length for the four demonstration examples are explicitly marked in Fig. 2-10.

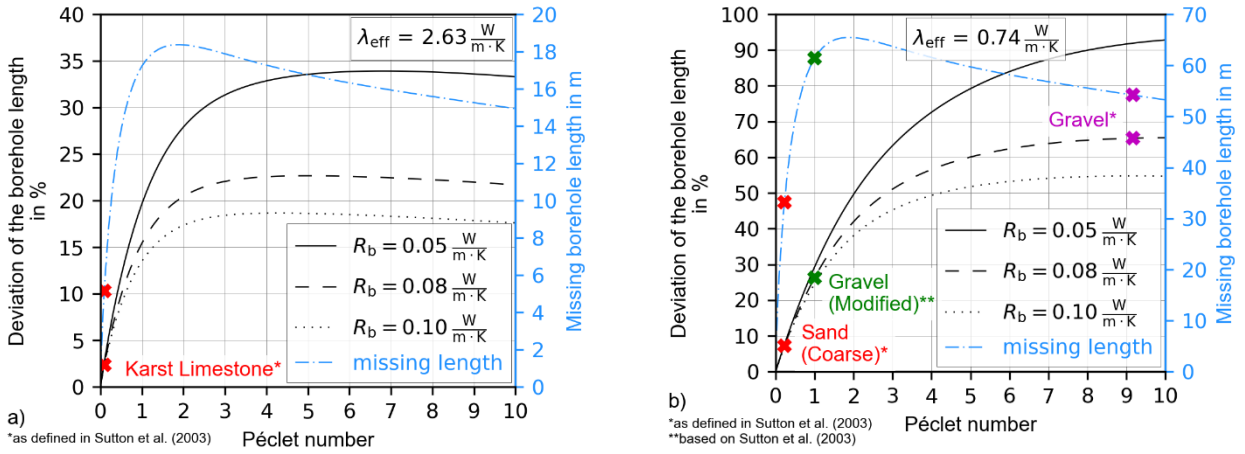

Fig. 2-10: Deviation in borehole length depending on the Péclet number for the thermal properties as listed in Table 2-3 of a) Karst Limestone and b) Gravel and Sand (coarse).

2.5 Interim conclusions

This study assesses the suitability of the analytical IMLS model for the dimensioning of vertical finite and grouted BHEs with horizontal groundwater advection for steady-state conditions. Therefore, the relevant aspects for the analytically based determination of the operating temperature of BHEs are investigated concerning the use of the IMLS model.

The initial step was the investigation of the applicability of established thermal borehole resistance models for BHEs under purely conductive conditions concerning groundwater advection. Due to the non-radially symmetric temperature distribution around the borehole, the suitability of the mean borehole temperature for the determination of the borehole resistance is investigated. It is found that established analytical methods to determine the borehole thermal resistance as a mean value over the borehole radius can also be applied to BHEs with groundwater advection.

In the second step, the applicability of the IMLS model to boreholes of finite length is evaluated by comparing the *g*-functions resulting from the infinite and the finite MLS. For a FMLS with an isothermal boundary condition, the deviation is less than 5% for BHEs of a depth of 30 m or more, and for Péclet

numbers greater than 0.05. Here, the use of the IMLS leads to only slightly larger *g*-function values and temperature changes at the borehole wall than the more realistic FMLS model.

The major discrepancy when applying the IMLS model to finite, grouted BHEs is due to the grouting of the borehole, since the grouting is almost impermeable for groundwater flow, while the IMLS model represents a homogeneous groundwater flow (also within the borehole region). This discrepancy is investigated by comparing the IMLS model with numerical simulations in an extensive parameter study. The deviation could be traced back to one main parameter: the Péclet number. Using the Péclet number, a correction function is introduced to overcome the discrepancy of the IMLS model. The described correction procedure allows for a more precise estimation of the temperature change at the borehole wall for steady-state conditions. A calculation of the BHE operating temperature that is too optimistic is thereby avoided, which is necessary to ensure operational safety. It is shown that, depending on the Péclet number, the use of the IMLS model without correction will lead to an underestimation of the required borehole length.

With the correction function found in this study, the IMLS model, together with established borehole resistance models, has been found to be well-suited for the dimensioning of finite, vertical, and grouted boreholes in the presence of groundwater advection for steady-state conditions, boreholes of at least 30 m length, and Péclet numbers from 0.05 on. Since the developed correction function is valid for single boreholes and steady-state conditions only, further development will focus on transient conditions and borehole fields.

3 Analytical simulation of heat conduction around planar trench collectors

3.1 Chapter overview

Vertical planar installations in very shallow ground are uncommon technological variants for geothermal heat supply. Still, they are of increasing interest when depth and space restrictions do not allow the drilling of boreholes or the installation of horizontal collectors. This work is dedicated to planar closed-loop heat exchangers that are installed in trenches at a few meters depth. A novel three-dimensional analytical model is presented that accounts for the thermal properties as well as seasonal temperature variation in the ground. The model represents the trench collector as a finite plane source (FPS) with a specific thermal resistance to simulate the mean temperature of the circulating heat carrier fluid. Both a detailed dimensional analysis and a successful comparison to numerical simulation are presented. Even though only conductive heat transport is simulated, the model could be validated to the conditions observed at an experimental field site with a trench collector installed at Biberach, Germany. The presented analytical method can serve as an ideal tool for the fast dimensioning of vertical planar heat collectors in practice, and it represents a fundamental framework for the integration of advection or latent heat transfer in frozen ground.

3.2 Introduction

Ground heat collectors represent a family of closed-loop devices used for feeding ground-source heat pumps (GSHP). As a common feature, they are installed at only a few meters depth, where they still experience seasonal temperature fluctuations. There are various types of ground heat collectors (GHCs) such as horizontal ground heat collectors, trench collectors, or geothermal baskets. Hou et al. (2022) classified them according to their geometry into four categories: linear-loops, slinky-coils, helical-coils and others (e.g., planar, tunnel-lining). Each geometry can be installed either vertically or horizontally, and either compactly in trenches or covering a wide area in the subsurface. Obviously, the ideal choice is highly dependent on the available space, and for instance, horizontal collectors are more common in rural areas than in densely populated cities. The state of the art in this field reveals that a growing number of geometries are applied in practice, while appropriate planning tools are lacking. This is due to the challenge of sufficiently resolving the heat transport processes in shallow ground to predict the performance of a given geometry. Therefore, further development of models that can reliably simulate the full system, and which are validated by experimental field measurements, is recommended to increase accuracy, reliability, safety and efficiency of the GSHPs (Hou et al., 2022; Rashid et al., 2023). This motivates the following investigations.

This chapter focuses on three-dimensional analytical modelling of plate-shaped heat exchangers installed vertically in trenches. Recent field applications of these technological variants are reported for instance by Suft and Bertermann (2022) and Oh and Beckers (2023). Analytical models in particular are appealing due to their computational efficiency and compactness in comparison to numerical implementations. This has been demonstrated for example for the simulation of related geothermal devices such as slinky coils implemented as very shallow horizontal heat exchangers in vertical arrangement by Xiong et al. (2015) and in horizontal orientation by Larwa et al. (2019). Another related variant of growing interest is the vertical energy wall, with numerical simulation concepts presented by Kürten et al. (2015) and Gerola et al. (2023). For the selected vertical trench geometry in our work, so far only a two-dimensional, analytical model is available (Ciriello et al., 2015b). Aside from this, Bortoloni and Bottarelli (2015) used an analytical solution based on the line source method, which is assumed to be an equivalent slinky-coil having the same heat transfer surface per trench length. Compared with their two-dimensional numerical model, they achieve promising results for the minimum design temperature. Further related work deals with numerical simulations or experimental measurements for feasibility studies, the comparison of planar heat exchangers with other geometries and performance analysis (Amadeh et al., 2020; Bottarelli, 2013; Bottarelli et al., 2014; Bottarelli et al., 2019; Bottarelli and Di Federico, 2012; Cao et al., 2018; Ciriello et al., 2015b; Ciriello et al., 2015a; Gabrielli and Bottarelli, 2016; Habibi et al., 2020; Schwarz et al., 2022; Zhou et al., 2021). For example, Habibi et al. (2020) revealed by numerical simulation the benefits of planar vertical collectors in comparison to linear heat exchangers. However, to the best of our knowledge, no analytical three-dimensional model that accurately describes a plate-shaped trench collector has been developed by this time. Thus, our objective is to close this gap. A new analytical model of planar ground heat collectors installed vertically in trenches for heat conduction in the subsurface is presented and validated with numerical simulations and experimental data.

3.3 Models and methods

3.3.1 Analytical model

3.3.1.1 Finite plane source

Heat conduction in the subsurface influenced by a planar trench collector is mathematically best represented by a FPS with an isothermal boundary condition (Fig. 3-1). Analogous to the popular finite line source used for the thermal design of borehole heat exchangers (Cimmino, 2018; Fascì et al., 2021; Rivera et al., 2015a), the FPS is deduced from the three-dimensional, transient heat conduction equation:

$$\frac{\partial T}{\partial t} = \alpha \left(\frac{\partial^2 T}{\partial x^2} + \frac{\partial^2 T}{\partial y^2} + \frac{\partial^2 T}{\partial z^2} \right) \tag{3-1}$$

in which t is time in s, $T(x, y, z, t)$ is temperature in K (or °C) and α is the thermal diffusivity in m²/s. A planar heat source of strength $\dot{q}$ in W/m² is applied at $y = 0$ (see Fig. 3-1). It has a constant value W within the dimensions of the vertical planar trench collector, i.e. L_c in m in x-direction and H_c in m in z-direction (see Fig. 3-1), and is zero outside:

$$\dot{q}(x, y, z, t) = \begin{cases} W \; for \; 0 \leq x \leq L_\mathrm{c} \wedge y = 0 \wedge H_\mathrm{inst} \leq z \leq (H_\mathrm{inst} + H_\mathrm{c}) \\ 0 \end{cases} \tag{3-2}$$

Furthermore, the boundary condition at infinity, at the ground surface, and the initial condition are given in Eqs. (3-3) and (3-4), respectively:

$$T|_{|x|\to\infty} = T|_{|y|\to\infty} = T|_{z\to\infty} = T|_{z=0} = 0 \tag{3-3}$$

$$T|_{t=0} = 0 \tag{3-4}$$

Taking the instantaneous point source as a fundamental solution of potential theory (Carslaw and Jaeger, 1959), it can be used to solve the above-described problem for heat conduction. For this, the instantaneous point source has to be integrated over time from 0 to t to obtain the continuous point source at x', y', z' in an infinite solid (Carslaw and Jaeger, 1959). Its solution is given as:

$$T(x, y, z, t) = \frac{\dot{Q}}{4\pi\lambda} \frac{\operatorname{erfc}\left(\frac{\sqrt{(x-x')^2 + (y-y')^2 + (z-z')^2}}{2\sqrt{\alpha t}} \right)}{\sqrt{(x-x')^2 + (y-y')^2 + (z-z')^2}} \tag{3-5}$$

where the temperature T at the location (x, y, z) is considered to be the solution of a point source if heat is liberated at the rate $\dot{Q}$ (in W) per unit time from $t = 0$ to $t = t$. Here x, y, z are the evaluation points, whereas x', y', z' define the location of the heat source. Furthermore, λ is the thermal conductivity in W/(m·K).

Next, the continuous point source solution must be integrated to the required dimensions of the collector under consideration, to gain the solution of the FPS in an infinite solid. With a collector of length L_c and height H_c, i.e. the plane source is located at $\{(0 \leq x' \leq L_\mathrm{c}), (y' = 0), (0 \leq z' \leq H_\mathrm{c})\}$ (see Fig. 3-1), the integral formulation reads as:

$$T(x, y, z, t) = \frac{\dot{q}}{4\pi\lambda} \int_0^{L_\mathrm{c}} \int_0^{H_\mathrm{c}} \frac{\operatorname{erfc}\left(\frac{\sqrt{(x-x')^2 + (y-y')^2 + (z-z')^2}}{2\sqrt{\alpha t}} \right)}{\sqrt{(x-x')^2 + (y-y')^2 + (z-z')^2}} \, dz' dx' \tag{3-6}$$

Finally, the method of image is used to create the solution within a semi-infinite solid with an isothermal boundary condition at $z = 0$, which represents the ground surface as depicted in

Fig. 3-1. The general solution of the FPS with an isothermal boundary condition at the surface, T_{FPS}, reads:

$$T_{\mathrm{FPS}}(x,y,z,t) = \frac{\dot{q}}{4\pi\lambda}\int_0^{L_\mathrm{c}}\int_{H_\mathrm{inst}}^{H_\mathrm{inst}+H_\mathrm{c}}\left(\frac{\operatorname{erfc}\left(\frac{\sqrt{(x-x')^2+(y-y')^2+(z-z')^2}}{2\sqrt{\alpha t}}\right)}{\sqrt{(x-x')^2+(y-y')^2+(z-z')^2}} - \frac{\operatorname{erfc}\left(\frac{\sqrt{(x-x')^2+(y-y')^2+(z+z')^2}}{2\sqrt{\alpha t}}\right)}{\sqrt{(x-x')^2+(y-y')^2+(z+z')^2}}\right) dz'dx' \tag{3-7}$$

where H_inst is the installation depth of the trench collector in m, i.e. the distance between the ground surface and the upper edge of the GHC. Eq. (3-7) is the solution of Eq. (3-1) for the homogeneous boundary condition at $z = 0$ and allows the determination of the temperature at any point x, y, z around the planar collector apart from the location of the source for times $t > 0$. For design purposes, however, the mean temperature at the wall of the trench collector $\bar{T}_\mathrm{cw}\left(\frac{d_\mathrm{c}}{2}, t\right)$ is to be considered and can be calculated by Eq. (3-8) for $y = \frac{d_\mathrm{c}}{2}$. d_c is the thickness of the GHC in m, which in this specific case is 6 mm (see Fig. 3-4). Since the source itself has no width, it is centred so that an evaluation at the collector wall corresponds to $y = \frac{d_\mathrm{c}}{2}$ or $y = \frac{-d_\mathrm{c}}{2}$. In this case, it is sufficient to consider only one side of the collector wall, as the heat transfer is symmetrical.

$$\bar{T}_{\mathrm{FPS}}(y,t) = \frac{\dot{q}}{4\pi\lambda L_\mathrm{c} H_\mathrm{c}} \int_0^{L_c}\int_{H_\mathrm{inst}}^{H_\mathrm{inst}+H_\mathrm{c}}\int_0^{L_\mathrm{c}}\int_{H_\mathrm{inst}}^{H_\mathrm{inst}+H_\mathrm{c}}\left(\frac{\operatorname{erfc}\left(\frac{\sqrt{(x-x')^2+(y-y')^2+(z-z')^2}}{2\sqrt{\alpha t}}\right)}{\sqrt{(x-x')^2+(y-y')^2+(z-z')^2}} - \frac{\operatorname{erfc}\left(\frac{\sqrt{(x-x')^2+(y-y')^2+(z+z')^2}}{2\sqrt{\alpha t}}\right)}{\sqrt{(x-x')^2+(y-y')^2+(z+z')^2}}\right) dz'dx'dz\ dx \tag{3-8}$$

By simplifying the quadruple integral in Eq. (3-8) to a sum of only double and single integrals, the formula becomes more manageable. The reduction of the multiple integrals in Eq. (3-8) leads to the long but computationally optimised Eq. (A I) contained in the appendix. Evaluating Eq. (3-8) at $y = \frac{d_\mathrm{c}}{2}$ results in the mean collector wall temperature $\bar{T}_\mathrm{cw}$.

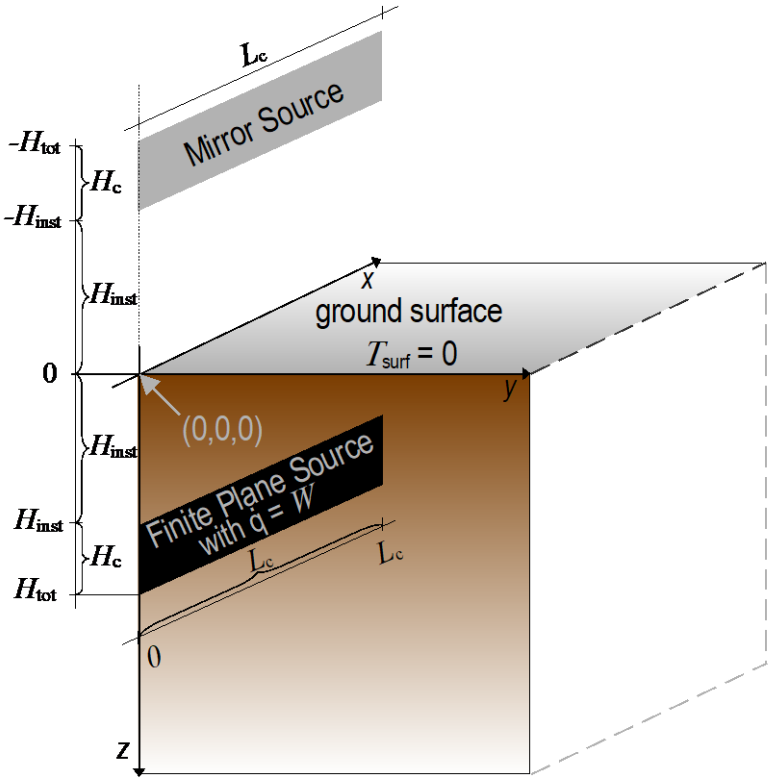

Fig. 3-1: Geometrical settings for the finite plane source in a semi-infinite solid with an isothermal boundary to simulate a vertical trench collector.

3.3.1.2 Dimensional analysis

The dimensional analysis of the given heat conduction problem allows, analogous to the common *g*-functions of borehole heat exchangers (Cimmino, 2018; Eskilson, 1987; Miocic et al., 2024; Rivera et al., 2017), the development of dimensionless response functions at the collector wall. The use of these functions enables a broad range of application of a certain solution independent of case-specific geometrical and thermal properties. The total height from the ground surface down to the bottom of the ground heat collector H_{tot} in m (see Fig. 3-1) is used for non-dimensionalisation of all geometry parameters and is calculated as follows:

$$H_{\mathrm{tot}} = H_{\mathrm{inst}} + H_{\mathrm{c}} \tag{3-9}$$

This height is chosen for the non-dimensionalisation since it comprises two relevant geometrical parameters influencing the dimensionless temperature response, i.e. the installation depth H_{inst} and the collector height H_{c}. These heights are governing parameters for the heat transfer between the collector and the ground surface; whereas the influence of the collector length L_{c} is less pronounced, because typically L_{c} is larger than the heights. Particularly with very long collectors or several collectors in a row, the influence of L_{c} becomes increasingly less relevant, approaching a two-dimensional situation which would result in values of the non-dimensional coordinates towards zero if L_{c} was used for non-dimensionalisation.

Then, the following dimensionless variables are used in the dimensional analysis:

$$x^* = \frac{x}{H_{\mathrm{tot}}} \qquad y^* = \frac{y}{H_{\mathrm{tot}}} = \frac{d_c}{2H_{\mathrm{tot}}} \qquad z^* = \frac{z}{H_{\mathrm{tot}}} \tag{3-10}$$

$$x'^* = \frac{x'}{H_{\mathrm{tot}}} \qquad y'^* = \frac{y'}{H_{\mathrm{tot}}} = 0 \qquad z'^* = \frac{z'}{H_{\mathrm{tot}}} \tag{3-11}$$

$$Fo_{H_{\mathrm{tot}}} = \frac{\alpha t}{{H_{\mathrm{tot}}}^2} \tag{3-12}$$

$$\theta\left(Fo_{H_{\mathrm{tot}}}\right) = \Delta T(t)\ \frac{\lambda}{\dot{q} H_{\mathrm{tot}}} \tag{3-13}$$

where the dimensionless coordinates $x^*, y^*, z^*, x'^*, y'^*, z'^*$ are marked by a superscript asterisk, $Fo_{H_{\mathrm{tot}}}$ corresponds to the dimensionless time and $\theta\left(Fo_{H_{\mathrm{tot}}}\right)$ is the dimensionless temperature response of the ground heat collector.

Hence, the dimensionless form of Eq. (3-1) is defined as:

$$\frac{\dot{q} H_{\mathrm{tot}}}{\lambda}\ \frac{\alpha}{{H_{\mathrm{tot}}}^2}\ \frac{\partial \theta}{\partial Fo_{H_{\mathrm{tot}}}} = \frac{\dot{q} H_{\mathrm{tot}}}{\lambda}\ \frac{1}{{H_{\mathrm{tot}}}^2}\ \alpha\left(\frac{\partial^2 \theta}{\partial {x^*}^2} + \frac{\partial^2 \theta}{\partial {y^*}^2} + \frac{\partial^2 \theta}{\partial {z^*}^2}\right) \tag{3-14}$$

$$\frac{\partial \theta}{\partial Fo_{H_{\mathrm{tot}}}} = \left(\frac{\partial^2 \theta}{\partial {x^*}^2} + \frac{\partial^2 \theta}{\partial {y^*}^2} + \frac{\partial^2 \theta}{\partial {z^*}^2}\right) \tag{3-15}$$

Thus, it can be deduced that the dimensionless temperature response resulting from the FPS for one trench collector depends on the Fourier number, the dimensionless time, Eq. (3-12) and the following dimensionless geometrical parameters:

$$\frac{L_{\mathrm{c}}}{H_{\mathrm{tot}}} \tag{3-16}$$

$$\frac{H_{\mathrm{inst}}}{H_{\mathrm{tot}}} \tag{3-17}$$

$$\frac{d_{\mathrm{c}}}{2H_{\mathrm{tot}}} \tag{3-18}$$

Using Eq. (3-8) and the dimensional analysis, the mean dimensionless temperature response at the collector wall of the continuous FPS solution with an isothermal boundary condition at the ground surface is derived:

$$\bar{\theta}\left(Fo_{H_{\mathrm{tot}}}, \frac{d_{\mathrm{c}}}{2H_{\mathrm{tot}}}, x^*, z^*, x'^*, z'^*\right) = \frac{H_{\mathrm{tot}}}{4\pi \frac{L_{\mathrm{c}}}{H_{\mathrm{tot}}}\left(1 - \frac{H_{\mathrm{inst}}}{H_{\mathrm{tot}}}\right)} \tag{3-19}$$

$$\int_0^{\frac{L_{\mathrm{c}}}{H_{\mathrm{tot}}}} \int_{\frac{H_{\mathrm{inst}}}{H_{\mathrm{tot}}}}^{1} \int_0^{\frac{L_{\mathrm{c}}}{H_{\mathrm{tot}}}} \int_{\frac{H_{\mathrm{inst}}}{H_{\mathrm{tot}}}}^{1} \left(\frac{\operatorname{erfc}\left(\frac{\sqrt{\left(x^* - x'^*\right)^2 + \left(\frac{d_{\mathrm{c}}}{2H_{\mathrm{tot}}}\right)^2 + \left(z^* - z'^*\right)^2}}{2\sqrt{Fo_{H_{\mathrm{tot}}}}} \right)}{\sqrt{\left(x^* - x'^*\right)^2 + \left(\frac{d_{\mathrm{c}}}{2H_{\mathrm{tot}}}\right)^2 + \left(z^* - z'^*\right)^2}} - \frac{\operatorname{erfc}\left(\frac{\sqrt{\left(x^* - x'^*\right)^2 + \left(\frac{d_{\mathrm{c}}}{2H_{\mathrm{tot}}}\right)^2 + \left(z^* + z'^*\right)^2}}{2\sqrt{Fo_{H_{\mathrm{tot}}}}} \right)}{\sqrt{\left(x^* - x'^*\right)^2 + \left(\frac{d_{\mathrm{c}}}{2H_{\mathrm{tot}}}\right)^2 + \left(z^* + z'^*\right)^2}} \right) dz'^* dx'^* dz^* dx^*$$

An exemplary curve of the dimensionless temperature response for an experimental plant (described in detail in Chapter 3.3.3) is shown in Fig. 3-2.

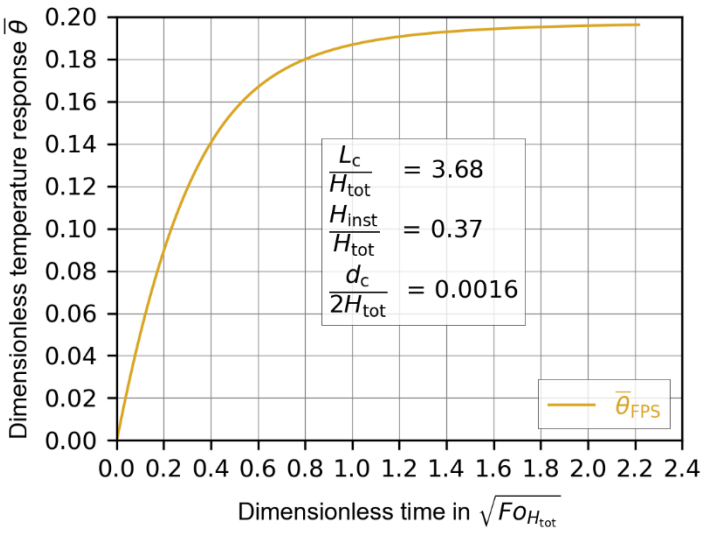

Fig. 3-2: Mean dimensionless temperature response of the FPS with a heat injection rate at the source and a source geometry corresponding to the one of the experimental plant at the Biberach University of Applied Sciences (see technical details given in Chapter 3.3.3).

3.3.1.3 Seasonal temperature variation

Generally, GHCs are installed at a depth of 1 to 1.5 m below the ground surface (Koenigsdorff, 2011) and can affect the subsurface at a depth down to 5 to 10 m. Therefore, the annual temperature oscillation at the ground surface and its impact at the installation depth have to be considered. Since the temperature in these depths varies within a broad range, Kusuda

and Achenbach (1965) proposed Eq. (3-20) to calculate the seasonal varying ground temperature $T_{\mathrm{undist\,sub}}(z,t)$ depending on its depth *z* in m:

$$T_{\mathrm{undist\,sub}}(z,t) = \bar{T}_{\mathrm{a}} - \Delta T_{\mathrm{am}}\ \mathrm{e}^{-z\sqrt{\frac{\pi}{t_{\mathrm{p}}\alpha}}}\ \cos\left(\frac{2\,\pi}{t_{\mathrm{p}}}\left[t - t_0 - \frac{z}{2}\sqrt{\frac{t_{\mathrm{p}}}{\pi\alpha}}\right]\right) \tag{3-20}$$

The phase constant t_0 in Eq. (3-20) corresponds to the time of the year in s at which the temperature of the ground surface reaches its minimum. The considered time period t_{p} in s is one year, as after this period the seasonal oscillation restarts. This oscillation with the amplitude ΔT_{am} is subtracted from the annual mean air temperature $\bar{T}_{\mathrm{a}}$. As can be seen in Fig. 3-3, the seasonal temperature at a specific time of the year can vary by several degrees over the collector height, e.g., at the end of the second month the undisturbed subsurface temperature varies between 3.6 °C at the installation depth and 6.4 °C at the bottom of the collector, whereas at the end of the fourth month there is barely a temperature difference. Analysing Eq. (3-20), the damping of the ground surface temperature oscillation depends on $-z\sqrt{\frac{\pi}{t_{\mathrm{p}}\alpha}}$, which corresponds to $\sqrt{\frac{\pi}{Fo_z}}$, i.e. the damping includes the dimensionless time Fo_z. Only for values of Fo_z smaller than 0.025 the seasonal oscillation is regarded to be negligible, larger values show a clear influence of the seasonal temperature oscillation. Since the undisturbed subsurface temperature is crucial for both the determination of the minimum temperature and for natural regeneration, and additionally varies within a broad range over the collector height, it is important to average this temperature spatially (over the collector height). The spatial averaging of the seasonal temperature variation of the undisturbed subsurface within the installation depth is carried out over the collector height, starting at the installation depth H_{inst} and reaching down to the collector bottom edge H_{tot}. Eqs. (3-21) and (3-22) specify the average of the seasonal undisturbed temperature over the collector height:

$$\overline{T}_{\text{undist sub}}(t) = \overline{T}_{\text{a}} + \Delta\overline{T}_{\text{undist sub}}(t) \tag{3-21}$$

$$\Delta\overline{T}_{\text{undist sub}}(t) = \frac{-\Delta T_{\text{am}}}{2\,H_{\text{c}}\sqrt{\frac{\pi}{t_{\text{p}}\,\alpha}}} \left\{ \begin{aligned} & \mathrm{e}^{-H_{\text{inst}}\sqrt{\frac{\pi}{t_{\text{p}}\alpha}}} \left[\sin\left(\frac{2\pi}{t_{\text{p}}}(t-t_0) - H_{\text{inst}}\sqrt{\frac{\pi}{t_{\text{p}}\alpha}}\right) \right. \\ & \left. + \cos\left(\frac{2\pi}{t_{\text{p}}}(t-t_0) - H_{\text{inst}}\sqrt{\frac{\pi}{t_{\text{p}}\alpha}}\right) \right] \\ & -\mathrm{e}^{-H_{\text{tot}}\sqrt{\frac{\pi}{t_{\text{p}}\alpha}}} \left[\sin\left(\frac{2\pi}{t_{\text{p}}}(t-t_0) - H_{\text{tot}}\sqrt{\frac{\pi}{t_{\text{p}}\alpha}}\right) \right. \\ & \left. + \cos\left(\frac{2\pi}{t_{\text{p}}}(t-t_0) - H_{\text{tot}}\sqrt{\frac{\pi}{t_{\text{p}}\alpha}}\right) \right] \end{aligned} \right\} \tag{3-22}$$

here $\overline{T}_{\text{undist sub}}(t)$ is the spatial mean undisturbed subsurface temperature in °C over the installation depth of the trench collector and $\Delta\overline{T}_{\text{undist sub}}(t)$ is the spatial average (over the installation depth) of the temperature change of the seasonal oscillation. Eq. (3-20) is a quasi-stationary solution of Eq. (3-1) for the inhomogeneous temperature boundary condition which corresponds to Eq. (3-20) for $z = 0$.

For a trench collector buried at a depth of 1.2 m, a collector height of 1.2 m and the properties listed in Table 3-1, the seasonal temperature variations in the collector depth and its mean temperature variation are depicted in Fig. 3-3.

Table 3-1: Parameters used to calculate undisturbed subsurface temperatures.

Parameter description	**Value**	**Unit**
Annual mean air temperature $\overline{T}_{\text{a}}$	10	°C
Annual amplitude of the mean ground surface temperature ΔT_{am}	10	K
Phase constant t_0	840	h
Period t_{p}	8760	h
Thermal diffusivity of the subsurface α	0.002477064	m²/h

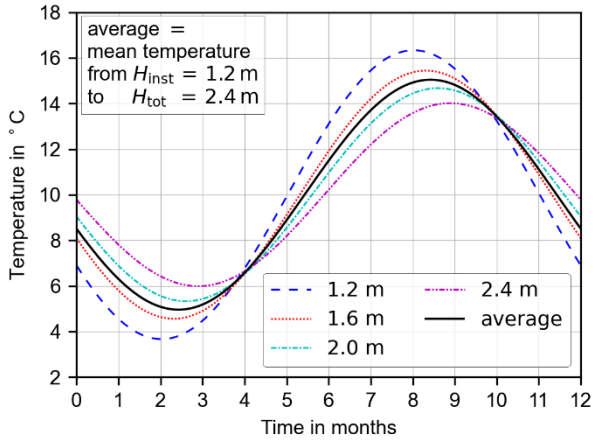

Fig. 3-3: Seasonal temperature variations of the subsurface at various depths over the collector height and its mean value for the parameters defined in Table 3-1.

3.3.1.4 Ground heat exchanger resistance

Analogous to referring to the thermal resistance R_b of borehole heat exchangers (Eskilson, 1987; Hellström, 1991; Lamarche, 2021; Ozudogru et al., 2014; Wagner et al., 2013; Yoon et al., 2014) the heat transfer through the GHC itself is modelled with a so-called collector resistance, R_c (Van de Ven et al., 2018). All thermal resistances in this chapter have the unit m²·K/W. A cross-section of the collector geometry, a twin-wall sheet, is depicted in Fig. 3-4. Fig. 3-4 b shows the analytical resistance model for one collector element (one fluid channel with corresponding plate section), which consists of a convective resistance R_h between fluid and collector material and a conductive resistance R_{pp} through the polypropylene. These resistances are connected in series. The convective resistance R_h can be defined analytically, whereas the conductive resistance R_{pp} is defined by numerical simulations and both are combined by an analytical resistance model. The entire model is based on assumptions which are described below. The first assumption is a uniform flow through each element of the trench collector, which means that the heat carrier fluid temperature in each channel is uniform as well. Thus, the interaction between the channels is considered negligible, i.e. the interaction resistance R_{ia} may be omitted. As a consequence, adiabatic boundary conditions between the collector elements as depicted in Fig. 3-4 a allow a parallel connection of all element resistances ${}^1R_c$ except for the five elements each at the top and at the bottom of the trench collector. These are excluded since no flow occurs through these channels for safety reasons and are thus treated as inactive. Accordingly, in the model, the sixth element both from the top and the bottom has only one adiabatic boundary towards the neighbouring active element. This means that two kinds of conductive resistances R_{pp} must be considered, and as a consequence two numerical simulations must be carried out for the different collector elements: one for the centre element with two adiabatic boundary conditions, and one for a corner element which has one adiabatic boundary condition and borders on five

non-flow-through elements on the other side. Furthermore, the boundary condition towards the subsurface is set to have a constant temperature, whereas the collector interior boundary of the active elements is simulated with a Robin boundary condition. The collector consists of 199 elements, 189 of which are active and 187 of which correspond to the resistance model in Fig. 3-4 b.

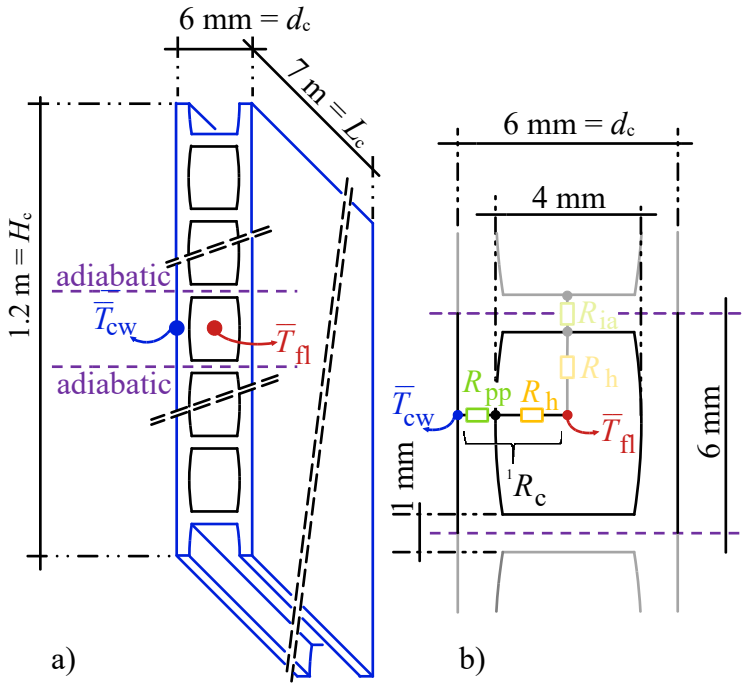

Fig. 3-4: a) Geometry and cross-section of the trench collector in a three-dimensional perspective, and b) the analytical resistance model for one channel with two adiabatic boundaries.

The heat transfer coefficient h in W/(m²·K) is the inverse of the convective resistance R_h and is calculated by Eqs. (3-23) and (3-24) for laminar flow in the collector. Due to the small chambers of the collector, only laminar flow will occur within this kind of trench collector. Thus, h can be calculated from Schramek et al. (2005).

$$h = \frac{Nu\lambda_{fl}}{D_{hydr}} \tag{3-23}$$

with

$$Nu = \left[49.028 + 4.173\, RePr\, \frac{D_{hydr}}{L_c}\right]^{0.333} \quad for\ Re < 2320 \tag{3-24}$$

where Nu is the dimensionless Nusselt number, characterising the convective heat transfer, D_{hydr} the representative dimension in m, which in this specific case is the hydraulic diameter of the collector channel, and λ_{fl} is the thermal conductivity of the fluid in W/(m·K). In order to calculate the Nusselt number Nu, the Prandtl number Pr is needed. Furthermore, it hast to be checked if the condition for the Reynolds number Re is fulfilled. Considering material properties

of a mixture of water and ethylene glycol with 25% glycol for the fluid and a nominal volume flow rate of 6 l/min through the entire collector, the heat transfer coefficient h reaches a value of 368.46 W/(m²·K) at a fluid temperature of 0 °C. In order to determine the collector resistance, the results of the numerical simulations from Van de Ven et al. (2018) are used, resulting in a temperature-specific heat flux density of 246.58 W/(m²·K) and 41.17 W/(m²·K), for each middle element and each edge element, respectively. With these results and the installation area serving as a reference surface, the overall collector resistance R_c is 0.00429 (m²·K)/W. Using the collector resistance R_c and the heat extraction or injection rate $\dot{q}$, the temperature change due the trench collector resistance, ΔT_{R_c}, is calculated as:

$$\Delta T_{R_\mathrm{c}} = \dot{q} R_\mathrm{c} \tag{3-25}$$

3.3.1.5 Analytical algorithm for ground thermal conditions around a planar trench collector

The major benefit of the analytical model presented here is the fast calculation of the collector outlet temperature. The collector outlet temperature is often the main limitation in the design of such systems due to operational safety or to avoid environmental damage (Ramming, 2007; Verein Deutscher Ingenieure e. V., 2019). The prerequisite for its calculation is that the heat extraction rate $\dot{q}$, the temperature spread over the collector $\Delta T_\mathrm{sp}(t)$ (difference between fluid inlet and outlet temperature), the thermal subsurface properties, and the collector geometry are known. The heat transfer in the subsurface due to the planar trench collector including the undisturbed seasonal temperature oscillation is decomposed into a homogeneous and an inhomogeneous boundary value problem. In this case, the FPS (Eq. (3-7)) is the solution of the homogeneous boundary value problem, while the seasonal temperature oscillation (Eq. (3-20)) represents the solution of the inhomogeneous boundary value problem (Carslaw and Jaeger, 1959). Therefore, the dimensionless temperature response function $\theta\left(Fo_{H_\mathrm{tot}}, \frac{L_\mathrm{c}}{H_\mathrm{tot}}, \frac{H_\mathrm{inst}}{H_\mathrm{tot}}, \frac{d_\mathrm{c}}{2H_\mathrm{tot}}\right)$ with the corresponding dimensionless parameters can be selected. Now the temperatures from Chapter 3.3.1.1 and 3.3.1.3 can be calculated and superposed to determine the mean collector wall temperature $\overline{T}_\mathrm{cw}(t)$. Thereupon, the temperature change due to the collector resistance as described in Chapter 3.3.1.4 can be applied, so that finally the collector outlet temperature $T_\mathrm{c,fl,o}$ is determined as in the following equations:

$$\bar{T}_{\mathrm{c,fl}}(t) = \bar{T}_{\mathrm{undist\,sub}}(t) + \bar{T}_{\mathrm{cw}}(t) + \Delta T_{R_{\mathrm{c}}}(t) \tag{3-26}$$

$$T_{\mathrm{c,fl,o}} = \bar{T}_{\mathrm{c,fl}}(t) + \frac{\Delta T_{\mathrm{sp}}(t)}{2} \tag{3-27}$$

The collector outlet temperature $T_{\mathrm{c,fl,o}}$ has to be determined in the design phase, since this temperature is limited, e.g., in the VDI-guideline in Germany (Verein Deutscher Ingenieure e. V., 2019).

3.3.2 Numerical model

The numerical model serves as a reference for the verification of the analytical model. The basic model is set up in COMSOL Multiphysics using the Heat Transfer in Porous Media module. Since the FPS model simulates heat conduction only in the subsurface, the numerical model does not consider the detailed geometry of the planar trench collector but focuses on the relevant heat transfer processes in the surrounding ground. Therefore, the collector is represented as a planar heat sink/source installed at a depth of 1.2 m below the surface. The seasonal temperature fluctuations at the ground surface are represented using Eq. (3-20) for the time-dependent temperature variation at the surface by setting z = 0 m. The initial temperature distribution of the simulation domain due to the seasonal fluctuations is also calculated by Eq. (3-20) using t = 0 s as a starting point in time. The domain was defined empirically by varying its size, while both the temperature at the collector wall and the dimensionless temperature were monitored for different boundary conditions. Furthermore, the calculation speed is optimised by quartering the simulation domain and using symmetry boundary conditions. As a result of the domain reduction due to symmetry, the heat injection rate specified in COMSOL is halved compared to the analytical model to ensure consistency of both models. In addition to the domain reduction, infinite regions at the border of the domain allow a reduction of the simulation domain whilst avoiding their boundary influence at the collector surface. The grid of the numerical model consists mainly of a free-tetrahedral mesh extended by a structured mesh in the infinite regions. At the collector surface, the grid is extremely fine and becomes coarser towards the edge.

3.3.3 Experimental plant

To validate practical suitability, the proposed analytical model is compared with measurement data of an experimental plant. The experimental plant is located at the Biberach University of Applied Sciences in Biberach (Riß) in southern Germany. The collector is 7 m long, 1.2 m high, 6 mm thick and installed in a trench at a depth of 70 cm below the ground surface. The collector consists of 199 polypropylene channels as depicted in Fig. 3-4. A more detailed description of the ground heat collector plant and the installed measuring equipment can be found in Van de Ven et al. (2025). In addition to the trench collector and measurement equipment system

described in Van de Ven et al. (2025), the thermal response test (TRT) device of the Biberach University of Applied Sciences shown Fig. 3-5 b is used to increase the inlet temperature in the trench collector while assuring a constant heat transfer rate. Further details on the trench collector itself can be found in planning and operating instructions (MEFA Befestigungs- und Montagesysteme GmbH, 2022).

Fig. 3-5: a) Trench collector and measurement equipment during installation, b) thermal response test device attached to the trench collector plant at the experimental site.

For the validation of the FPS model with measurement data from the experimental plant, the dimensionless temperature response of the FPS model with the dimensionless parameter values matching the ones of the experimental plant is used. The site-specific values are as follows:

$$\frac{L_\mathrm{c}}{H_\mathrm{tot}} = 3.68 \quad ; \quad \frac{H_\mathrm{inst}}{H_\mathrm{tot}} = 0.37 \quad ; \quad \frac{d_\mathrm{c}}{2H_\mathrm{tot}} = 0.0016 \tag{3-28}$$

Fig. 3-2 shows the corresponding mean dimensionless temperature response for the installed trench collector.

3.4 Results and discussion

3.4.1 Verification of the analytical model

For the mathematical verification of the analytical model equations derived here, a period of one year is analysed, as GHCs should be regenerated within one year to ensure the same output in the following year. Note that the collector and subsurface properties for the theoretical investigations in this chapter correspond to recommended installation conditions. Thus, parameter settings for verification as listed in Table 3-2 are hypothetical and vary from the ones of the experimental plant that is subject to the following chapter.

Table 3-2: Collector and subsurface properties for the comparison of the analytical and the numerical model.

Collector properties				**Subsurface properties**			
Collector length	L_c	7	m	Thermal conductivity of the solid	λ_s	1.5	W/(m·K)
Collector height	H_c	1.2	m	Porosity	ϕ	0.2	
Collector thickness	d_c	0.006	m	Density of the solid matrix	ρ_s	2180	kg/m³
Installation depth	H_inst	1.2	m	Specific heat capacity of the solid matrix	$c_{p,s}$	1000	J/(kg·K)
Heat load	$\dot{Q}$	−200	W	Thermal conductivity of the groundwater	λ_w	0.58	W/(m·K)
Seasonal temperature oscillation				Density of the groundwater	ρ_w	1000	kg/m³
Period	t_p	8760	h	Specific heat capacity of the groundwater	$c_{p,\mathrm{w}}$	4200	J/(kg·K)
Phase constant	t_0	840	h				
Annual amplitude of the surface temperature	ΔT_am	10	K	Annual mean air temperature	$\bar{T}_\mathrm{a}$	10	°C

The verification is carried out systematically. First, a constant heat extraction rate and a constant temperature at the ground surface as in Eq. (3-8) is investigated followed by the model for the mean seasonal temperature variation in the installation depth as in Eqs. (3-21) and (3-22). After that, the combination of both models, i.e. the superposing of the temperature change in Eqs. (3-8), (3-21) and (3-22), is investigated and compared with the corresponding numerical model. Finally, a simulation is carried out considering a six-month collector operation followed by six months of regeneration while including the seasonal temperature variation.

If only the FPS model is compared with the numerical simulation, it can be seen in Fig. 3-6 and Fig. 3-7 that both models agree very well. The absolute temperature deviation is less than 0.04 K, and the percentage deviation is less than 0.5% and can therefore be neglected.

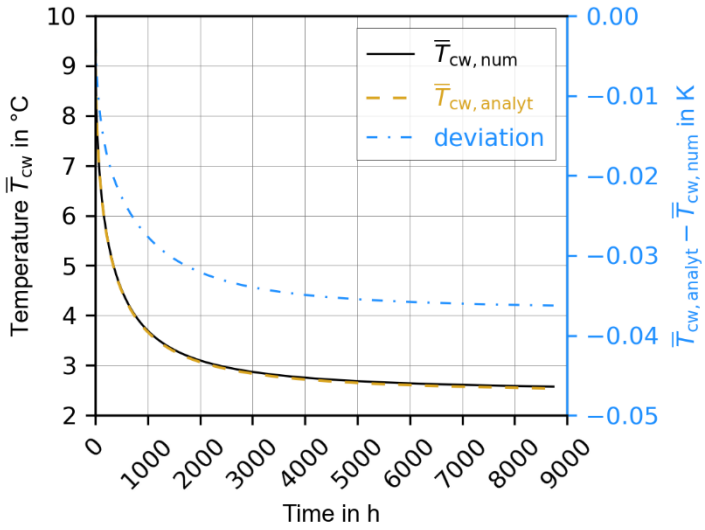

Fig. 3-6: Comparison of the temperature of the analytical and numerical model for a constant heat extraction rate and a constant temperature at the ground surface.

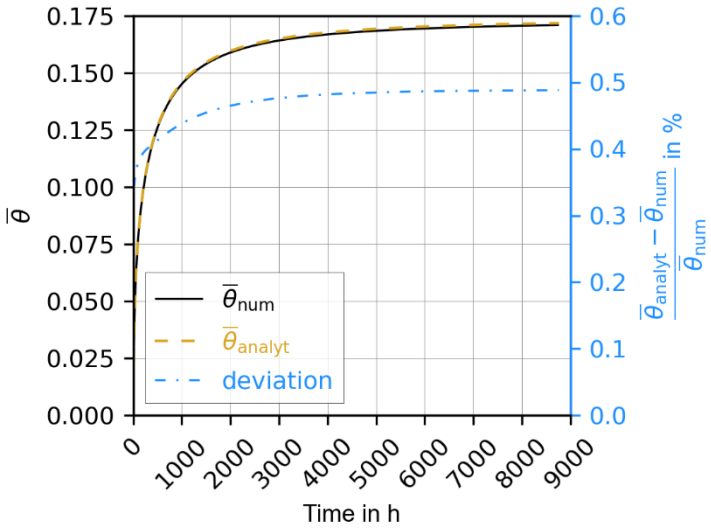

Fig. 3-7: Comparison of the dimensionless temperature response of the analytical and numerical model for a constant heat extraction rate and a constant temperature at the ground surface.

The spatial integral mean of the undisturbed subsurface temperature in the installation depth of the trench collector for both the numerical simulation and the analytical solution from Eqs. (3-21) and (3-22) are shown in Fig. 3-8. The deviation between both models reaches a maximum of ca. 0.009 K, which is very small and considered negligible.

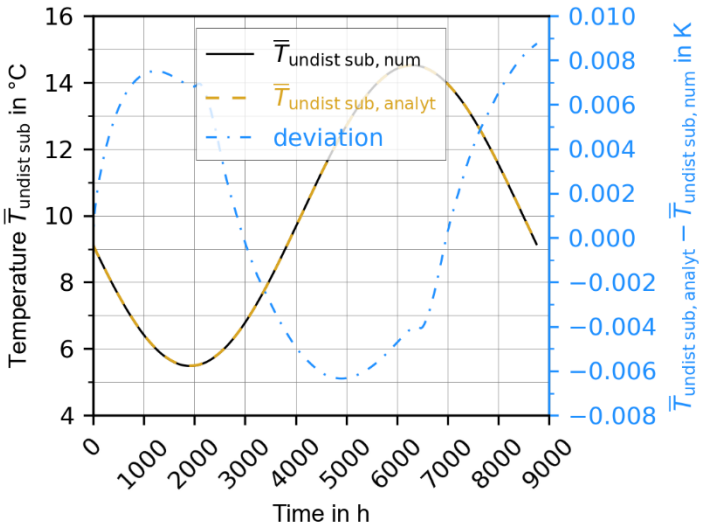

Fig. 3-8: Comparison of the spatial mean seasonal temperature in the installation depth of the analytical and numerical model.

For the combination of the model with constant heat extraction and the seasonal temperature variation in the subsurface, the deviation is higher than in the two individual models, as revealed in Fig. 3-9. However, the maximum deviation is smaller than 0.05 K. This value is so small that it can be considered negligible for practical purposes. This very good agreement proves that by decomposition of the problem in an inhomogeneous and a homogeneous boundary value problem the single solutions can be superposed. If calculation time is considered, the numerical model takes 7 h 48 min. with an Intel Xeon Gold 6230R @ 2.10 GHz processor. In contrast, the analytical model takes less than eight minutes on a standard laptop. The reduction in computing time by a factor of 65 clearly shows the advantage of the analytical model.

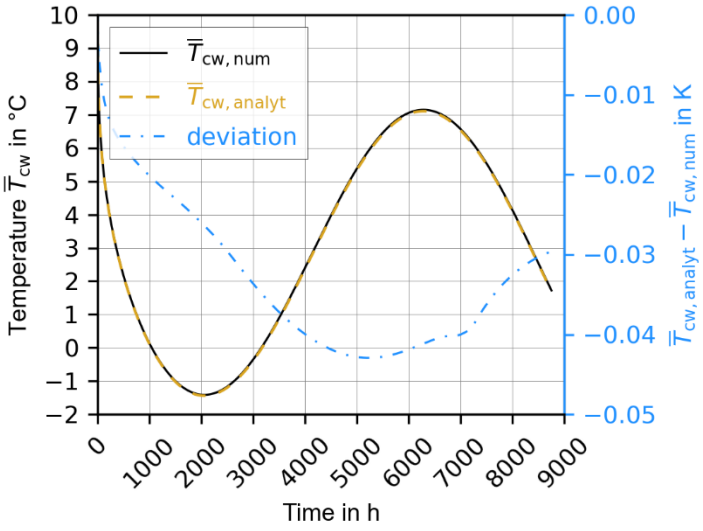

Fig. 3-9: Comparison of the temperature of the analytical and numerical model for a constant heat extraction rate and a seasonal temperature variation at the ground surface.

Typically, a ground heat collector will extract heat during the winter season, i.e. from November to April in the northern hemisphere. In the cases where no active regeneration is foreseen, the ground heat collector uses natural regeneration during the summer half of the year (from May to October in the northern hemisphere) to be able to ensure the same amount of heat extraction the following year. For representing such conditions, the last verification scenario applies six months of constant heat extraction followed by six months of natural regeneration. Fig. 3-10 shows the results of both the analytical and the numerical model for the afore-described heat extraction profile. A very good match is achieved between both models. The deviation only increases abruptly as the heat extraction stops but decreases again afterwards. Apart from this short switchover time, the deviation is smaller than 0.05 K.

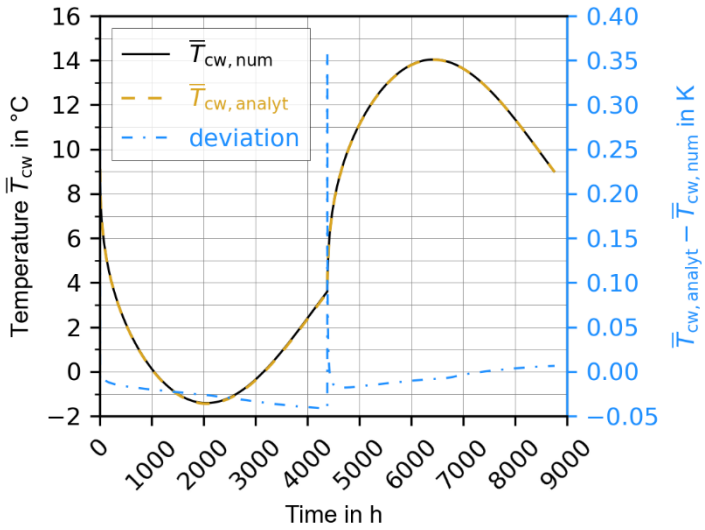

Fig. 3-10: Comparison of the mean temperature at the collector wall of the analytical and numerical model for a constant heat extraction rate over 4380 h and a seasonal temperature variation at the ground surface.

Based on the various model comparisons, it can be stated that the analytical model corresponds very well to the numerical model. After the successful verification, the next step is the validation of the analytical model with measurement data.

3.4.2 Validation of the analytical model

In order to demonstrate the practical applicability of the FPS model, a comparison with measurement data is performed. Three experiments were conducted, in each of which a constant volume flow and heat transfer rate were employed to the trench collector at the field site similar to a standard TRT for borehole heat exchangers (Spitler and Gehlin, 2015). The main parameters of the experiments, the determined undisturbed subsurface temperatures, the estimated thermal conductivities, and collector resistances are listed in Table 3-3 for each experiment. The three experiments are carried out under slightly different conditions. The first experiment was carried out in 2022 with the lowest heat injection rate of 0.88 kW to avoid

excessive overheating of the subsurface, since the undisturbed subsurface temperature was rather high at that time. The two other experiments are conducted in spring 2023 starting with considerably lower undisturbed subsurface temperatures, especially for Experiment 2. This range of possible different initial parameters creates a solid basis for validating the analytical model. The constant heat injection rate and the constant volume flow are induced by the TRT device. For all experiments, first the undisturbed subsurface temperature at the installation depth was determined using the buried PT100 sensors directly next to the collector. Then, a fitting procedure, i.e. the Levenberg-Marquardt algorithm for nonlinear least squares curve-fitting problems, was conducted to estimate the thermal conductivity, λ, and the collector resistance, R_c. To avoid the influence of the starting behaviour, the measurement data within the first hour of heat injection was neglected.

Table 3-3: Experiment descriptions and results.

Description	**Unit**	**Experiment 1**	**Experiment 2**	**Experiment 3**
Date of the experiment	DD.MM.YYY	28.04.2022 – 03.05.2022	28.02.2023 – 6.03.2023	06.04.2023 – 11.04.2023
Heat injection rate $\dot{Q}$	kW	0.88	1.51	1.54
Volume flow $\dot{V}$	m³/h	1.00	0.88	0.88
Mean undisturbed temperature $T_{\mathrm{undist\,sub}}$	°C	8.9	6.2	8.1
Thermal conductivity λ	W/(m·K)	1.47	1.84	1.76
Collector resistance R_c	(m²·K)/W	0.0245	0.0303	0.0233

A comparison of the measurement data and the FPS model is shown in Fig. 3-11, Fig. 3-12 and Fig. 3-13. These figures show a good agreement for all three experiments. However, it is noticeable that the fitted values for the thermal conductivity and the collector resistance vary depending on the experiment. In particular, the range of thermal conductivity values is relatively wide, especially between the first experiment and the last two experiments. One reason for the higher thermal conductivities in the experiments of 2023 may be the fact that there was a relatively high precipitation in 2023 (Deutscher Wetterdienst, 2023). Related studies indicate that the influence of moisture may be significant for the heat conduction of a ground heat exchanger, especially in low-moisture soils (Li et al., 2022).

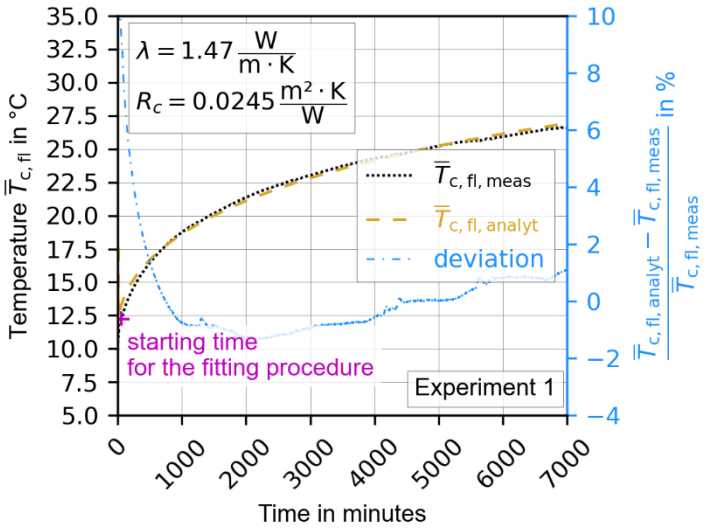

Fig. 3-11: Comparison of the finite plane source and the measurement data of Experiment 1.

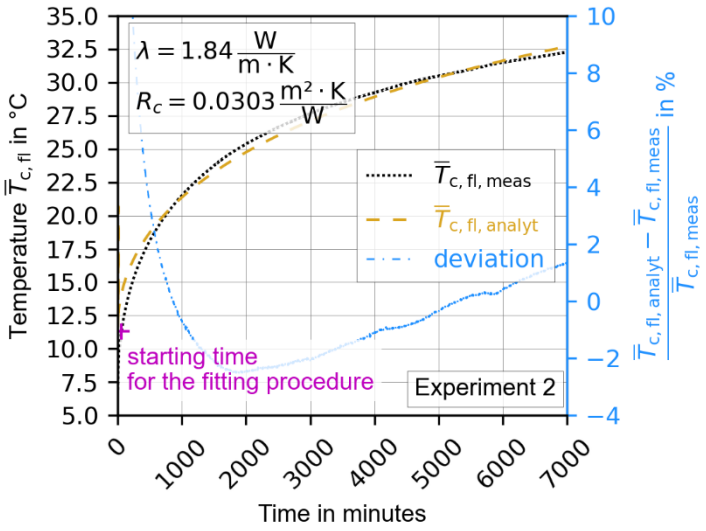

Fig. 3-12: Comparison of the finite plane source and the measurement data of Experiment 2.

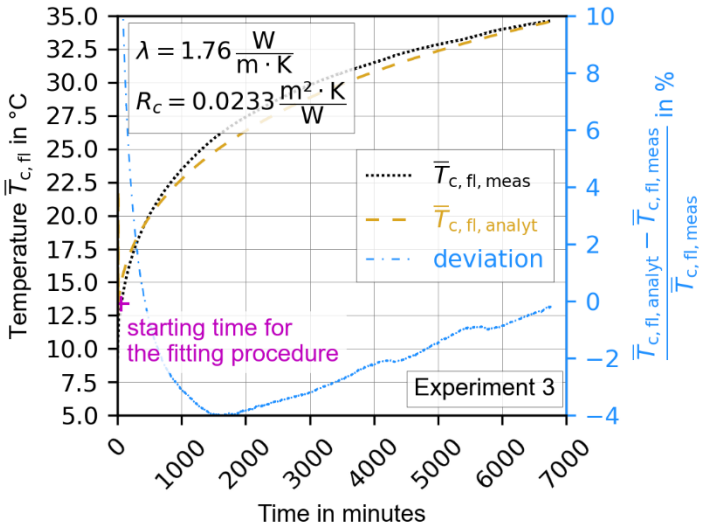

Fig. 3-13: Comparison of the finite plane source and the measurement data of Experiment 3.

To evaluate the quality of the fitting and the resulting parameters for the thermal conductivity and the collector resistance, an exhaustive grid search was carried out for all experiments. The thermal conductivity was evaluated from 0.01 to 5.0 in 0.01 steps and the collector resistance from 0.0001 to 0.1 in 0.0001 steps leading to a total number of about 500,000 value pairs. The root mean square error (RMSE) for each pair of values is determined for all three experiments and visualised in Fig. 3-14 for RMSE-values less than or equal to 1. Physical thermal conductivity measurements of the soil at the site are conducted both in situ and from bucket samples. The in-situ measurements are done with the hot wire method with a needle probe (ISOMET 2104, Applied Precision Ltd., Slovakia), whereas the bucket samples are conducted with the transient plane source method (HotDisk TPS1500, C3 Prozess- und Analysentechnik, Germany). The measurements showed values between 1.3 and 2.0 W/(m·K). As depicted in Fig. 3-14, the smallest deviation to the measurement data lies within this range. The steepness of the RMSE trend in the figures shows that the thermal conductivity is very sensitive and, thus, can be estimated well. The feasible range of the collector resistance, however, is large. In complementary numerical simulations, the collector resistance for the installed collector type is determined to be 0.00429 (m²·K)/W. However, as soon as the contact between the subsurface and the collector is not ideal, the resistance increases substantially. Even with an air gap of only 0.5 mm on both collector sides, the resistance triples. The real value of the collector resistance is likely to be higher than the simulated value due to the assumed ideal contact with the subsurface and the assumption of a uniform flow through the collector in the simulation model. As an upper limit, an air gap of 1.5 mm on both collector sides is added to the simulated resistance value, leading to a collector resistance of 0.03554 (m²·K)/W. Furthermore, it is to be mentioned that the assumed uniform flow in the resistance model does not perfectly apply over the entire collector height in practice. For this reason, a higher collector

resistance is to be expected. In addition, it is possible that, analogous to the findings of Marcotte and Pasquier (2008) for borehole resistances, the collector resistance is overestimated by the curve fitting based on least-squares. As with the thermal conductivity, the collector resistance is also within the expected range due to the non-ideal connection to the subsurface and flow into the collector.

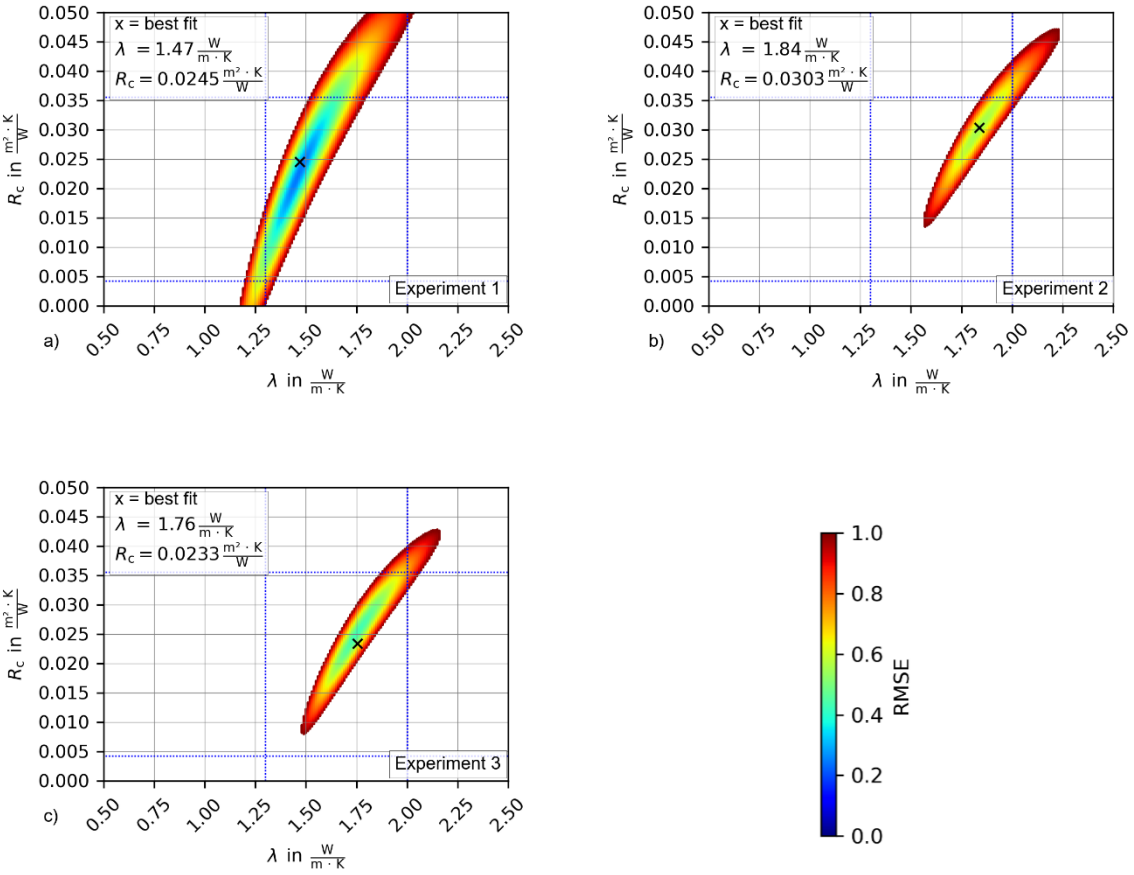

Fig. 3-14: RMSE of the collector resistance and the thermal conductivity pairs for simulation of a) Experiment 1, b) Experiment 2, c) Experiment 3.

3.5 Interim conclusions

This chapter presents a three-dimensional, analytical model for planar ground heat collectors vertically installed in trenches for dimensioning purposes. The model not only considers the correct geometry of the source system but also the seasonal temperature fluctuation in the ground as well as the thermal resistance through the heat exchanger plate and its influence on the fluid temperature in the collector. If the subsurface parameters, the heat extraction or injection rate are known, the mean fluid temperature in the collector can be calculated for the case of pure heat conduction in the ground.

The FPS is used to represent the heat extraction or injection and the heat conduction in the subsurface. A mathematical solution for the quadruple integrals of the FPS is presented

containing only double or single integrals. A dimensional analysis is performed which allows the use of dimensionless temperature responses to cover a wider range of similar geometries. Furthermore, a mathematical solution for the spatially averaged seasonal temperature variation over the installation depth of the collector is presented and the use of a ground heat exchanger resistance is introduced. The calculation algorithm presented uses the superposition principle of all the aforementioned temperature responses in order to determine the mean fluid temperature in the GHC.

The developed novel model was verified with numerical simulations and validated satisfactorily with measured values of an experimental plant. Compared to numerical simulations, which do not even directly calculate the mean fluid temperature, the calculation time of the presented analytical model is 65 times smaller. Characterised by a lower complexity, analytical models in general are easier to handle and therefore more suitable for dimensioning.

These promising results should be further investigated to be able to map load profiles of GHCs through temporal superposition in the analytical model. Finally, it is strongly recommended to extend the analytical model to take the phase change within the subsurface into account since GHCs are characterised by freezing the ground during winter.

4 Analytical simulation of ground freezing and thawing around ground heat collectors

4.1 Chapter overview

Ground heat collectors (GHCs) represent shallow geothermal devices that are buried in the upper metres of the ground with strong thermal coupling to ground surface. Therefore, during seasonal operation, heat extraction in winter can cause temporal freezing of the soil surrounding the collector. The transient latent heat transfer during freezing and thawing can be crucial for the performance of a collector, and it adds complexity to the model-based representation of the devices. Here, a novel analytical model is presented that accounts for these processes and simulates the evolution of thermal ground conditions during operation of different collector variants. It combines heat source-based solutions with thermal power balancing depending on a given collector geometry and temporal superposition for varying heat loads. By comparison with high-resolution numerical model results, the obtained fast analytical predictions represent the thermal regime around horizontal pipe installations and vertical planar trench collectors within seconds very well, achieving temperature deviations of less than 1.4 K and accuracies over 85.6% for predicting of the thickness of the frozen ground. This regime is inspected in particular with respect to collector wall temperature and the maximum horizontal extension of the frozen soil. The findings demonstrate the suitability of the new model framework to be used in the planning and design phase for optimal layout of collectors, as well for straightforward representation of complex freezing and thawing processes during operation.

4.2 Introduction

The need for renewable heating solutions has contributed to a worldwide growth of the heat pump market, particularly of air-source heat pumps (Westring et al., 2024). However, in 2023, there was a notable decline in the overall sales of heat pumps across Europe (Westring et al., 2024). This can be attributed to various factors such as energy price volatility, economic stagnation, political uncertainty, and regulatory challenges (Milagros Garcia Salciarini, 2024). To enhance the attractiveness of especially ground-source heat pumps, given their superior environmental performance compared to air-source systems, it is essential to maximise their operational reliability. One way to contribute to this is by competent design models, which is also the focus of this study. More specifically, a new analytical modelling technique for ground heat collectors is introduced, taking into account freezing and thawing of the adjacent soil. This technique is based on the consistent modelling method defined in Van de Ven et al. (2018) for closed-loop shallow geothermal systems, which allows for the comparison of different source systems without deviations arising from varying modelling philosophies. This method draws on

the established analytical model for borehole heat exchangers (BHEs) of Eskilson (1987), while generalising it for application to other shallow geothermal closed-loop systems. It divides the domain of interest into two parts:

1. The source system (including the installation situation).
2. The surrounding subsurface (including boundary effects at the ground surface).

The source system is modelled by analytical resistance models extended by capacity models, if necessary. Whereas the surrounding subsurface is represented by extensions of the analytical solution of the instantaneous point source, e.g., continuous finite line source, cylinder source, ring source, etc. These source solutions can be extended by approximations if relevant thermal effects are not included in these fundamental solutions of potential theory. Furthermore, varying heat loads are considered by temporal superposition (Van de Ven et al., 2018). This approach ensures that, when comparing different source systems (e.g. borehole heat exchanger, ground heat collector, etc.), the underlying modelling methodology remains consistent, and that differences in performance can be attributed to the system itself rather than to the modelling approach.

GHCs are closed-loop heat exchangers installed in a few metres depth in order to provide thermal energy for a heat pump heating system. Fig. 4-1 illustrates the variety of different shapes of ground heat collectors. In contrast to the more widely used BHEs, GHCs operate at lower temperatures during the heating period (winter) due to their exposure to seasonal temperature variations at the ground surface. Additionally, they interact with a smaller volume of soil compared to BHEs, resulting in lower heat storage capacity. These factors lead to operating temperatures falling below the freezing point for a substantial portion of the heating season. As a result, a significant part of the thermal energy extracted is gained from the latent heat, which is released during freezing of water contained in the soil. Since significant interactions with the ground surface, such as heat transfer from the ambient air, solar radiation, and precipitation, govern the regeneration process, it is essential that such systems are installed beneath unsealed surfaces as long as no active thermal regeneration is applied (Koenigsdorff, 2011). In addition to temperature restrictions, GHCs must also meet the design criterion of ensuring that the frozen soil of adjacent collector pipes or plates do not merge (Verein Deutscher Ingenieure e. V., 2019). The reason for this is to ensure the infiltration of meltwater and rainwater in order to avoid the formation of mud accumulation. By complying with both criteria, excessive uplift and settlement caused by freezing and thawing of the soil is avoided.

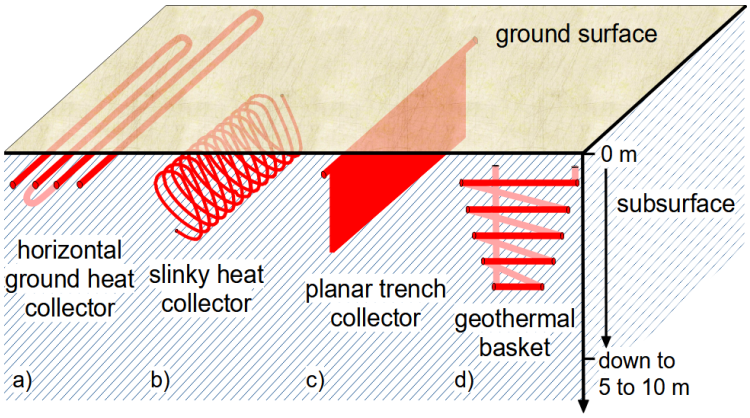

Fig. 4-1: Various types of ground heat collectors, including the two variants (a) and (c), which are the focus of this paper.

The main advantage of analytical models is their computational efficiency, as they are faster and easier to apply than intricate numerical methods. Analytical models typically involve simplifications of the complex reality, such as an average effective thermal conductivity of the soil, or a uniform heat extraction rate over the entire ground-source system (Lamarche, 2023; Stauffer et al., 2017). These simplifications have proven suitable for planning the layout of BHEs, and they have been successfully employed for years in design tools such as EWS (Programm EWS), EED (Earth Energy Designer), and GLHEPro (Ground Loop Heat Exchanger Design Software) (Spitler et al. 2016; Blocon AB 2020; Arthur Huber 2016). In contrast, the operating conditions of ground heat collectors differ from those of the more widespread BHEs, as the latter extend much deeper into the ground, maintaining a relatively constant undisturbed subsurface temperature over the borehole length throughout the year. Furthermore, it is a distinctive feature of ground heat collectors that they induce freezing of the soil immediately surrounding the collector. This aspect is not considered in the analytical models for BHEs as it is irrelevant for their operation.

Within numerical models for geothermal energy systems, freezing and thawing of the soil is frequently neglected (Liu et al., 2025). It is more prevalent in models for construction and mining purposes, where artificial ground freezing is used to stabilise the subsurface and to avoid groundwater seepage (Alzoubi et al., 2019; Huang et al., 2018; Zhou and Meschke, 2013). Two distinct methodologies are primarily employed in these models to represent the freezing and thawing in the soil: the apparent heat capacity method and the enthalpy method (Liu et al., 2025). The apparent heat capacity method incorporates the latent heat of the phase change into the material's heat capacity over a defined temperature range (Yang et al., 2015). This method is implemented in COMSOL Multiphysics' phase change material model (COMSOL Multiphysics, 2019). This approach is more frequently employed as it simpler and easier to implement, although the exact phase boundary cannot be tracked (Liu et al., 2025). The enthalpy method is more complex as it accounts for the latent heat phase change into the energy conservation equation. With this method, a mushy region is introduced between the

two phases in order to avoid sharp discontinuities (Jiménez-Xamán et al., 2019). In the context of closed-loop shallow geothermal systems, only a limited number of numerical models incorporate subsurface phase change processes alongside the operation of the heat source system. Liu et al. (2025) analyses the performance of coaxial BHEs under soil freezing conditions by applying the apparent heat capacity method in a finite difference framework. The apparent heat capacity method is also employed by Yang et al. (2015) in their 2D model to evaluate the influence of soil freezing on ground heat exchangers. Eslami-Nejad and Bernier (2012) likewise used the apparent heat capacity method for their one-dimensional radial numerical heat transfer model. This 1D model is coupled with a BHE model to investigate the effect of ground freezing on the borehole wall temperature. Arzanfudi and Al-Khoury (2018) on the other hand use the enthalpy method in their model to evaluate the processes occurring in the vicinity of energy piles. Bottarelli et al. (2015) presented a GHC model, which includes freezing in the subsurface considering the phase change of water and an addition phase change material. As in this study, an additional phase change material is added by mixing water and micro-encapsulated paraffin with the soil, which is then used as backfill material for the trench. Accordingly, heat extraction from the subsurface in this case is facilitated by two materials undergoing phase transition. Therefore, the numerical model was simplified to a heat conduction model with an equivalent solid domain, which combines all relevant thermal properties (Bottarelli et al., 2015). Gan (2013) developed a numerical model for a horizontal ground heat exchanger, where freezing and thawing is included within the energy conservation equation. According to their investigations, the specific heat extraction rate increases up to 8.6% (Gan, 2013). Hüsing et al. (2016) developed a finite difference model for a horizontal ground heat exchanger in TRNSYS, which accounts for ground freezing. They apply the apparent heat capacity method to model phase change in the subsurface in their 2D simulation (Hüsing et al., 2018). Moreover, they claim that their model represents an improvement over existing numerical models for horizontal ground heat exchangers proposed by Giardina (1995), Ramming (2007) and Glück (2009). Hirsch et al. (2019) developed a numerical model for ground heat exchangers in DELPHIN, highlighting that moisture transport and ice formation are taken into account. However, they share little information on how freezing is represented in the model.

Existing analytical models for GHCs commonly consider heat conduction in the subsurface – for example, Claesson and Dunand (1983) for horizontal pipes, Li et al. (2012a) for slinky coil ground heat exchanger and Jeon et al. (2018) for spiral-coil ground heat exchanger or geothermal baskets. Some analytical models consider additional effects such as seasonal temperature variation and the air-soil boundary effect (Bahmani and Hakkaki-Fard, 2022; Ciriello et al., 2015b; Lamarche, 2019; Wang et al., 2016) or freezing and thawing due to heat transfer to and from the surface (Xiong et al., 2015). Although Xiong et al. (2015)

account for freezing and thawing at the surface for the calculation of the undisturbed ground temperature, their approach does not capture the soil freezing and thawing occurring around the collector pipes. In addition, the model representing the undisturbed ground temperature is a numerical one, which is subsequently superposed with the analytical ring source model. Previous studies have applied thermal response tests to ground heat collectors for model-based estimation of soil parameters (Urresta et al., 2021; Van de Ven et al., 2022; Van de Ven et al., 2023). Beyond that, the impact of groundwater advection on the operation of a slinky-coil heat exchanger has been investigated (Li et al., 2012b).

Freezing and thawing are crucial heat transfer processes for all kinds of GHCs that use the latent heat of the soil moisture. The governing differential equations for these processes are nonlinear and not included in the fundamental solution of potential theory (Carslaw and Jaeger, 1959), which is widely used in the form of the continuous infinite or finite (moving) line source (I(M)LS or F(M)LS) (ILS: Spitler and Gehlin (2015); IMLS: Sutton et al. (2003), Wagner et al. (2013); FLS: Abdelaziz et al. (2014), Lamarche (2019), Fontaine et al. (2011); FMLS: Erol and François (2018), Molina-Giraldo et al. (2011)), the infinite or finite plane source (IPS or FPS) (IPS: Gupta et al. (2022); FPS: Van de Ven et al. (2024)), or the ring source (Li et al., 2012a; Witte et al., 2022; Xiong et al., 2015) for dimensioning of shallow geothermal closed-loop systems. To our knowledge, one analytical model exists, which simulates both the operational temperature and the propagation of the frozen ground (Ramming, 2007). However, the model of Ramming (2007) focuses only on different pipe configurations and does not conform to the consistent modelling approach as defined in Chapter 1.2.3. The consistent modelling approach only allows completely coupled fundamental solutions of potential theory (Carslaw and Jaeger, 1959) supplemented by approximations not included in potential theory. Ramming (2007) primary focusses on horizontal GHCs consisting of pipes installed horizontally in the soil, for which a detailed analytical model has been developed. While additional collector configurations are discussed, their actual geometries are only approximated and treated as variations of the horizontal pipe model. These approaches involve assumptions that are not further verified. Furthermore, the analytical model proposed by Ramming (2007) cannot be suitably adapted to align with the consistent modelling framework described in Chapter 1.2.3 and is therefore excluded as a basis for comparative analysis of different source systems.

The presented study closes this gap and introduces an approximate solution for analytical simulation of the subsurface freezing caused by geothermal heat collector operation. In the following, a general formulation is presented that is subsequently specified for two geometric collector variants. A detailed numerical implementation is employed for comparison and exemplary calculations are presented to reveal the suitability of the analytical approach.

4.3 Models and methods

4.3.1 Analytical models

4.3.1.1 General approach

The analytical model is set up to simulate different collector configurations that operate in shallow ground in the vicinity of the ground surface. The initial temperature of the ground in the height range of the collector is assumed to be above freezing temperature and no previous geothermal use is considered. For above-freezing temperatures solely source solutions are used to calculate the temperature field around the GHC. The use of source solutions provides consistency with established model methods in shallow geothermal applications, e.g., BHEs (Cimmino et al., 2013; Eskilson, 1987). Given the solution for a basic step pulse with a constant heat load, the temperature difference from the initial value $T = 0$ is calculated and a varying heat extraction rate is accounted for by superposition. The corresponding absolute temperature resulting from one step pulse with its starting time set to $t = 0$ is:

$$T(t, x, y, z) = \gamma \dot{q} \theta(t, x, y, z) \tag{4-1}$$

Specifically, T is the solution for a given source geometry (point, line, plane, ring, etc.) at the time t and the location x, y, z. The applied constant heat extraction or injection rate $\dot{q}$ is defined in W/m or W/m² depending on the selected collector geometry. In Eq. (4-1), γ is the dimensional factor belonging to the dimensionless temperature response θ. Both, γ and θ depend on the main geometry of the model, i.e. line, plane, ring, etc. The dimensionless temperature response depends on further dimensionless parameters. The unit of the dimensional factor is related to the unit of $\dot{q}$ and can be in m·K/W or m²·K/W. Subsequently, the dimensional factor is specified with a subscript, γ_{unfr} and γ_{fr}, in which it considers the properties of the unfrozen and frozen ground, respectively. The equations defining the dimensional factors are specified in detail in the Chapters 4.3.1.2 and 4.3.1.3.

The resulting temperature field calculated with Eq. (4-1) is superposed with seasonal temperature variations and a collector resistance model. The natural seasonal varying ground temperature depending on its depth $T_{\mathrm{undist\,sub}}(z, t)$ is calculated by Kusuda and Achenbach (1965) and has already been described in Eq. (3-20) in Chapter 3.3.1.3. If the collector extends over a few tenths of a metre in depth, it is reasonable to average the undisturbed ground temperature over the collector height, as in Eqs. (3-21) and (3-22).

This modelling approach uses the temporal superposition technique to apply a realistic heat load profile. This technique makes it possible to take the effects of previous heat loads into account, and thus, it can be used to model the history of previous thermal loads (Eskilson, 1987). Here, the solution is again defined as the temperature difference with respect to an initial temperature of 0. Thus, this can also be written as an absolute temperature T in Eq. (4-2).

Since the model is applied in discrete, equidistant time steps, the temporal superposition is formulated stepwise in time, with n being the number of the considered time steps and Δt the time step interval:

$$T(n\Delta t) = \sum_{i=1}^{n} \gamma \dot{q}_\theta(i\Delta t)\left[\theta\left((n-i+1)\Delta t\right) - \theta\left((n-i)\Delta t\right)\right] \tag{4-2}$$

$$T(n\Delta t) = \gamma \dot{q}_\theta(n\Delta t)\theta(\Delta t) + T_{\mathrm{hist}}(n\Delta t) \tag{4-3}$$

with

$$T_{\mathrm{hist}}(n\Delta t) = \sum_{i=1}^{n-1} \gamma_{\mathrm{unfr}} \dot{q}_\theta(i\Delta t)\left[\theta\left((n-i+1)\Delta t\right) - \theta\left((n-i)\Delta t\right)\right] \tag{4-4}$$

and

$$\theta(0) = 0 \tag{4-5}$$

Here, $\dot{q}_\theta$ is the conductive heat injection or extraction rate in W/m or W/m². $T_{\mathrm{hist}}(n\Delta t)$ represents the impact of previous thermal loads from the time step 1 to $n-1$ at the specified time $n\Delta t$. Eq. (4-2) is rewritten in Eq. (4-3) as a decomposition of a contribution from the past $T_{\mathrm{hist}}(n\Delta t)$ and the current time step $\gamma \dot{q}_\theta(n\Delta t)\theta(\Delta t)$. This decomposition into a past and a current component in Eq. (4-3) is intended for the modelling of ground freezing. In the case of freezing, the history-dependent term is evaluated using the dimensional factor corresponding to the unfrozen state γ_{unfr}, whereas the current time step reflects the prevailing phase of the soil and is calculated differently, as described later by Eq. (4-12). Evaluating the history term based on the unfrozen dimensional parameter represents a methodological simplification designed to reduce computational complexity. This, however, may lead to discrepancies compared to actual physical behaviour. Eqs. (4-2), (4-3) and (4-4) apply for equidistant time steps with constant heat injection or extraction rates within each time step. Furthermore, the corresponding dimensionless temperature response must be used, i.e. the dimensionless variables must match both the collector geometry and the desired evaluation point. By superposing Eqs. (3-20) and (4-2), the collector wall temperature T_{cw} can be determined at each point in time under consideration by Eq. (4-6) as long as the resulting temperature, T_{cw}, is above freezing temperature T_{lat}:

$$T_{\mathrm{cw}}(n\Delta t) = T_{\mathrm{undist\,sub}}(z, n\Delta t) + \gamma\, \dot{q}_\theta(n\Delta t)\, \theta(\Delta t) + T_{\mathrm{hist}}(n\Delta t) \tag{4-6}$$

$T_{\mathrm{undist\,sub}}(z, n\,\Delta t)$ can be replaced by the average of the undisturbed ground temperature over the collector height, if necessary. In addition to Eq. (4-6), a heat balance at the collector wall is applied, where the total heat flow rate $\dot{q}_{\mathrm{tot}}$ extracted, or injected, by the collector is divided

into the conductive heat flow rate between the ground and the collector wall $\dot{q}_\theta$ and the latent heat flow rate $\dot{q}_{\mathrm{lat}}$.

$$0 = \dot{q}_{\mathrm{tot}}(n\Delta t) + \dot{q}_{\mathrm{lat}}(n\Delta t) - \dot{q}_\theta(n\Delta t) \tag{4-7}$$

The total heat flow rate, $\dot{q}_{\mathrm{tot}}$, is negative when heat is extracted and becomes positive when heat is injected. The same applies for the conductive heat flow rate $\dot{q}_\theta$. The latent heat flow rate $\dot{q}_{\mathrm{lat}}$, in contrast, is positive during the formation of ice and turns negative as the frozen ground thaws. As soon as the subsurface freezes, i.e. $T_{\mathrm{cw}} < T_{\mathrm{lat}}$, the conductive heat flow rate, $\dot{q}_\theta$, is divided into an unfrozen and a frozen conductive heat flow rate, $\dot{q}_{\theta,unfr}$ and $\dot{q}_{\theta,fr}$, respectively. Both sum up to the conductive heat flow rate $\dot{q}_\theta$:

$$\dot{q}_\theta(n\Delta t) = \dot{q}_{\theta,\mathrm{unfr}}(n\Delta t) + \dot{q}_{\theta,\mathrm{fr}}(n\Delta t) \tag{4-8}$$

The modelling approach distinguishes four cases:

I. No frost is present at the beginning of the current time step, and no freezing occurs within in the current time step n.

II. No frost is present at the beginning of the current time step, but the soil adjacent to the collector wall starts freezing within the current time step.

III. Frost is present at the beginning of the current time step, and the subsurface freezes further or partially thaws with residual frost within the current time step.

IV. Frost is present at the beginning of the current time step, and the subsurface thaws completely within the current time step.

In case I, i.e. for temperatures above the freezing point, the latent heat flow rate $\dot{q}_{\mathrm{lat}}$ is zero, and thus, the conductive heat flow rate, $\dot{q}_\theta$, equals the total heat flow rate $\dot{q}_{\mathrm{tot}}$. The collector wall temperature can directly be calculated with Eq. (4-6) and $\gamma = \gamma_{\mathrm{unfr}}$.

Once the collector wall temperature drops below the freezing temperature, the latent heat flow rate, $\dot{q}_{\mathrm{lat}}$, is used as a source term, which stores heat during freezing and releases the stored heat during thawing.

In case II, when the collector wall temperature falls below the freezing temperature, the frozen conductive heat flow rate for the current time step $\dot{q}_{\theta,\mathrm{fr}}(n\Delta t)$ is set to zero. The unfrozen part of the conductive heat flow rate is determined by setting the collector wall temperature equal to the freezing temperature and using the unfrozen properties for the dimensional factor, i.e. $\gamma = \gamma_{\mathrm{unfr}}$, in Eq. (4-6). Thus, the resulting equation for the conductive heat flow rate in the unfrozen subsurface $\dot{q}_{\theta,\mathrm{unfr}}$ is:

$$\dot{q}_{\theta,\mathrm{unfr}}(n\Delta t) = \frac{T_{\mathrm{lat}} - \left(T_{\mathrm{undist\,sub}}(z, n\Delta t) + T_{\mathrm{hist}}(n\Delta t)\right)}{\gamma_{\mathrm{unfr}}\theta(\Delta t)} \tag{4-9}$$

Since $\dot{q}_{\theta,\mathrm{fr}}$ in case II is zero, $\dot{q}_{\theta}$ equals $\dot{q}_{\theta,\mathrm{unfr}}$. Given the known value of the conductive heat flow rate, $\dot{q}_{\theta}$, Eq. (4-7) can be solved for the latent heat flow rate, $\dot{q}_{\mathrm{lat}}$, leading to:

$$\dot{q}_{\mathrm{lat}}(n\Delta t) = \dot{q}_{\theta}(n\Delta t) - \dot{q}_{\mathrm{tot}}(n\Delta t) \tag{4-10}$$

Subsequently, the scale-representative amount of frozen soil built up in the current time step, $\Delta Fr(t)$, can be calculated as follows:

$$\Delta Fr(n\Delta t) = \frac{\dot{q}_{\mathrm{lat}}(n\Delta t)\Delta t}{\Lambda_{\mathrm{lat}}\phi\rho_{\mathrm{ice}}} \tag{4-11}$$

Here, Λ_{lat} is the specific phase change enthalpy of the groundwater, ϕ is the porosity of the subsurface, and ρ_{ice} is the density of the frozen soil water. Since the representative amount of frozen soil built up in the current time step, $\Delta Fr(n\Delta t)$, i.e. the change in amount of frozen soil, directly depends on the heat extraction or injection rates $\dot{q}_{\mathrm{tot}}$, and thus, on the associated geometry model, it is expressed either in m² or m. A frozen quantity expressed in metres, for instance, refers to the distance perpendicular to the collector wall. A more detailed explanation follows in the subsequent Chapters 4.3.1.2 and 4.3.1.3. For case II, the scale-representative change in frozen soil, $\Delta Fr(n\Delta t)$, equals the overall amount of frozen soil at the considered time, $Fr(n\Delta t)$. Once the total amount of frozen soil until the current time is determined, the maximum extent of the frozen area can be calculated. This is highly dependent on the geometry of the collector, i.e. the specific geometry model, and therefore cannot be generalised. It must be individually determined for each collector configuration. The collector wall temperature, T_{cw}, for temperatures below the freezing point, T_{lat}, is calculated by simple, two-dimensional heat conduction equations using corresponding shape factors, $S(n\Delta t)$, as follows:

$$T_{\mathrm{cw}}(n\Delta t) = T_{\mathrm{lat}} + \gamma_{\mathrm{fr}}\dot{q}_{\theta}(n\Delta t)S(n\Delta t) \tag{4-12}$$

Similar to the dimensional factor γ_{fr}, the shape factor $S(n\Delta t)$ depends on the geometry model as well but is dimensionless. The temporal dependence of the shape factor is determined by the extent of frozen ground, which changes with time. The temperature gradient between the frost isotherm and the collector wall is calculated using the heat conduction equation, with the frost isotherm assumed to be at the boundary of the frozen soil.

Case III covers both the further freezing and partial thawing of the subsurface. This means, that a specific amount of frozen soil, Fr, is already present and the collector wall temperature, T_{cw}, is below the freezing point, T_{lat}. The only distinction from the previous case is that the frozen conductive heat flow rate $\dot{q}_{\theta,\mathrm{fr}}$ is non-zero and calculated as follows:

$$\dot{q}_{\theta,\mathrm{fr}}(n\Delta t) = \frac{T_{\mathrm{cw}}\big((n-1)\,\Delta t\big) - T_{\mathrm{lat}}}{\gamma_{\mathrm{fr}}\theta(\Delta t)} \tag{4-13}$$

The unfrozen conductive heat flow rate, $\dot{q}_{\theta,\mathrm{unfr}}$, is to be calculated with Eq. (4-9). By applying the result into Eqs. (4-8), (4-10), and (4-11), the latent heat flow rate, $\dot{q}_{\mathrm{lat}}$, and the amount of frozen soil built up in the current time step, ΔFr, can be determined. If the sum of the change in the amount of frozen soil, $\Delta Fr(n\Delta t)$, and the frozen soil from the previous time step, $Fr\big((n-1)\Delta t\big)$, is greater than or equal to zero, the total amount of frozen soil at the current time step, $Fr(n\Delta t)$, can be determined as follows:

$$Fr(n\Delta t) = Fr\big((n-1)\Delta t\big) + \Delta Fr(n\Delta t) \tag{4-14}$$

Similar to case II, the collector wall temperature for case III can be computed using Eq. (4-12).

Upon thawing of the soil, i.e. for case IV, the change of the amount of frozen soil at the current time step will lead to a value below zero for the total amount of frozen soil. Thus, similar to case III, the heat balance model is based on Eq. (4-7) and solved for the latent heat flow rate, $\dot{q}_{\mathrm{lat}}$. This is done by applying Eqs. (4-9) and (4-13), allowing the determination of the change in amount of frozen soil, ΔFr. If case IV applies, the entire soil thaws, leading to the following change in the amount of frozen soil:

$$\Delta Fr(n\Delta t) = Fr\big((n-1)\Delta t\big)\,(-1) \tag{4-15}$$

By applying Eq. (4-14), an amount of frozen soil in the current time step of 0 is obtained. In the time step during which the soil undergoes complete thawing, the latent heat injection rate can be determined with the defined change of the frozen soil amount by reformulating Eq. (4-11) as follows:

$$\dot{q}_{\mathrm{lat}}(n\Delta t) = \Delta Fr(n\Delta t)\Lambda_{\mathrm{lat}}\phi\rho_{\mathrm{ice}}\Delta t \tag{4-16}$$

Furthermore, Eq. (4-13) can still be applied to determine the frozen conductive heat injection rate at the time step in which the complete soil thaws, whereas the unfrozen conductive heat injection rate must be determined by balancing the heat rates from Eq. (4-7) and solving for the unfrozen conductive heat injection or extraction rate, $\dot{q}_{\theta,\mathrm{unfr}}$:

$$\dot{q}_{\theta,\mathrm{unfr}}(n\Delta t) = q_{\mathrm{lat}}(n\Delta t) + \dot{q}_{\mathrm{tot}}(n\Delta t) - q_{\theta,\mathrm{fr}}(n\Delta t) \tag{4-17}$$

The collector wall temperature, however, can be determined using Eq. (4-6) in the time step during which the soil undergoes complete thawing.

The calculation algorithm, incorporating all defined four cases, is presented in the flow chart in Fig. 4-2.

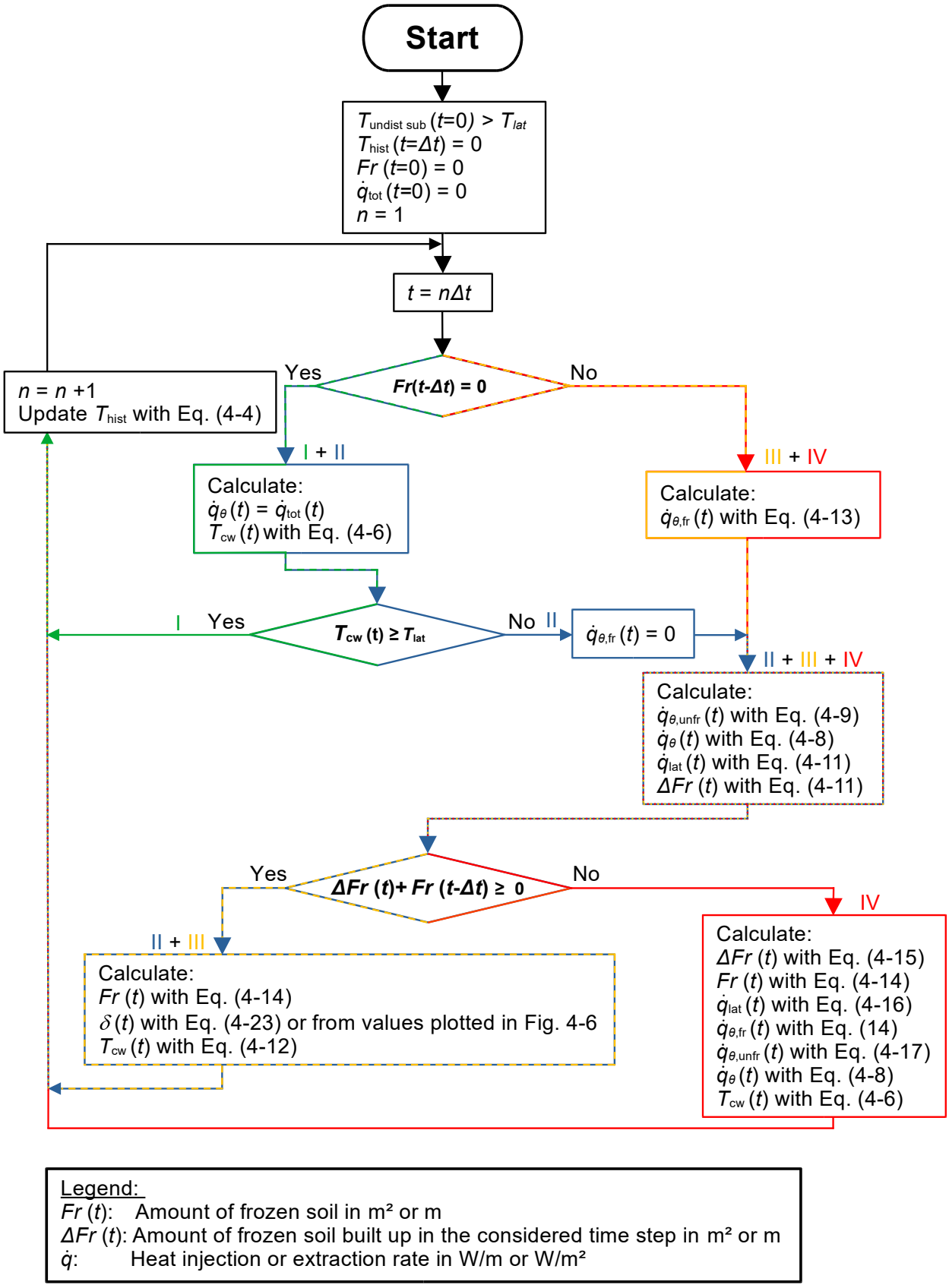

Fig. 4-2: Flow chart of the calculation algorithm.

The described methodology is exemplified for a horizontal pipe and a planar trench collector in the following chapters.

4.3.1.2 Horizontal pipe

The source solution used for the analytical simulation of a horizontal pipe is the 2D, ILS model with an isothermal boundary condition at the ground surface. The ILS is located parallel to the ground surface as depicted in Fig. 4-3. For the applied 2D model, the units of $\dot{q}$, γ, ΔFr, and Fr, are W/m, m·K/W, m², and m², respectively.

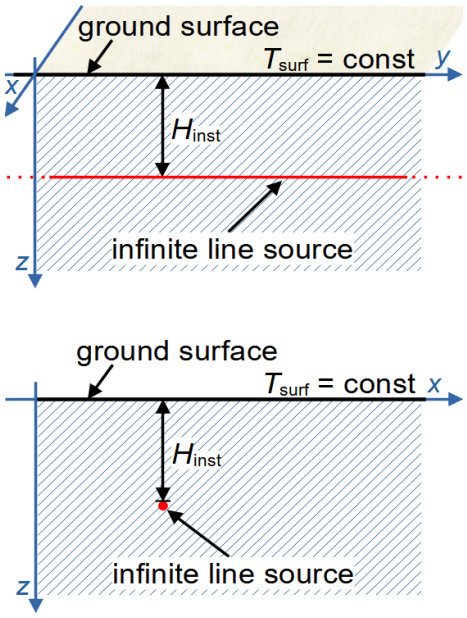

Fig. 4-3: Infinite line source with an isothermal boundary condition at the ground surface.

The mathematical solution of the ILS with an isothermal boundary condition can be deduced from the point source. Similar as in Eq. (4-1), it is formulated as an absolute temperature:

$$T(x,z,t) = -\frac{\dot{q}}{4\pi\lambda}\left[\mathrm{Ei}\left(-\frac{(x-x')^2+(z-z')^2}{4\alpha t}\right)-\mathrm{Ei}\left(-\frac{(x-x')^2+(z+z')^2}{4\alpha t}\right)\right] \quad (4\text{-}18)$$

(Carslaw and Jaeger, 1959)

Here, x and z represent the coordinates of the evaluation point at which the temperature is calculated as depicted in Fig. 4-3, t is the time in s that has elapsed since the heat load was applied, $\dot{q}$ is the heat extraction (negative) or injection (positive) rate in W/m , λ is the thermal conductivity of the subsurface, Ei is the exponential integral, x' and z' indicate the location of the source and α is the thermal diffusivity of the subsurface in m²/s. This source model is used for the heat conduction in the subsurface as described in Chapter 4.3.1.1 The dimensionless form of Eq. (4-18), which is needed as an input for the general approach, is:

$$\theta(t) = -\frac{1}{2}\left[\mathrm{Ei}\left(-\frac{(x-x')^2+(z-z')^2}{4at}\right)-\mathrm{Ei}\left(-\frac{(x-x')^2+(z+z')^2}{4at}\right)\right] \quad (4\text{-}19)$$

Furthermore, γ_{unfr} and γ_{fr} are defined in Eq. (4-20) and (4-21) for the ILS model:

$$\gamma_{\mathrm{unfr}} = \frac{1}{2\pi\lambda_{\mathrm{unfr}}} \tag{4-20}$$

$$\gamma_{\mathrm{fr}} = \frac{1}{2\pi\lambda_{\mathrm{fr}}} \tag{4-21}$$

Here, both dimensional factors have the unit m·K/W. With Eqs. (4-19) and (4-20) or (4-21), Eq. (4-18) can be reformulated as follows:

$$T(n\Delta t) = \dot{q}_{\theta,\mathrm{unfr/fr}}\gamma_{\mathrm{unfr/fr}}\theta(n\Delta t) \tag{4-22}$$

Within the calculation algorithm, Eq. (4-22) represents a reformulation of Eqs. (4-9) and (4-13) corresponding to the formula structure of Eq. (4-18). Thus, it is primarily used to divide the heat extraction or injection rate into frozen and unfrozen fractions.

Ground heat collectors are generally installed at frost-free depths; additionally, their minimum collector outlet temperature should not fall below −5 °C (Verein Deutscher Ingenieure e. V., 2019). This combination results in a nearly radial symmetry of the formation of the frozen ground, as can be seen in Fig. 4-4 . However, if the collector is positioned very close to the surface, limiting the amount of heat flowing in from above during the heating season, this symmetry is disrupted. In such cases, the expansion of the frozen ground takes on a droplet-like shape, as can be seen in Fig. 4-5 for a horizontal pipe installed in 20 cm depth. This installation depth leads to a non-homogeneous temperature distribution around the collector pipe.

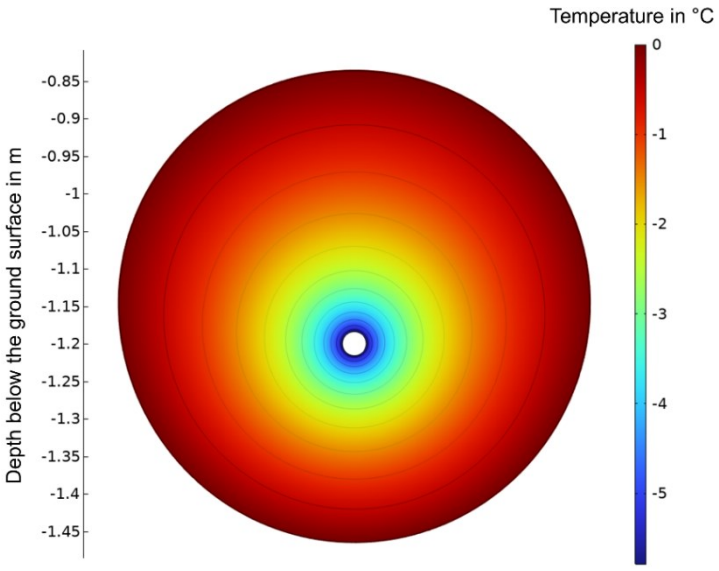

Fig. 4-4: Temperature distribution around a horizontal pipe including the seasonal temperature variation at the surface and after a heat extraction of 2000 hours.

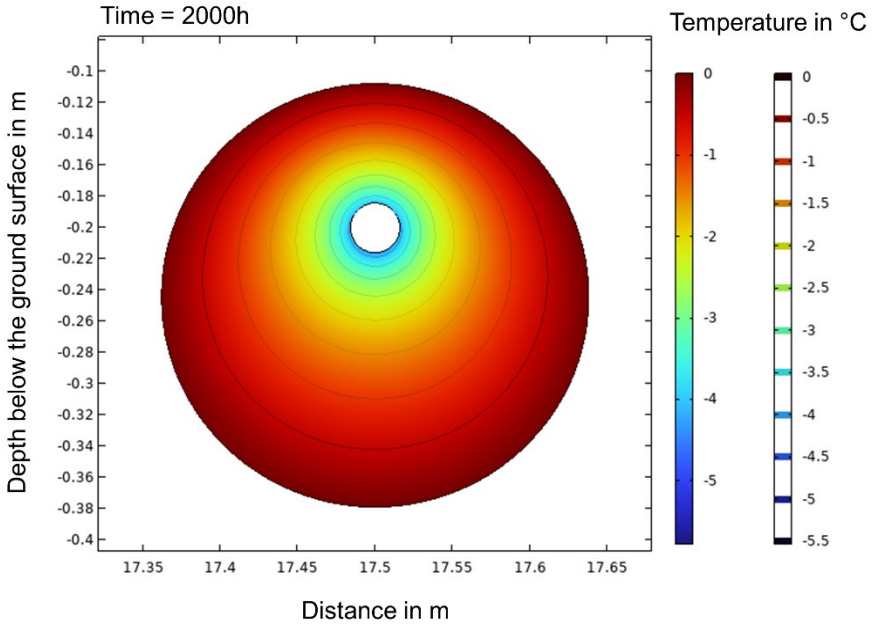

Fig. 4-5: Temperature distribution around a horizontal pipe installed at 20 cm depth with seasonal temperature variation at the surface and after a heat extraction of 2000 hours.

In this model a radially symmetric freezing of the subsurface around the collector pipe is assumed. With r_{pipe} being the pipe radius in m, A_{pipe} being the cross-sectional area of the pipe, and the scale-representative amount of frozen ground being $Fr(t)$, the maximum extension of the frozen ground $\delta(n\Delta t)$ in m between the pipe wall and the frost isotherm, T_{lat}, is determined:

$$\delta(n\Delta t) = \sqrt{\frac{Fr(n\Delta t) + A_{\mathrm{pipe}}}{\pi}} - r_{\mathrm{pipe}} \tag{4-23}$$

The shape factor for the horizontal pipe with freezing of the subsurface is determined based on the well-known formula for heat conduction in concentric circles:

$$\Delta T = \frac{\dot{q}}{2\pi\lambda} \ln\left(\frac{r_{\mathrm{outer}}}{r_{\mathrm{inner}}}\right) \tag{4-24}$$

(VDI-Gesellschaft Verfahrenstechnik und Chemieingenieurwesen, 2013)

By combining Eq. (4-12) and (4-24) the shape factor for the horizontal pipe is determined as follows:

$$S(t) = \ln\left(\frac{\delta(n\Delta t) + r_{\mathrm{pipe}}}{r_{\mathrm{pipe}}}\right) = \ln\left(\frac{\delta(n\,\Delta t)}{r_{\mathrm{pipe}}} + 1\right) \tag{4-25}$$

This approach is valid as long as freezing of the ground develops closely to the radial symmetry assumed here. If the shape of the frozen ground deviates significantly from radial symmetry, the model becomes increasingly imprecise.

Using this straightforward model, a horizontal pipe that serves as a geothermal ground collector can be efficiently and accurately designed, while accounting for the freezing of the subsurface. However, it is crucial to select appropriate time step sizes to ensure that the steady-state condition of the shape factor is achieved. Failure to do so will lead to instability in the method, as the growth of the frozen radius is initially overestimated, which is subsequently corrected by thawing the frozen radius in the following step. This correction, in turn, leads to an overestimation of the thawing process, thereby exacerbating the error and initiating a cycle of continuously overestimating the freezing or thawing process. Therefore, the lower limit for the time step duration of the analytical solution for the horizontal pipe is four hours. This time step size is applied in the exemplary application studies presented in the following chapters, as it provides stable results for the chosen parameters without compromising accuracy.

4.3.1.3 Planar trench collector

The analytical model employed for heat conduction in the subsurface for planar trench collectors is the analytical FPS model, which is described in Chapter 3.3.1.1 (Van de Ven et al., 2024). The units of $\dot{q}$ and γ are W/m² and m²·K/W respectively. The dimensionless temperature response of the FPS model is expressed as follows:

$$\theta(t) = \frac{1}{4\pi L_c H_c H_{tot}} \tag{4-26}$$

$$\int_0^{L_c}\int_{H_{inst}}^{H_{inst}+H_c}\int_0^{L_c}\int_{H_{inst}}^{H_{inst}+H_c}\left(\frac{\operatorname{erfc}\left(\frac{\sqrt{(x-x')^2+(y-y')^2+(z-z')^2}}{2\sqrt{\alpha t}}\right)}{\sqrt{(x-x')^2+(y-y')^2+(z-z')^2}} - \frac{\operatorname{erfc}\left(\frac{\sqrt{(x-x')^2+(y-y')^2+(z+z')^2}}{2\sqrt{\alpha t}}\right)}{\sqrt{(x-x')^2+(y-y')^2+(z+z')^2}}\right) dz'dx'dz\,dx$$

Here L_c, H_c, H_{inst}, and H_{tot} represent the collector dimensions, i.e. its length, its height, its installation depth, and its overall depth, respectively. erfc is the complementary error function, (x, y, z) describe the evaluation plane, and (x', y', z')) define the location of the plane source. More detailed information on the FPS model can be found in Chapter 3. Furthermore, the dimensional factors for this model are defined as:

$$\gamma_{unfr} = \frac{H_{tot}}{\lambda_{unfr}} \tag{4-27}$$

$$\gamma_{fr} = \frac{H_{tot}}{\lambda_{fr}} \tag{4-28}$$

To determine the maximum horizontal extension of the frozen ground for planar trench collectors, a so-called equivalent volume $V_{fr,eq}$ is calculated based on amount of the frozen ground, Fr. It is assumed that the expansion of the frozen volume occurs in all three

dimensions, i.e. the distance perpendicular to the collector wall of the frozen layer corresponds to Fr and both the collector length L_c and the collector height H_c are lengthened by Fr as well. Consequently, the equivalent frozen volume for the determination of the maximum extension of the frozen ground is described by:

$$V_{fr,eq}(n\Delta t) = Fr(n\Delta t)\,(L_c + Fr(n\Delta t)\,(H_c + Fr(n\Delta t)) \tag{4-29}$$

The maximum horizontal extension of the frozen ground, $\delta(n\Delta t)$, is defined based on various steady-state, three-dimensional, numerical simulations for the considered collector geometry and various thermal conductivities of the solid matrix. In order to minimise errors from correlation curves, the maximum extension of the frozen ground is directly determined through linear interpolation of the simulated results for a given equivalent frozen volume $V_{fr,eq}$. The results of the numerical, steady-state simulations used for the linear interpolation are shown in Fig. 4-6. The figure illustrates that the maximum horizontal extension of the frozen ground is independent of the soil properties.

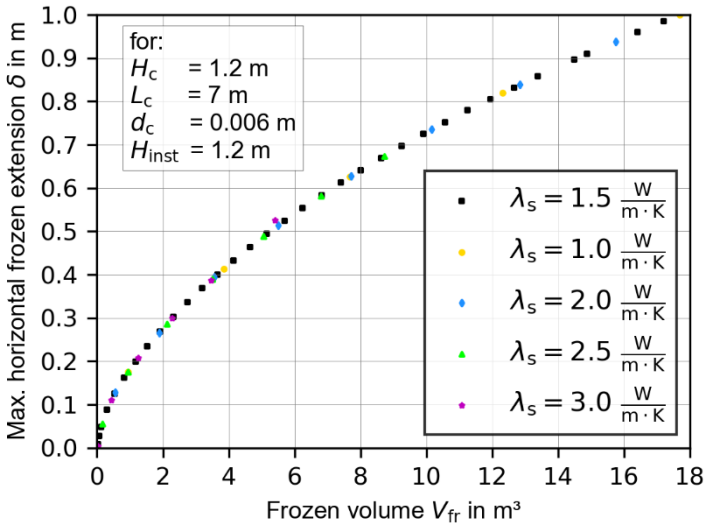

Fig. 4-6: Relationship between frozen volume and maximum horizontal extension of the frozen ground, based on steady-state, 3D numerical simulations for various thermal conductivities.

However, for the calculation of the collector wall temperature, a dimensional transition occurs. As in the horizontal pipe model, the shape factor that is applied for the heat conduction between the collector wall temperature T_{cw} and the freezing isotherm T_{lat} is derived in analogy to the well-known 2D, steady-state solution of heat conduction in a plane wall. Applied to the distance L_{fr} between the collector wall temperature T_{cw} and the freezing isotherm T_{lat}, this yields Eq. (4-30).

$$T_{\mathrm{cw}} - T_{\mathrm{lat}} = \frac{\dot{q}}{\lambda} L_{\mathrm{fr}} \tag{4-30}$$

(Incropera et al., 2013)

By transforming Eq. (4-30) into Eq. (4-12), the shape factor S can be determined directly. However, it should be pointed out that L_{fr} represents the distance between the mean temperature at the collector wall and the freezing isotherm, i.e. it represents half of the scale-representative amount of the frozen ground, $Fr(t)/2$, as on both sides of the collector the ground freezes. Furthermore, it is important to note that, in the context of heat conduction, not only the scale-representative amount of frozen ground $Fr(t)$ must be halved, but also the heat extraction or injection rate $\dot{q}$, as the thermal power acts on both sides of the collector. Consequently, the shape factor can be defined as follows:

$$S(n\Delta t) = \frac{Fr(n\Delta t)}{4H_{\mathrm{tot}}} \tag{4-31}$$

As previously noted for the horizontal pipe model, selecting the appropriate time step is crucial for the analytical trench collector model as well. Therefore, the lower limit of the time step size for this collector is a 48-hour size. This time step duration is employed to ensure reliable results for the chosen parameters.

4.3.2 Numerical models

The numerical models serve as a reference for the validation of the introduced analytical approach. For both geometric variants, horizontal pipe and planar trench collector, a separate model is set up in COMSOL Multiphysics (COMSOL Multiphysics, 2019). In both models, the Heat Transfer in Porous Media module is utilised, assigning a fluid phase and a solid matrix to characterise the porous structure. Furthermore, a local thermal equilibrium is applied, and the effective conductivity of the porous medium is simulated as the weighted arithmetic mean (volume average) of the conductivities of the fluid and the solid matrix. Within the fully saturated porous medium, the liquid medium is designated as a phase change material, i.e. freezing is restricted to the fluid phase, while the solid matrix remains unaffected. The phase change within the fluid is modelled employing the apparent heat capacity method, applied over a transition interval of 2 K between phase 1 (ice) and phase 2 (water). Thus, the applied model accounts for the gradual freezing process within the finite elements, it remains a simplification of all complex processes occurring in the soil while freezing. Nonetheless, it is adequately precise for this application. If complex thermo-hydro-mechanical processes are to be considered, e.g., soil uplift caused by frost, sophisticated models incorporating multiple physical processes such as described in Zhou and Meschke (2013) are to be applied. The collectors themselves are modelled as boundary heat sources and in their vicinity, where gradients are the biggest, the mesh is very fine and progressively gets coarser towards the

boundaries. In a preliminary study, the influence on the accuracy of the element order on the temperature at collector wall and the maximum extension of the frozen soil was investigated. The temperature at the collector wall barely deviates (< 0.02%) between a linear and a second-degree discretisation of the temperature. The maximum extension of the frozen soil on the other hand differs significantly within the first hours of ground freezing but declines already within less than a day. Thereafter, the remaining deviation of the extension of the frozen soil is less than 1.3%. The significant discrepancy is due to a time shift in the onset of ground freezing and is irrelevant for the design of these systems. Given the minor differences between the linear and second-order discretisation and the fact that the simulation time increased by a factor of more than 18 for the second-order variant, further simulations were carried out using a linear temperature discretisation.

4.3.2.1 Horizontal pipe

The numerical model for the horizontal pipe is based on the parameters of the analytical model and is thus 2D as well. The horizontal pipe in the subsurface is represented by a circular void within a rectangular calculation region. Therefore, the heat extraction rate of the ILS model $\dot{q}_{\mathrm{ILS}}$ in W/m is to be converted into the heat flux density set in the numerical model in W/m² to ensure equal conditions:

$$\dot{q}_{\mathrm{num}} = \frac{\dot{q}_{\mathrm{ILS}}}{2\pi r_{\mathrm{pipe}}} \tag{4-32}$$

The upper boundary of the rectangular calculation region represents the ground surface with the corresponding temperature boundary condition. The remaining boundaries of the domain are specified as adiabatic. The domain was defined empirically by varying its size, while both the accuracy of the temperature at the collector wall and at the border of the domain were monitored. At the left and right side, as well as at the lower border of the domain, so-called infinite regions are assigned to reduce the simulation domain, whilst avoiding their boundary influencing the collector operation. The numerical calculation grid consists of a free-triangle mesh extended by a structured mesh in the infinite regions. At the pipe boundary, the mesh resolution is significantly finer and gradually coarsens towards the outer regions. A figure of the mesh is provided in the appendix.

4.3.2.2 Planar trench collector

The numerical model of the planar trench collector is an extension of the numerical model described in Chapter 3.3.2. The collector is represented by a planar heat sink, i.e. the detailed geometry and internal flow dynamics of the collector are not considered. The computational domain was established through an empirical approach, involving systematic variation of its dimensions while monitoring the collector wall temperature for different boundary conditions.

To enhance computational efficiency, the numerical model applies two key simplifications: a quarter domain approach using symmetry boundary conditions, and the implementation of infinite element domains at the outer boundaries. Together, these measures reduce the computational load while maintaining physical accuracy by eliminating boundary-induced effects at the collector wall. The mesh mainly consists of a free-tetrahedral grid, which is supplemented by a structured mesh in the infinite element regions. A finer mesh is used near the collector surface to capture thermal gradients, while the element size increases gradually towards the domain boundaries. A figure of the mesh is provided in the appendix.

4.4 Results

4.4.1 Definition of scenarios for validation

The validation of the derived analytical model is carried out by comparison with the results of the numerical models. A period of twelve months is applied in all cases, as GHCs need to be regenerated within this time frame to ensure consistent performance in the following period. The parameters employed for the validation process for both the horizontal pipe and the planar trench collector are presented in Table 4-1. The subsequent analysis is conducted for three distinct scenarios: In scenario I a constant temperature is imposed at the ground surface, with a constant heat extraction rate applied over the course of one year for both types of collectors. For scenario II, a seasonal temperature variation at the ground surface is introduced, while the heat extraction is reduced to six months in order to assess the natural regeneration process for both collector types. Finally, the most realistic conditions are represented in scenario III. This is implemented for the horizontal pipe model, where a load profile is applied alongside the actual temperature fluctuations at the ground surface. This load profile, representing typical conditions in the Northern Hemisphere, starts in October and ends in April (see Fig. 4-7).

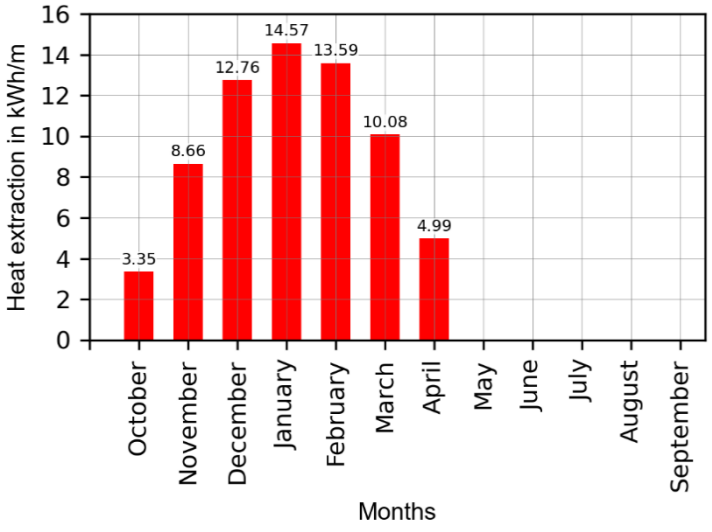

Fig. 4-7: Heat extraction profile used for the most realistic scenario III.

The subsurface and collector properties used for the validation process are listed in Table 4-1. It is assumed that the soil is fully saturated. Although this is not always the case in practice, as the water content in the pore spaces increases after the phase transition, the assumption of complete saturation after the phase change is generally a close approximation of the actual conditions in humid climates such as in Central Europe.

Table 4-1: Collector and surface properties for the comparison of the analytical and numerical models.

Subsurface properties			
Thermal conductivity of the solid matrix	λ_{s}	1.5	W/(m K)
Porosity	ϕ	0.25	
Density of the solid matrix	ρ_{s}	2180	kg/m³
Specific heat capacity of the solid matrix	$c_{p,\mathrm{s}}$	1000	J/(kg K)
Thermal conductivity of the groundwater	λ_{w}	0.58	W/(m K)
Density of the groundwater	ρ_{w}	1000	kg/m³
Specific heat capacity of the groundwater	$c_{p,\mathrm{w}}$	4200	J/(kg K)
Thermal conductivity of the ice	λ_{ice}	2.33	W/(m K)
Density of the ice	ρ_{ice}	900	kg/m³
Specific heat capacity of the ice	$c_{p,\mathrm{ice}}$	2000	J/(kg K)
Latent heat	Λ_{lat}	333500	J/kg
Annual mean surface temperature	$T_{\mathrm{undist\,sub}}$	10	°C
Seasonal temperature oscillation			
Period	t_{p}	8760	h
Phase constant	t_0	840	h
Annual amplitude of the Surface temperature	ΔT_{am}	10	K
Properties horizontal pipe			
Pipe radius	r_{pipe}	0.016	m
Installation depth	H_{inst}	1.2	m
Specific heat load rate	$\dot{q}_{\mathrm{tot}}$	−20	W/m
Properties planar trench collector			
Collector length	L_{c}	7	m
Collector height	H_{c}	1.2	m
Collector thickness	d_{c}	0.006	m
Installation depth	H_{inst}	1.2	m
Specific heat load rate	$\dot{q}_{\mathrm{tot}}$	−47.62	W/m²

To highlight the importance of considering soil freezing during the operation of GHCs, additional numerical simulations without accounting for the phase change of the water content in the soil for all scenarios are presented, while keeping all other conditions the same.

For the suitability of the analytical model as a design model, both design criteria, the collector outlet temperature and the maximum horizontal extent of the frozen ground, must be considered. Since the collector outlet temperature can rather precisely be determined based on the average collector wall temperature by using resistance models for the mean fluid temperature and subsequently assuming a temperature spread over the collector length, results of the collector wall temperature of both models are compared with each other. It should be noted that, for the calculation, the mean collector wall temperature must necessarily be determined based on the corresponding mean dimensionless temperature response applied consistently throughout the entire modelling approach. Suitable analytical resistance models to determine the mean fluid temperature of the planar trench collector can be found in Chapter 3.3.1.4. In the case of a horizontal pipe, the analytical solution for heat conduction in concentric circles, presented in Eq. (4-24), can be applied to determine the mean fluid temperature. For the comparison of the maximum horizontal frozen extension, δ, between the analytical and numerical model, only the results for a collector wall temperature T_{cw} below −1 °C are considered. This is done since in the analytical model the phase change occurs at −1 °C, whereas in the numerical model the phase change occurs between 0 °C and −2 °C.

4.4.2 Horizontal pipe

The first scenario (constant heat extraction rate and constant temperature at the surface) for the horizontal pipe model demonstrates excellent agreement for both examined parameters. It reveals a maximum deviation of 0.14 K for the collector wall temperature, T_{cw}, whereas the maximum horizontal extent of the frozen ground, δ, reaches a maximum deviation of 1 mm or 10% (Fig. 4-8). If freezing of the soil was not considered, the mean temperature at the collector wall would be around 0.5 K lower. The comparison of computing times clearly demonstrates the advantage of the analytical model: with precalculated dimensionless temperatures as an input matrix, the analytical model takes less than 14 seconds of calculation time for this scenario, whereas the numerical models takes one hour and two minutes. Both calculations were executed for a time step size of 4 h on a machine equipped with an Intel® CoreTM i7-6700 processor (8 logical cores at 3.40 GHz) and 38 GB RAM.

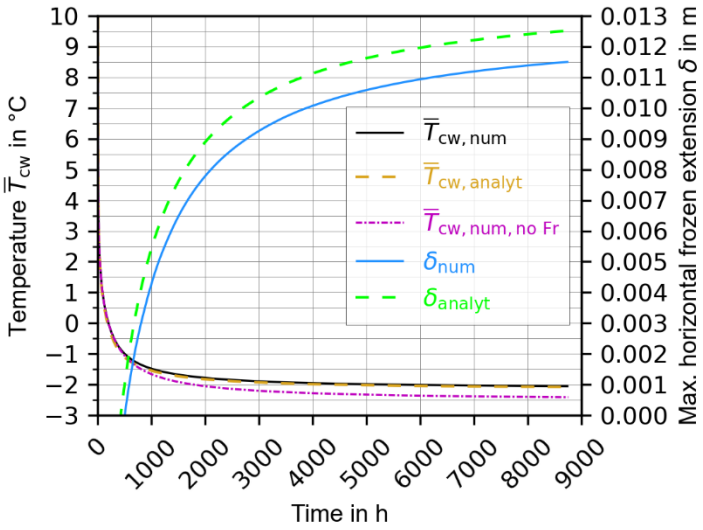

Fig. 4-8: Mean collector wall temperature and maximum horizontal extension of the frozen soil in scenario I, comparing the numerical and analytical simulations for a horizontal pipe.

The results for the second scenario are shown in Fig. 4-9, where a constant heat extraction rate over six months is superposed with the temperature fluctuations at the ground surface. It has larger deviations in temperature at the collector wall, with a maximum absolute deviation of 0.60 K. The discrepancy in the maximum horizontal extent of the frozen ground is up to 5 mm, which corresponds to a deviation of 3% relative to the maximum frozen radius. This is notably smaller than the deviation in the previous scenario I. In this scenario, the freezing of the subsurface results in a maximum temperature change that is more than 2 K smaller than in the case without freezing.

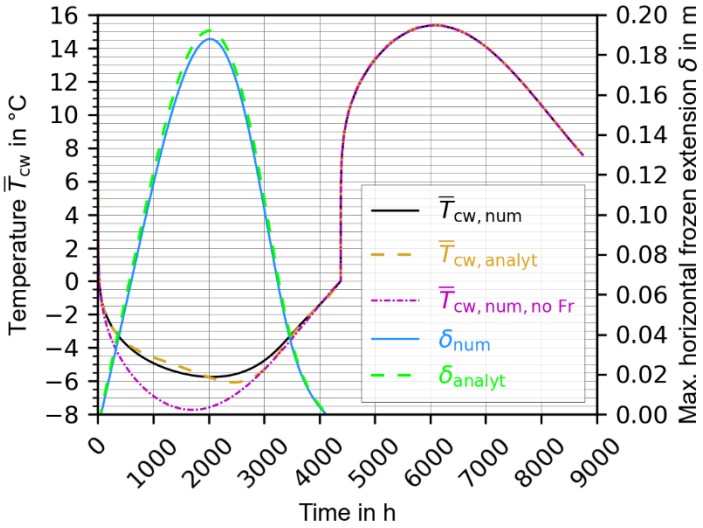

Fig. 4-9: Mean collector wall temperature and maximum horizontal extension of the frozen soil in scenario II, comparing the numerical and analytical simulations for a horizontal pipe.

The third scenario uses the heat extraction profile shown in Fig. 4-7 and also accounts for seasonal temperature fluctuations at the ground surface. It is assumed that the energy profile

depicted in Fig. 4-7 is extracted continuously, i.e. a constant heat extraction rate is applied over each month. This scenario with a more realistic heat extraction profile that is concentrated on the heating period reveals the largest deviations in both the temperature and the maximum extension, as depicted in Fig. 4-10. The largest temperature difference between the results of the numerical and analytical model is 1.33 K. The maximum frozen extension deviates up to 1.73 cm, which corresponds to 11% relative to the maximum extent of the frozen ground. A noticeable difference can also be observed in this scenario between the temperature at the collector wall if phase change in the soil is considered or not, again proving the influence of the freezing process.

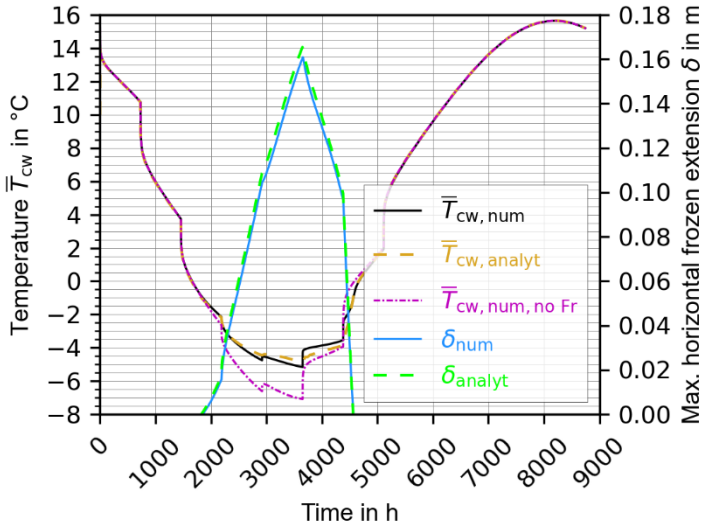

Fig. 4-10: Mean collector wall temperature and maximum horizontal extension of the frozen soil in scenario III, comparing the numerical and analytical model results for a horizontal pipe and assuming the heat extraction profile depicted in Fig. 4-7.

4.4.3 Planar trench collector

Fig. 4-11 shows the results for scenario I with a constant heat extraction rate and a constant temperature at the ground surface for the planar trench collector. The absolute temperature deviations are within a similar range as for the horizontal pipe model and reach a maximum of 0.80 K for the planar trench collector. The extent of the frozen ground deviates by up to 6.7 cm, which represents 13% relative to the maximum extent of the frozen ground with the most significant relative deviation occurring at the beginning of the transient state. However, towards the end of the simulation period of one year, the deviation decreases to 4%. Compared to the horizontal pipe results, accounting for the phase change in the surrounding soil has a larger impact on the temperature profile of the planar trench collector. The temperature difference between simulations with and without phase change in the soil is over 1 K larger for this collector type, making it roughly twice as large as for the horizontal pipe. The calculation time comparison for this collector is conducted in 48 h time steps. Like the horizontal pipe model,

the analytical trench collector model also relies on precalculated dimensionless temperature responses and is executed on the same machine as the horizontal pipe calculations (Intel® CoreTM i7-6700 processor (8 logical cores at 3.40 GHz); 38 GB RAM). The computation takes around 0.14 s on this machine, demonstrating the model´s efficiency. In contrast, the numerical model requires more than 13.5 h to run on a high-performance cluster with the cpu partition, one node and 32 tasks per node.

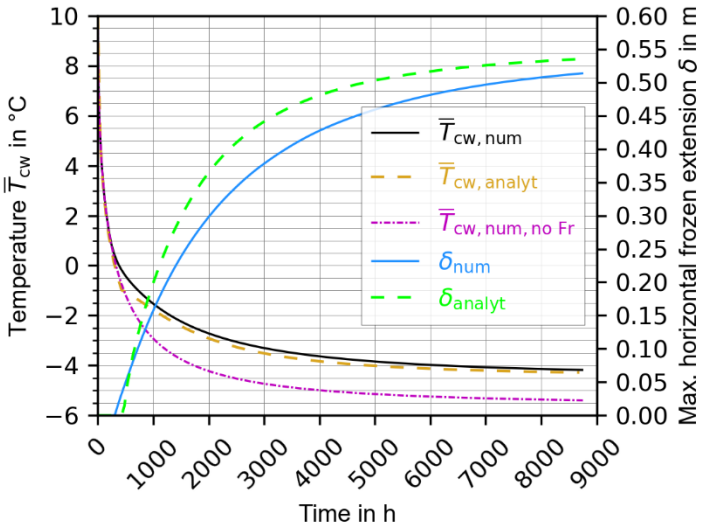

Fig. 4-11: Mean collector wall temperature and maximum horizontal extension of the frozen soil in scenario I, comparing the numerical and analytical model results for a planar trench collector.

The results of both the analytical and numerical simulations for scenario II are shown in Fig. 4-12. At first sight, the analytical model seems to represent the numerical results less accurately as in the case of the horizontal pipe model. However, upon closer examination and consideration of the design parameters, there is a temporal shift of the maximum horizontal extension of the frozen ground and the temperature development during thawing. By comparison of the design critical parameters, i.e. the overall minimum temperature and maximum horizonal extent of the frozen ground, the discrepancy is less significant. This specific consideration was neglected in the previous comparisons, as the overall agreement was regarded as satisfactory. The deviations of both parameters are visually emphasised in red in Fig. 4-12. The minimal temperature at the collector wall simulated with the analytical model is only 0.7 K lower than the numerical result. On the other hand, the maximum horizontal extension of the frozen ground is approximately 10 cm (or 14.4%) larger in the analytical solution. Both deviations lead to a more conservative estimation of the collector's performance, ensuring that no underdimensioning occurs. Without considering frost formation in the soil, the calculated temperature change would be more than 2 K larger than the one predicted by the proposed model, leading to a significant deviation from reality and an overly conservative design.

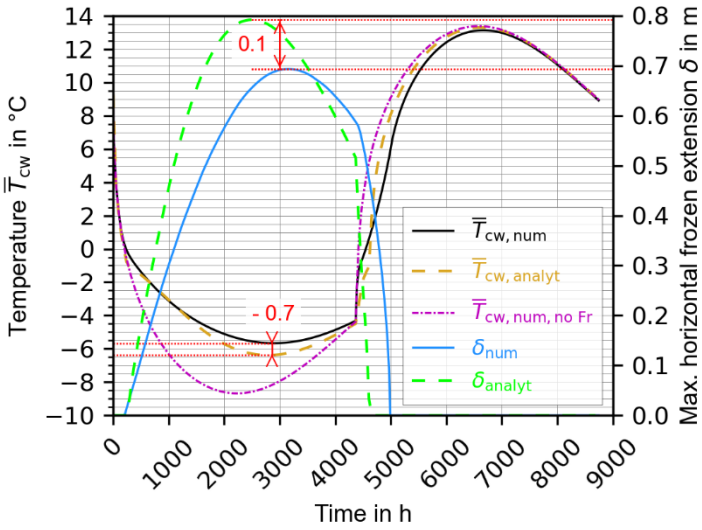

Fig. 4-12: Mean collector wall temperature and maximum horizontal extension of the frozen ground for scenario II, comparing both the numerical and analytical models for a planar trench collector.

4.5 Discussion

The presented analytical modelling approach shows very good results for the mean collector wall temperature with deviations below 1.4 K for both analysed collector variants. Through the application of the dimensionless temperature response of the linear conduction problem, the dynamics of such temperature responses can be seamlessly preserved, even below the freezing temperature. This is achieved by adjusting the soil properties to account for the frozen state as soon as the freezing temperature is exceeded. Even though the temperature below the freezing point does not precisely match the numerical simulation, it is still sufficiently accurate, leaving little need for further adjustments.

However, the maximum extension of the frozen ground, especially for the planar trench collector, shows larger deviations of the analytical model compared to the numerical simulation. For the horizontal pipe, the deviation is not significant, ranging from a few millimetres to under 2 cm, and within a maximum range of approximately 10% for the investigated scenarios. Considering the temporal shift in the planar trench collector results, the deviation between the maximum horizontal extension of the frozen ground occurring in both models reaches a maximum of approximately 10 cm or 14%. To comprehend the greater discrepancy of the planar trench collector results, it is essential to analyse the frost expansion and the temperature distribution at the collector surfaces of the numerical simulations.

Fig. 4-4 depicts the temperature distribution of the horizontal pipe investigated. It is clearly evident that the temperature distribution at the collector pipe wall is homogeneous, and the temperature profile (and thus, the propagation of the frozen ground) expands outward in a nearly radially symmetric manner. Additionally, due to the model's 2D geometry, no secondary

effects arise, such as temperature gradients at the pipe's inlet or outlet. Consequently, the shape factor of the analytical model corresponds very closely to the numerical results. The minor deviation in the maximum extent of the frozen ground can be attributed to the minimally asymmetric temperature and thus, frost distribution around the collector pipe.

Fig. 4-13 shows the temperature distribution of the planar trench collector. It can be observed that the temperature distribution at the collector surface is pronounced non-uniform, with variations extending over a range greater than 6 K and even a small area with temperatures remaining above 0 °C. This significant temperature inhomogeneity, along with the non-uniform distribution of the frozen ground around the collector surface, complicates the determination of the correct frozen volume and its corresponding maximum extent.

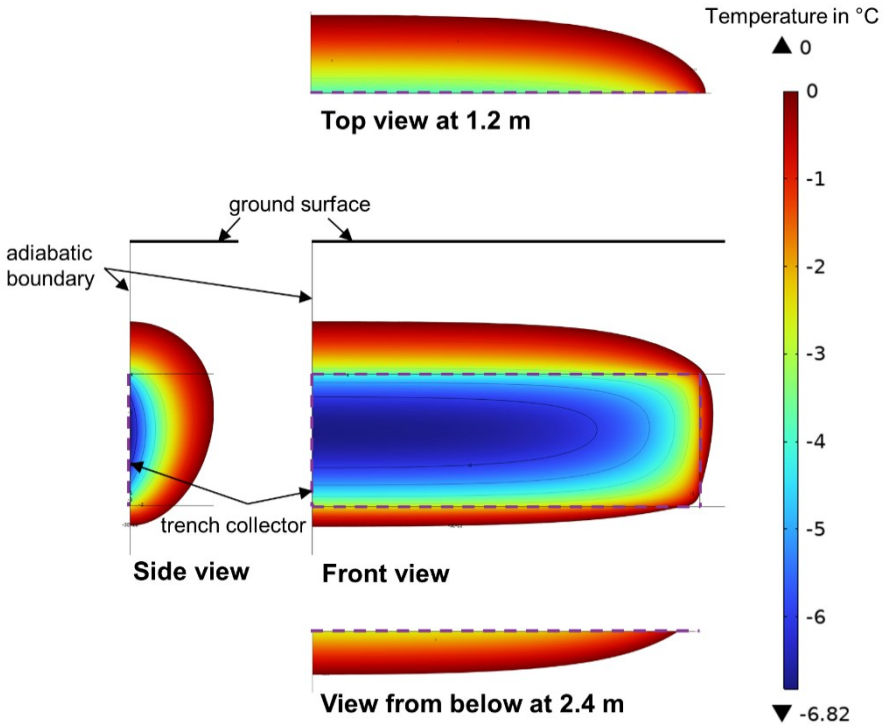

Fig. 4-13: Orthogonal projection of the temperature distribution around the planar trench collector of the second scenario after 2016 hours of heat extraction.

4.6 Interim conclusions

This study presents an analytical modelling methodology for geothermal heat collectors, which freeze the subsurface around them. The method is structured as follows:

- Up to the freezing temperature, solely an analytical source solution is used, which matches the corresponding collector geometry.
- Once the subsurface freezes, a thermal power balance is set up, consisting of the total extracted heat flow rate, the conductive heat flow rate from the surrounding ground, and the latent heat flow rate stored during the freezing process. The conductive heat

flow rate is split up into so-called frozen and unfrozen components. The unfrozen component defines the conductive heat flow rate up to the frost temperature using unfrozen subsurface properties, whereas the frozen part is defined by the temperature difference between the frost temperature and the temperature at the collector wall of the previous time step and using frozen subsurface properties.

- The spatially averaged collector wall temperature is calculated by simple heat conduction equations over the distance between the source and the isotherm at freezing temperature. Since the extent of the frozen ground highly depends on the collector geometry, a suitable shape factor for each collector geometry has to be applied.
- The maximum extension of the frozen soil also highly depends on the collector geometry and consequently must be determined individually for each collector geometry under consideration.

The methodology outlined was applied to both a horizontal pipe configuration and a planar trench collector for various scenarios. All scenarios were subjected to a comparison with numerical results. The horizontal pipe model shows good agreement for both the collector wall temperature as well as the maximum extent of the frozen ground. With a deviation of around 10%, this model provides a solid foundation for the design of such systems. Considering the design critical parameters, the planar trench collector model exhibits slightly higher deviations of up to 14% for the maximum extension of the frozen ground. This is due to the more complex geometry and the non-homogeneous temperature distribution at the collector wall, and thus, directly influences the corresponding extent of the frozen ground. However, the collector wall temperature can be determined quite accurate with this model.

Thus, it can be concluded that the presented model approach is basically highly effective for the design of ground-source heat collector systems, as the temperature at the collector wall can be determined with deviations of less than 1.4 K, while the accuracy for predicting the maximum extent of the frozen ground reaches at least 85.6%. For a horizontal pipe, the presented method enables accurate calculation of both the mean temperature at the collector wall and the extent of the frozen ground, making it suitable for the design of such systems. For the planar trench collector, the analytical model shows greater deviations but provides satisfactory results for the design of such systems. However, for a precise transient development of the collector wall temperature and the propagation of the frozen ground, the model used to determine the maximum horizontal extent of the frozen ground should be optimised. Furthermore, the current modelling approach does not yet account for adjacent collector pipes or collector plates within a ground-coupled heat pump system, which remains an area for future development.

5 Synthesis of findings

Given the need of increasing ground-source heat pumps as a sustainable heating and cooling technology, the conclusions drawn from this thesis provide further perspectives for improving and extending the contributions to the presented, analytical, consistent modelling methodology, which serves as a tool to enhance and facilitate broader adoption of shallow geothermal applications. First, the key findings of this work are summarised and concluded, followed by proposals for future investigations, which are identified from open questions.

5.1 General summary and conclusions

The presented analytical, consistent modelling method serves the purpose of a neutral comparison of the performance of shallow geothermal, closed-loop systems at a particular location. This provides a valuable decision support for the most suitable source system(s) at the considered location – supporting an optimal balance of initial investigation costs and performance efficiency for the client, while offering easy-to-use modelling approaches for design engineers. The methodology breaks-down the calculation domain into two parts: the source system itself, including the installation situation, and the surrounding subsurface, including surface influences. The source system itself is modelled by analytical resistance models and, if applicable, extended by capacity models; whereas the surrounding subsurface is represented by extensions of the instantaneous point source. Relevant heat transfer processes, which cannot be represented by one of the aforementioned modelling approaches, are to be considered as approximations by complementary solutions. The last modelling aspect to mention is the principle of superposition, which can be applied for time-varying heat loads as well as for considering thermal interference within a source field.

The applied use of the consistent modelling methodology is demonstrated through three examples. The first application focusses on grouted borehole heat exchangers (BHEs) with groundwater advection, i.e. the application of moving sources extended with a complementary solution for the grouted area of the borehole, which is not subjected to groundwater flow. Furthermore, the applicability of borehole resistance models for BHEs with groundwater advection are assessed as suitable. The second example shows the use of extensions of the instantaneous point source for alternative geometries, an application of a resistance model for a planar ground heat collector (GHC) and the consideration of seasonal temperature variations within the installation depth. As a final point, an analytical modelling approach for freezing and thawing around GHCs is developed and the applicability of the complementary solution is shown for two variants through validation with numerical simulations.

The investigations of BHEs in Chapter 2 first addressed the compatibility of thermal borehole resistance models for BHEs with groundwater advection, as this thermal effect leads to a non-radially symmetric distribution of temperature around the borehole. Since resistance models assume this radially symmetric distribution, numerical simulations with and without groundwater advection are evaluated, as well as an analytical solution of heat conduction in an annulus. With a deviation of less than 1%, the borehole resistance averaged over the borehole wall is identical for a subsurface with and without groundwater advection. Thereafter, the applicability of the infinite moving line source (IMLS) to a BHE with finite length is examined, revealing discrepancies of less than 5% for BHEs of at least 30 m and having Péclet numbers of greater than 0.05. Finally, and central to the topic of BHEs, detailed investigations are conducted to understand the deviations between the analytical steady-state solution of the IMLS and the numerical simulation with a sealed backfilling within the borehole. The extensive analysis of the parameter impacts led to the conclusion that the discrepancy depends on the Péclet number. With this knowledge, a correction function was proposed to overcome the underestimation by the steady-state *g*-function. The impact of using the IMLS, the finite line source and the IMLS with a correction function is demonstrated for various subsurface types, illustrating the potential savings in both drilling depth and heat extraction rate when applying the IMLS. In addition, the consequences of underestimating the steady-state *g*-function in backfilled boreholes – if no correction is applied – are also highlighted. These examples emphasise the importance of the introduced correction function for backfilled BHEs.

Chapter 3 covers an example of extending the instantaneous point source for a planar geometry and isothermal boundary condition. For this purpose, the mathematical formulation of a finite plane source is derived alongside a computational optimisation and a dimensional analysis, forming the foundation for understanding the heat transfer characteristics of planar trench collectors. The dimensional analysis facilitates the formulation and derivation of the dimensionless temperature response, along with the corresponding dimensionless parameters. By reducing the number of governing variables, it simplifies the complexity and minimises the variety of dimensionless temperature responses needed. Furthermore, a collector resistance to represent the heat transfer from the circulating fluid to the subsurface is introduced, as well as the consideration of the spatial-mean of seasonal temperature variations over the collector height. Finally, Chapter 3.3.1.5 outlines the algorithm for determining the collector outlet temperature based on the aforementioned thermal models. Beyond verification through numerical simulations, the algorithm is further validated through measurement data obtained from three thermal response tests (TRTs) conducted at the test field in Biberach (Riß), demonstrating the applicability of the presented model.

A general, analytical approach to represent freezing and thawing around GHCs, in conformity with the defined analytical, consistent modelling methodology, is introduced in Chapter 4. This

contributes directly to the third objective, which extends the analysis of GHCs by examining the effects of freezing and thawing processes on their thermal performance. The general formulation of the modelling concept further allows for its application to all conceivable geometries of GHCs. The thermal impact of GHCs up to the freezing point can be effectively determined by applying dimensionless temperature responses, combined with the principle of superposition, as outlined in Chapter 3. Once the collector initiates freezing of the surrounding ground, a thermal power balance is established. Beyond the latent heat flow rate, the conductive heat flow, divided into an unfrozen and a frozen part are considered in the power balance. The unfrozen, conductive component quantifies the extracted heat flow rate down to the freezing temperature. In contrast, the frozen, conductive component represents the heat flow rate between the freezing temperature and the collector wall temperature from the previous time step. Both the unfrozen and frozen conductive components are calculated using the corresponding subsurface thermal properties. The subcooled mean collector wall temperature is defined by conductive heat transfer over the distance between the heat source and the freezing isotherm. This distance is inherently influenced by the collector geometry, which can be analytically described through an appropriate shape factor. Furthermore, the maximum extent of the frozen ground, similar to the shape factor, is highly dependent on the collector geometry and must be determined individually. This is important, as the maximum extension of the frozen ground represents a critical design criterion to prevent the merging of frozen zones between neighbouring collectors, thereby mitigating the risk of mud accumulation and ensuring sufficient infiltration of precipitation. Previous heat injection or extraction loads are accounted for by applying the principle of superposition. Beyond the general description, the method is implemented for horizontal pipes and planar trench collectors. Three scenarios are formulated to systematically validate both analytical models against numerical simulations. As the collector wall temperatures reached a temperature deviation of less than 1.4 K, it can be stated, that the presented approach is highly effective for the temperature prediction. In contrast, the calculated maximum extension of the frozen ground reaches an accuracy of 85.6% which offers opportunity for further optimisations of the model. Overall, the horizontal pipe model yields more accurate results compared to the planar trench collector model.

In summary, the developed approaches in Chapter 2, 3 and 4 highlight the potential of the proposed analytical, consistent modelling methodology for shallow geothermal closed-loop systems. Building on this foundation, it is essential to further pursue and refine these developments to fully exploit their capabilities and ensure further advancements in this field.

5.2 Outlook

Although this work has made valuable contributions towards closing the modelling gaps in thermal characterisation of various phenomena of BHEs and GHCs, as well as in the application of the analytical, consistent modelling methodology, several opportunities remain for optimising the presented approaches and extending the methodology to additional shallow geothermal sources, while other thermal phenomena of shallow geothermal closed-loop systems are yet to be explored.

With regard to optimisations of the presented approach for BHEs with groundwater advection, investigations on the transient behaviour of the IMLS for backfilled BHEs remain pending. This is particularly relevant under conditions of low-velocity groundwater flow or when short-term BHE behaviour is analysed. Furthermore, as the subsurface typically comprises a variety of soil types – including both permeable and impermeable layers alongside unsaturated zones – it is essential to incorporate multiple subsurface layers into the design model. Therefore, it is necessary to assess the correction function and adapt it to the finite moving line source (FMLS) model as part of a multilayer model if required. The modelling of BHE fields with groundwater advection using the IMLS and the impact of backfilled boreholes on the modelling accuracy is already investigated in Koenigsdorff et al. (2023). Based on these investigations, a transient and layered model – yet to be developed – for a single BHE with groundwater advection can readily be extended to a model for BHE fields.

Open issues concerning GHCs comprise an extensive validation of the presented analytical models through measurement data of ground freezing around a horizontal pipe and a planar trench collector. However, to accomplish this, a methodology must be developed for the conduction of experiments and the subsequent evaluation of its measurement data to enable model validation for ground freezing and thawing. In doing so, the key challenge lies in the accurate determination of soil properties such as porosity and thermal conductivity, while adequate measuring devices are required or need to be developed to meet demands not previously encountered. Within the QEWSplus research project, a prototype of such a measuring device and initial evaluation methods are developed, which, however, offer significant potential for optimisation (Van de Ven et al., 2022; Van de Ven et al., submitted 2025), and is therefore part of a further research proposal. Beyond that, the validation of the planar trench collector model through numerical simulations revealed optimisation potential for the estimation of the maximum extension of the frozen ground. A further research objective is the thermal characterisation of GHC fields, i.e. the thermal interference of neighbouring collectors and its influence on the system performance. Methodologically, this can be addressed by the development of dimensionless temperature responses for GHC fields and their embedding in the modelling approach for ground freezing and thawing around GHCs.

This objective is not limited to the geometries discussed in this work but also applies to further GHC geometries, for which a model already exists that conforms to the defined analytical, consistent modelling methodology but considers only a single collector. Finally, the application of the modelling approach for freezing and thawing around GHCs can be extended to additional collector geometries, e.g., slinky-coil collectors, geothermal baskets, etc. As extensions of the instantaneous point source for the characterisation of the heat conduction in the subsurface already exist to some degree (e.g. ring source), the main challenge lies in determining the maximum extent of the frozen ground. Especially for ring source models, the freezing of the soil within the ring, which is likely to be the limiting factor, is of particular interest for investigation.

To establish full applicability of the analytical, consistent modelling methodology for closed-loop sources, a key element is the characterisation of geothermally activated building structures and infrastructure (gTABS) and the development of a modelling approach within the defined consistent modelling framework. An essential distinction in terms of thermal modelling between these systems and BHEs or GHCs is the use of partially modified surface boundary conditions, e.g., energy piles (Sani et al., 2019), energy diaphragm walls (Di Donna et al., 2017) or slab absorbers (Neth and Koenigsdorff, 2024) underneath buildings, thermally activated sewers with challenging boundaries conditions inside the sewer (Kugler and Moormann, 2023), etc. Additionally, the capacity of the source system often has a significant impact on the thermal behaviour of these systems. Furthermore, it should be noted and considered in the design that for these systems structural requirements always take precedence over their thermal function. The aforementioned characteristics makes such systems highly relevant for detailed investigation and thermal analysis. By focusing on infrastructure such as sewers or tunnels, the importance of their thermal activation becomes increasingly significant in Germany, particularly with the obligation to implement municipal heat planning. To estimate their potential, for example, as part of a cold district heating network, user-friendly modelling tools are necessary to ensure they can be effectively considered in an early stage.

In addition to validating the models with short-term measurement data, a comparison with long-term measurement data is of particular interest, as the design phase aims to represent the long-term behaviour of the systems. The definition of long-term measurement data in this context highly depends on the source system and must therefore be chosen accordingly. While the long-term behaviour of BHEs spans several years, GHCs are typically designed to regenerate within one year. This validation would provide definitive proof of the suitability of the models avoiding both over- and underdimensioning. Initials steps have already been taken in the QEWSplus Research project, and the results will soon be published as part of the final

research report (Van de Ven et al., submitted 2025). Further work on this topic is planned in another proposed research project.

To expand the range of applications, a modelling framework for open-loop shallow geothermal systems that conforms to the defined analytical, consistent modelling methodology for closed-loop shallow geothermal systems can be developed. These include, for example, geothermal wells, whose performance significantly depend on the specific hydrogeology on-site. While the understanding of the associated heat and mass transfer processes is exciting, it poses a new challenge for representation within the analytical, consistent modelling methodology. The same applies to earth-air heat exchangers, although hydrogeology is not a factor in this context. Integrating these open-loop systems into the presented, analytical, consistent modelling methodology would allow a comprehensive, neutral comparison of all shallow geothermal source systems for the plot under consideration.

Lastly, the development of in-situ-system-TRTs – i.e. measurement and evaluation methods at the time of commissioning of the overall heat supply system, including the geothermal source, connecting pipes and manifold, and the heat pump – can enhance the quality of shallow geothermal systems and allow for early detection of issues such as insufficient heating performance or inefficiency. Initial results are already available on this topic for BHEs coupled to heat pump systems (Van de Ven et al., 2022). Nevertheless, there remain unaddressed analysis and tasks for BHE systems, as well as the development of such methods for other source systems. Therefore, this topic will also be explored further in a subsequent research project that is currently being proposed.

By investigating and implementing the previously mentioned points, essential planning tools for shallow geothermal systems would be established, which, owing to their user-friendly nature, are likely to diminish the barriers faced by planning engineers. As presented by Buchmiller (2025), all developed and future models are being implemented in a single modelling library, enabling designers to switch directly between source systems without changing software, thereby further reducing barriers during the design process. Consequently, this is expected to lead to an increased consideration of such systems and, ultimately, a higher frequency of their implementation, emphasising the importance of the additional proposed measures.

6 References

Abdelaziz, S.L., Ozudogru, T.Y., Olgun, C.G., Martin, J.R., 2014. Multilayer finite line source model for vertical heat exchangers. Geothermics 51, 406–416.

Aditya, G.R., Narsilio, G.A., 2020. Environmental assessment of hybrid ground source heat pump systems. Geothermics 87, 101868.

Ahmed, A.A., Assadi, M., Kalantar, A., Sliwa, T., Sapińska-Śliwa, A., 2022. A Critical Review on the Use of Shallow Geothermal Energy Systems for Heating and Cooling Purposes. Energies 15 (12), 4281.

Alzoubi, M.A., Zueter, A., Nie-Rouquette, A., Sasmito, A.P., 2019. Freezing on demand: A new concept for mine safety and energy savings in wet underground mines. International Journal of Mining Science and Technology 29 (4), 621–627.

Amadeh, A., Habibi, M., Hakkaki-Fard, A., 2020. Numerical simulation of a ground-coupled heat pump system with vertical plate heat exchangers: A comprehensive parametric study. Geothermics 88, 101913.

Angelotti, A., Ly, F., Zille, A., 2018. On the applicability of the moving line source theory to thermal response test under groundwater flow: considerations from real case studies. Geotherm Energy 6 (1).

Antelmi, M., Alberti, L., Angelotti, A., Curnis, S., Zille, A., Colombo, L., 2020. Thermal and hydrogeological aquifers characterization by coupling depth-resolved thermal response test with moving line source analysis. Energy Conversion and Management 225, 113400.

Arthur Huber, 2016. Bedienungsanleitung zum Programm EWS. Huber Energietechnik AG, Zürich, 73 pp.

Arzanfudi, M.M., Al-Khoury, R., 2018. Freezing-thawing of porous media: An extended finite element approach for soil freezing and thawing. Advances in Water Resources 119, 210–226.

Bahmani, M.H., Hakkaki-Fard, A., 2022. A hybrid analytical-numerical model for predicting the performance of the Horizontal Ground Heat Exchangers. Geothermics, 2022, 102369.

Bandos, T.V., Montero, Á., Fernández, E., Santander, J.L.G., Isidro, J.M., Pérez, J., Córdoba, P.J.F. de, Urchueguía, J.F., 2009. Finite line-source model for borehole heat exchangers: effect of vertical temperature variations. Geothermics 38 (2), 263–270.

Bandyopadhyay, G., Gosnold, W., Mann, M., 2008. Analytical and semi-analytical solutions for short-time transient response of ground heat exchangers. Energy and Buildings 40 (10), 1816–1824.

Barbieri, S., Antelmi, M., Panday, S., Baratto, M., Angelotti, A., Alberti, L., 2022. Innovative numerical procedure for simulating borehole heat exchangers operation and interpreting thermal response test through MODFLOW-USG code. Journal of Hydrology 614, 128556.

Bayer, P., Saner, D., Bolay, S., Rybach, L., Blum, P., 2012. Greenhouse gas emission savings of ground source heat pump systems in Europe: A review. Renewable and Sustainable Energy Reviews 16 (2), 1256–1267.

Bear, J., 1988. Dynamics of fluids in porous media, Repr. [d. Ausg.], New York, American Elsevier Pub., 1972, with corr ed. Dover books on physics and chemistry. Dover, New York, 764 pp.

Bennet, J., Claesson, J., Hellström, G., 1987. Multipole method to compute the conductive heat flows to and between pipes in a composite cylinder. Notes on Heat Transfer, Lund, Schweden.

Blocon AB, 2020. EED version 4 - Earth Energy Designer: Update manual. https://www.buildingphysics.com/manuals/EED4.pdf. Accessed 1 March 2021.

Blum, P., Campillo, G., Münch, W., Kölbel, T., 2010. CO2 savings of ground source heat pump systems – A regional analysis. Renewable Energy 35 (1), 122–127.

Bortoloni, M., Bottarelli, M., 2015. On the sizing of a flat-panel ground heat exchanger. Int J Energy Environ Eng 6 (1), 55–63.

Bottarelli, M., 2013. A preliminary testing of a flat panel ground heat exchanger. Int. J. Low-Carbon Tech. 8 (2), 80–87.

Bottarelli, M., Bortoloni, M., Su, Y., 2019. On the sizing of a novel Flat-Panel ground heat exchanger in coupling with a dual-source heat pump. Renewable Energy 142, 552–560.

Bottarelli, M., Bortoloni, M., Su, Y., Yousif, C., Aydın, A.A., Georgiev, A., 2015. Numerical analysis of a novel ground heat exchanger coupled with phase change materials. Applied Thermal Engineering 88, 369–375.

Bottarelli, M., Di Federico, V., 2012. Numerical comparison between two advanced HGHEs. Int. J. Low-Carbon Tech. 7 (2), 75–81.

Bottarelli, M., Fujii, H., Di Federico, V., 2014. Performance of a Drainage Trench Employed as Ground Heat Exchanger, in: International Heat Transfer Conference 15, Kyoto, Japan. 10-15.08.2014.

Buchmiller, D., 2025. GEO-HANDlight (GHL) & GEOSYST go GEO.Toolbox. Oberflächennahe Geothermie, 21 February 2025, Offenbach, Germany.

Cao, J., Bottarelli, M., Bortoloni, M., Pei, G., 2018. Small-scale lab analysis of the ground freezing effect on the thermal performance of a Flat-Panel ground heat exchanger. Geothermics 74, 247–254.

Carli, M. de, Tonon, M., Zarrella, A., Zecchin, R., 2010. A computational capacity resistance model (CaRM) for vertical ground-coupled heat exchangers. Renewable Energy 35 (7), 1537–1550.

Carslaw, H.S., Jaeger, J.C., 1959. Conduction of heat in solids, 2. ed. ed. Oxford science publications. Clarendon Press, Oxford, 510 pp.

Chaudhry, M.A., Zubair, S.M., 2001. On a Class of Incomplete Gamma Functions with Applications. Chapman and Hall/CRC.

Chiasson, A., O'Connell, A., 2011. New analytical solution for sizing vertical borehole ground heat exchangers in environments with significant groundwater flow: Parameter estimation from thermal response test data. HVAC&R Research 17 (6), 1000–1011.

Christodoulides, P., Vieira, A., Lenart, S., Maranha, J., Vidmar, G., Popov, R., Georgiev, A., Aresti, L., Florides, G., 2020. Reviewing the Modeling Aspects and Practices of Shallow Geothermal Energy Systems. Energies 13 (16), 4273.

Cimmino, M., 2018. Fast calculation of the g -functions of geothermal borehole fields using similarities in the evaluation of the finite line source solution. Journal of Building Performance Simulation 11 (6), 655–668.

Cimmino, M., 2021. An approximation of the finite line source solution to model thermal interactions between geothermal boreholes. International Communications in Heat and Mass Transfer 127, 105496.

Cimmino, M., Bernier, M., Adams, F., 2013. A contribution towards the determination of g-functions using the finite line source. Applied Thermal Engineering 51 (1-2), 401–412.

Ciriello, V., Bottarelli, M., Di Federico, V. (Eds.), 2015a. Uncertainty-based Analysis of Variations in Subsurface Thermal Field Due to Horizontal Flat-panel Heat Exchangers 25, 8 pp.

Ciriello, V., Bottarelli, M., Di Federico, V., Tartakovsky, D.M., 2015b. Temperature fields induced by geothermal devices. Energy 93, 1896–1903.

Claesson, J., Bennet, J., 1987. Multipole Method to Compute the Conductive Heat Flows to and Between Pipes in a Cylinder. Rapport: Institutionen för Byggnadsteknik. Department of Building Technology and [Department of] Mathematical Physics, University of Lund.

Claesson, J., Dunand, A., 1983. Heat extraction from the ground by horizontal pipes: a mathematical analysis.

Claesson, J., Hellström, G., 2000. Analytical Studies of the Influence of Regional Groundwater Flow by on the Performance of Borehole Heat Exchangers, in: Proceedings. TERRASTOCK 2000, 8th International Conference on Thermal Energy Storage : University of Stuttgart, Germany, August 28th until September 1st, 2000, Stuttgart, pp. 1–7.

Claesson, J., Hellström, G., 2011. Multipole method to calculate borehole thermal resistances in a borehole heat exchanger. HVAC&R Research 17 (6), 895–911.

COMSOL Multiphysics, 2019. COMSOL Multiphysics. COMSOL AB, Stockholm, Schweden.

COMSOL Multiphysics, 2021. Subsurface Flow Module: User´s Guide.

Congedo, P.M., Colangelo, G., Starace, G., 2012. CFD simulations of horizontal ground heat exchangers: A comparison among different configurations. Applied Thermal Engineering 33-34, 24–32.

Cui, P., Yang, W., Zhang, W., Zhu, K., Spitler, J.D., Yu, M., 2024. Advances in ground heat exchangers for space heating and cooling: Review and perspectives. Energy and Built Environment, 2024, 255–269.

Deutscher Wetterdienst, 2023. Deutschlandwetter im Jahr 2023: Erwärmungstrend hält an: 2023 mit neuem Rekord und reichlich Niederschlag, Offenbach, Germany.

Di Donna, A., Cecinato, F., Loveridge, F., Barla, M., 2017. Energy performance of diaphragm walls used as heat exchangers. Proceedings of the Institution of Civil Engineers - Geotechnical Engineering 170 (3), 232–245.

Diao, N., Li, Q., Fang, Z., 2004. Heat transfer in ground heat exchangers with groundwater advection. International Journal of Thermal Sciences 43 (12), 1203–1211.

Erol, S., François, B., 2018. Multilayer analytical model for vertical ground heat exchanger with groundwater flow. Geothermics 71, 294–305.

Eskilson, P., 1987. Thermal analysis of heat extraction boreholes. PhD. Thesis, Lund, Sweden.

Eslami-Nejad, P., Bernier, M., 2012. Freezing of geothermal borehole surroundings: A numerical and experimental assessment with applications. Applied Energy 98, 333–345.

European Commission, 2019. COMMUNICATION FROM THE COMMISSION TO THE EUROPEAN PARLIAMENT, THE EUROPEAN COUNCIL, THE COUNCIL, THE EUROPEAN ECONOMIC AND SOCIAL COMMITTEE AND THE COMMITTEE OF THE REGIONS The European Green Deal: COM(2019) 640 final, 24 pp.

European Parliament and Council, 2023a. DIRECTIVE (EU) 2023/1791 OF THE EUROPEAN PARLIAMENT AND OF THE COUNCIL of 13 September 2023 on energy efficiency and amending Regulation (EU) 2023/955 (recast): EED.

European Parliament and Council, 2023b. Directive (EU) 2023/2413 of the European Parliament and of the Council of 18 October 2023 amending Directive (EU) 2018/2001, Regulation (EU) 2018/1999 and Directive 98/70/EC as regards the promotion of energy from renewable sources, and repealing Council Directive (EU) 2015/652: RED III.

European Parliament and Council, 2024. Directive (EU) 2024/1275 of the European Parliament and of the Council of 24 April 2024 on the energy performance of buildings.: EPBD.

Fascì, M.L., Lazzarotto, A., Acuna, J., Claesson, J., 2019. Analysis of the thermal interference between ground source heat pump systems in dense neighborhoods. Science and Technology for the Built Environment 25 (8), 1069–1080.

Fascì, M.L., Lazzarotto, A., Acuña, J., Claesson, J., 2021. Simulation of thermal influence between independent geothermal boreholes in densely populated areas. Applied Thermal Engineering 196, 117241.

Figueira, J.S., García Gil, A., Vieira, A., Michopoulos, A.K., Boon, D.P., Loveridge, F., Cecinato, F., Götzl, G., Epting, J., Zosseder, K., Bloemendal, M., Woods, M., Christodoulides, P., Vardon, P.J., Borg, S.P., Erbs Poulsen, S., Andersen, T.R., 2024. Shallow geothermal energy systems for district heating and cooling networks: Review and technological progression through case studies. Renewable Energy 236, 121436.

Fontaine, P.-O., Marcotte, D., Pasquier, P., Thibodeau, D., 2011. Modeling of horizontal geoexchange systems for building heating and permafrost stabilization. Geothermics.

Fujii, H., Nishi, K., Komaniwa, Y., Chou, N., 2012. Numerical modeling of slinky-coil horizontal ground heat exchangers. Geothermics 41, 55–62.

Gabrielli, L., Bottarelli, M., 2016. Financial and economic analysis for ground-coupled heat pumps using shallow ground heat exchangers. Sustainable Cities and Society 20, 71–80.

Gan, G., 2013. Dynamic thermal modelling of horizontal ground-source heat pumps. Int. J. Low-Carbon Tech. 8 (2), 95–105.

Gehlin, S., 2002. Thermal Response Test: Method Development and Evaluation. Doctoral Thesis, Lulea, Schweden.

Gerola, M., Cecinato, F., Haasnoot, J.K., Vardon, P.J., 2023. Understanding the Thermal Efficiency of Energy Quay Walls: A Comprehensive Study Using Field Tests and Finite Element Simulations, in: Comsol conference Munich 2023. Comsol conference Munich 2023, Munich, pp. 1–6.

Giardina, J.J., 1995. Evaluation of ground coupled heat pumps for the state of wisconsin. Master thesis, Wisconsin.

Glück, B., 2009. Simulationsmodell “Erdwärmekollektor” zur wärmetechnischen Beurteilung von Wärmequellen, Wärmesenken und Wärme-Kältespeichern.

Go, G.-H., Lee, S.-R., Yoon, S., Kim, M.-J., 2016. Optimum design of horizontal ground-coupled heat pump systems using spiral-coil-loop heat exchangers. Applied Energy 162, 330–345.

Gossler, M.A., Bayer, P., Zosseder, K., 2019. Experimental investigation of thermal retardation and local thermal non-equilibrium effects on heat transport in highly permeable, porous aquifers. Journal of Hydrology 578, 124097.

Gu, Y., O´Neal, D. L., 1998. Development of an Equivalent Diameter Expression for Vertical U-Tubes Used in Ground-Coupled Heat Pumps. ASHRAE Transactions.

Gu, Y., O’Neal, D.L., 1995. An Analytical Solution to Transient Heat Conduction in a Composite Region With a Cylindrical Heat Source. Journal of Solar Energy Engineering 117 (3), 242–248.

Guo, Y., Hu, X., Banks, J., Liu, W.V., 2020. Considering buried depth in the moving finite line source model for vertical borehole heat exchangers—A new solution. Energy and Buildings 214, 109859.

Gupta, A., Loveridge, F., Shafagh, I., Rees, S., 2022. An Analytical Approach to Evaluate the Heat Transfer through the Embedded Retaining Walls, in: European Geothermal Congress 2022. Proceedings. European Geothermal Congress, Berlin. 18.10.2022 - 20.10.2022.

Habibi, M., Amadeh, A., Hakkaki-Fard, A., 2020. A numerical study on utilizing horizontal flat-panel ground heat exchangers in ground-coupled heat pumps. Renewable Energy 147, 996–1010.

Hecht-Méndez, J., Paly, M. de, Beck, M., Bayer, P., 2013. Optimization of energy extraction for vertical closed-loop geothermal systems considering groundwater flow. Energy Conversion and Management 66, 1–10.

Hellström, G., 1991. Ground heat storage: thermal analyses of duct storage systems. disseration, Lund, Sweden, 277 pp.

Hellström, G., Mazzarella, L., Pahud, D., 1996. Duct Ground Heat Storage Model (DST): TRNSYS. Department of Mathematical Physics, University of Lund, Lund, Sweden.

Helsen, L., 2016. Geothermally activated building structures. Advances in Ground-Source Heat Pump Systems, 423–452.

Hirsch, H., Petzold, H., Grunewald, J., 2019. Efficiency and area demand of multi-layer ground heat exchanger using phase change of water, in: fourth Central European Symposium on Building Physics. CESBP 2019, Prague, Czech Republic. 2.-5.09.2019, p. 2027.

Hou, G., Taherian, H., Song, Y., Jiang, W., Chen, D., 2022. A systematic review on optimal analysis of horizontal heat exchangers in ground source heat pump systems. Renewable and Sustainable Energy Reviews 154, 111830.

Huang, S., Guo, Y., Liu, Y., Ke, L., Liu, G., chen, C., 2018. Study on the influence of water flow on temperature around freeze pipes and its distribution optimization during artificial ground freezing. Applied Thermal Engineering 135, 435–445.

Hüsing, F., Hirsch, H., Rockendorf, G., 2016. Combination of Solar Thermal Collectors and Horizontal Ground Heat Exchangers as Optimized Source for Heat Pumps, in: EuroSun 2016, Palma de Mallorca, Spain. 11.-14.10.2016, pp. 1–11.

Hüsing, F., Mercker, O., Hirsch, H., Kuntz, D.C., Walker-Hertkorn, S., Sabel, M., 2018. Erdwärmekollektoren und Sonnenkollektoren als optimierte bivalente Quelle für hocheffiziente Wärmepumpensysteme : Kurzbezeichnung: Terra-Solar-Quelle : gemeinsamer Abschlussbericht zum Verbundvorhaben : Laufzeit: 01.02.2015-31.03.2018.

Incropera, F., DeWitt, D.P., Bergman, T.L., Lavine, A.S., 2013. Principles of heat and mass transfer, 7. ed., international student version ed. Wiley, Hoboken, NJ, 1048 pp.

Jaeger, J.G., 1944. XVIII. Some problems involving line sources in conduction of heat. The London, Edinburgh, and Dublin Philosophical Magazine and Journal of Science 35 (242), 169–179.

Javed, S., Claesson, J., 2011. New analytical and numerical solutions for the short-term analysis of vertical ground heat exchangers. ASHRAE Transactions 117 (1), 3–12.

Javed, S., Fahlén, P., Claesson, J., 2009. Vertical ground heat exchangers: A review of heat flow models. Effstock 2009, Stockholm - Proceedings.

Javed, S., Spitler, J.D., 2016. Calculation of borehole thermal resistance 35, 63–95.

Jeon, J.-S., Lee, S.-R., Kim, M.-J., 2018. A modified mathematical model for spiral coil-type horizontal ground heat exchangers. Energy, 2018, 732–743.

Jiménez-Xamán, C., Xamán, J., Moraga, N.O., Hernández-Pérez, I., Zavala-Guillén, I., Arce, J., Jiménez, M.J., 2019. Solar chimneys with a phase change material for buildings: An overview using CFD and global energy balance. Energy and Buildings 186, 384–404.

Karrer, H., Hagel, K., Kirschbaum, A., Kötting, I., Kuckelkorn, J.M., Osgyan, P., Pendzich, L., Pinnekamp, M., Reuß, M., Streib, G., Bachseitz, M., Koenigsdorff, R., Van de Ven, A., Meier, S., Fuchs, H., Koch, F., Steger, H., Wilke, S., Schindler, L., Schüppler, S., Zorn, R., Lutz, T., Reduth, Y., Riegger, M., Rolker, J., Burkhardt, F. (Eds.), 2020. Qualitätssicherung bei Erdwärmesonden II mit Beteiligung am IEA ECES ANNEX 27 - QEWS II : Schlussbericht : Laufzeit des Vorhabens: 01.10.2016-31.03.2020. ZAE Bayern.

Katsura, T., Nagano, K., Kindaichi, S., Shimakura, K., 2006. Heat transfer experiment in the ground with ground water advection. Proceedings of 10th Energy Conservation THerMal Energy Storage Conference.

Kavanaugh, S.P., 1985. Simulation and Experimental Verification of Vertical Ground-coupled Heat Pump Systems. Dissertation, Stillwater, Oklahoma, USA.

Kelvin, W.T.B., 1890. Mathematical and Physical Papers. University Press.

Koenigsdorff, R., 2011. Oberflächennahe Geothermie für Gebäude: Grundlagen und Anwendungen zukunftsfähiger Heizung und Kühlung. Fraunhofer IRB-Verl., Stuttgart, 332 pp.

Koenigsdorff, R., Schleichert, L., Van de Ven, A., 2023. Fast Calculation Method for Borehole Heat Exchanger Fields in Groundwater Flow, in: GeoTHERM Journal. GeoTHERM expo & Congress, Offenburg, Offenburg, pp. 17–25.

Kölbel, T., 2010. Grundwassereinfluss auf Erdwärmesonden: Geländeuntersuchungen und Modellrechnungen. Dissertation, Karlsruhe.

Kugler, T., Moormann, C., 2023. Thermal activation of sewers and embedding in a heating-cooling network. SEG, 1–2.

Kürten, S., Mottaghy, D., Ziegler, M., 2015. A new model for the description of the heat transfer for plane thermo-active geotechnical systems based on thermal resistances. Acta Geotech. 10 (2), 219–229.

Kusuda, T., Achenbach, P.R., 1965. Earth temperature and thermal diffusivity at selected stations in the United States, 236 pp.

Lamarche, L., 2019. Horizontal ground heat exchangers modelling. Applied Thermal Engineering 155, 534–545.

Lamarche, L., 2021. Analytic models and effective resistances for coaxial ground heat exchangers. Geothermics 97, 102224.

Lamarche, L., 2023. Fundamentals of Geothermal Heat Pump Systems: Design and Application, 1st ed. 2023 ed. Springer Nature Switzerland; Imprint Springer, Cham, 295214 pp.

Lamarche, L., Beauchamp, B., 2007a. A new contribution to the finite line-source model for geothermal boreholes. Energy and Buildings 39 (2), 188–198.

Lamarche, L., Beauchamp, B., 2007b. New solutions for the short-time analysis of geothermal vertical boreholes. International Journal of Heat and Mass Transfer 50 (7-8), 1408–1419.

Lamarche, L., Kajl, S., Beauchamp, B., 2010. A review of methods to evaluate borehole thermal resistances in geothermal heat-pump systems. Geothermics 39 (2), 187–200.

Larwa, B., Teper, M., Grzywacz, R., Kupiec, K., 2019. Study of a slinky-coil ground heat exchanger – Comparison of experimental and analytical solution. International Journal of Heat and Mass Transfer 142, 118438.

Lazzari, S., Priarone, A., Zanchini, E., 2010. Long-Term Performance of Borehole Heat Exchanger Fluids with Groundwater Movement: Excerpt from the Proceedings of the COMSOL Conference 2010 Paris. Proceedings COMSOL Conference 2010, 2010.

Lazzarotto, A., Pallard, W.M., 2019. Thermal Response Test Performance Evaluation with Drifting Heat Rate and Noisy Measurements, in: , European Geothermal Congress, pp. 1–9.

Li, H., Nagano, K., Lai, Y., 2012a. A new model and solutions for a spiral heat exchanger and its experimental validation. International Journal of Heat and Mass Transfer 55 (15-16), 4404–4414.

Li, H., Nagano, K., Lai, Y., 2012b. Heat transfer of a horizontal spiral heat exchanger under groundwater advection. International Journal of Heat and Mass Transfer 55 (23-24), 6819–6831.

Li, M., Lai, A.C., 2012. New temperature response functions (G functions) for pile and borehole ground heat exchangers based on composite-medium line-source theory. Energy 38 (1), 255–263.

Li, S., Sun, T., Du, Y., Li, M., 2022. Influence of moisture on heat transfer of ground heat exchangers in unsaturated soils. Renewable Energy 193, 1177–1185.

Liu, R., Zhang, W., Han, S., Du, H., Cui, P., Ma, Z., Feng, X., Zhang, W., 2025. A numerical heat transfer model and performance evaluation of coaxial geothermal heat exchanger under soil freezing conditions. Applied Thermal Engineering 266, 125538.

Man, Y., Yang, H., Diao, N., Liu, J., Fang, Z., 2010. A new model and analytical solutions for borehole and pile ground heat exchangers. International Journal of Heat and Mass Transfer 53 (13-14), 2593–2601.

Marcotte, D., Pasquier, P., 2008. On the estimation of thermal resistance in borehole thermal conductivity test. Renewable Energy 33 (11), 2407–2415.

MEFA Befestigungs- und Montagesysteme GmbH, 2022. Datenblatt mulitQ geo 1270. https://www.multiq.energy/Energy%20Systems/Dokumente/Datenblatt%20multiQ%20geo.pdf.

Milagros Garcia Salciarini, 2024. Pump it down: why heat pump sales dropped in 2023. https://www.ehpa.org/wp-content/uploads/2024/04/Pump-it-down-why-heat-pump-sales-dropped-in-2023_EHPA_April-2024.pdf. Accessed 23 January 2025.

Miocic, J.M., Schleichert, L., Van de Ven, A., Koenigsdorff, R., 2024. Fast calculation of the technical shallow geothermal energy potential of large areas with a steady-state solution of the finite line source. Geothermics 116, 102851.

Mohammadzadeh Bina, S., Fujii, H., Kosukegawa, H., Farabi-Asl, H., 2020. Evaluation of ground source heat pump system’s enhancement by extracting groundwater and making artificial groundwater velocity. Energy Conversion and Management 223, 113298.

Molina-Giraldo, N., Blum, P., Zhu, K., Bayer, P., Fang, Z., 2011. A moving finite line source model to simulate borehole heat exchangers with groundwater advection. International Journal of Thermal Sciences 50 (12), 2506–2513.

Neth, F., Koenigsdorff, R., 2024. Thermal investigation of geothermally activated building systems using Thermal-Response-Test method. Geothermics (123), 103–116.

Oh, H., Beckers, K., 2023. Cost and Performance Analysis for Five Existing Geothermal Heat Pump-Based District Energy Systems in the United States, 2023.

Ozudogru, T.Y., Olgun, C.G., Senol, A., 2014. 3D numerical modeling of vertical geothermal heat exchangers. Geothermics 51, 312–324.

Ramming, K., 2007. Bewertung und Optimierung oberflächennaher Erdwärmekollektoren für verschiedene Lastfälle. Zugl.: Dresden, Techn. Univ., Fak. Maschinenwesen, Diss., 2007. TUDpress, Dresden, 149 pp.

Rashid, F.L., Dhaidan, N.S., Hussein, A.K., Al-Mousawi, F.N., Younis, O., 2023. Ground heat exchanger in different configuration: Review of recent advances and development. Geoenergy Science and Engineering 227, 211872.

Rees, S.J., 2016a. An introduction to ground-source heat pump technology, in: Rees, S. (Ed.), Advances in Ground-Source Heat Pump Systems, 1. Aufl. ed. Elsevier Reference Monographs, s.l., pp. 1–25.

Rees, S.J., 2016b. Horizontal and compact ground heat exchangers, in: Rees, S. (Ed.), Advances in Ground-Source Heat Pump Systems, 1. Aufl. ed. Elsevier Reference Monographs, s.l., pp. 117–156.

Rees, S.J., He, M., 2013. A three-dimensional numerical model of borehole heat exchanger heat transfer and fluid flow. Geothermics 46, 1–13.

Reuß, M., Karrer, H., Gehlin, S., Andersson, O., Björn, H., Nagano, K., Katsura, T., Metzner, M., Boydens, W., Francois, L., Possemiers, M., Waucquez, B., Yang, L., Arola, T., Hussko, A., Lepphaharju, N., Söderlund, P., Burkhardt, F., Eckert, D., Heske, C., Koenigsdorff, R., Kudla, C., Kötting, I., Loeff, J., Proell, M., Riegger, M., Steger, H., Tekin, E., Van de Ven, A., Zorn, R., Paek, K.-N., Witte, H., Kalantar, A., Mazzotti, W., Cetin, A., Cetin, S., Girbalar, O.E., Kadioglu, Y.K., Kilkis, B., Oktay, M., Paksoy, H., 2020. Quality Management in Design, Construction and Operation of Borehole Systems IEA ECES ANNEX 27. International Energy Agency, 272 pp. https://www.iea-es.org/wp-content/uploads/public/IEA-ECES-ANNEX-27-Final-Report-20201118.pdf. Accessed 18 May 2025.

Rivera, J.A., Blum, P., Bayer, P., 2015a. Analytical simulation of groundwater flow and land surface effects on thermal plumes of borehole heat exchangers. Applied Energy 146, 421–433.

Rivera, J.A., Blum, P., Bayer, P., 2015b. Ground energy balance for borehole heat exchangers: Vertical fluxes, groundwater and storage. Renewable Energy 83, 1341–1351.

Rivera, J.A., Blum, P., Bayer, P., 2016. Influence of spatially variable ground heat flux on closed-loop geothermal systems: Line source model with nonhomogeneous Cauchy-type top boundary conditions. Applied Energy 180, 572–585.

Rivera, J.A., Blum, P., Bayer, P., 2017. Increased ground temperatures in urban areas: Estimation of the technical geothermal potential. Renewable Energy 103, 388–400.

Saner, D., Juraske, R., Kübert, M., Blum, P., Hellweg, S., Bayer, P., 2010. Is it only CO2 that matters? A life cycle perspective on shallow geothermal systems. Renewable and Sustainable Energy Reviews 14 (7), 1798–1813.

Sani, A.K., Singh, R.M., Amis, T., Cavarretta, I., 2019. A review on the performance of geothermal energy pile foundation, its design process and applications. Renewable and Sustainable Energy Reviews 106, 54–78.

Schramek, E.-R., Recknagel, H., Sprenger, E. (Eds.), 2005. Taschenbuch für Heizung und Klimatechnik: Einschließlich Warmwasser- und Kältetechnik : mit über 2100 Abbildungen und über 350 Tafeln sowie 4 Einschlagtafeln, 72. Aufl. ed. Münchner Beiträge zur Abwasser-, Fischerei- und Flußbiologie 55. Oldenbourg Industrieverlag, München, XXXIX, 2036, 56 str., [3] f. zganj. pril.

Schwarz, H., Jocic, N., Bertermann, D., 2022. Development of a Calculation Concept for Mapping Specific Heat Extraction for Very Shallow Geothermal Systems. Sustainability 14 (7), 4199.

Spitler, J.D., Gehlin, S.E., 2015. Thermal response testing for ground source heat pump systems—An historical review. Renewable and Sustainable Energy Reviews 50, 1125–1137.

Spitler, J.D., Marshall, C.L., Manickam, A., Dharapuram, M., Delahoussaye, R.D., Yeung, K.-W.D., Young, R., Bhargava, M., Mokashi, S., Yavuzturk, C., Haider, M., Xu, X., Cullin, J., Dickinson, B., Lee, E., Grundmann, R., 2016. GLHEPro 5.0 For Windows: Users' Guide. https://hvac.okstate.edu/sites/default/files/pubs/glhepro/GLHEPRO_5.0_Manual.pdf. Accessed 1 March 2021.

Stauffer, F., Bayer, P., Blum, P., Giraldo, N.M., Kinzelbach, W., 2017. THERMAL USE OF SHALLOW GROUNDWATER. CRC Press, [Place of publication not identified], 290 pp.

Suft, O., Bertermann, D., 2022. Long-term Monitoring of a Very Shallow Horizontal Collector System., in: European Geothermal Congress 2022. Proceedings. European Geothermal Congress, Berlin. 18.10.2022 - 20.10.2022, pp. 1–6.

Sutton, M.G., Nutter, D.W., Couvillion, R.J., 2003. A Ground Resistance for Vertical Bore Heat Exchangers With Groundwater Flow. Journal of Energy Recources Technology 125, 183–189.

Tye-Gingras, M., Gosselin, L., 2014. Generic ground response functions for ground exchangers in the presence of groundwater flow. Renewable Energy 72, 354–366.

Urchueguía, J.F., Badenes, B., Javadi, H., Mateo, M.Á., Armengot, B., 2023. Adapted composite two-region line source methods for evaluation of borehole heat exchangers with advanced materials. Applied Thermal Engineering 231, 120910.

Urresta, E., Moya, M., Campana, C., Cruz, C., 2021. Ground thermal conductivity estimation using the thermal response test with a horizontal ground heat exchanger. Geothermics, 2021, 102213.

Van de Ven, A., Bayer, P., Koenigsdorff, R., 2024. Analytical solution for the simulation of ground thermal conditions around planar trench collectors. Geothermics (124), 1–14.

Van de Ven, A., Braun, S., Denninger, M., Koenigsdorff, R., Neth, F., Schleichert, L., Kainzlsperger, M., Karrer, H., Kuckelkorn, J., Nienborg, B., Osgyan, P., Pendzich, L., Pinnekamp, M., Brand, T., Mangold, D., Reduth, Y., Theophil, T., Albers, A., Fuchs, H., Schilling, F., Steger, H., Huttenloch, P., Schindler, L., Zorn, R., Burkhardt, F., Bittscheidt, M., Hauri, F., Hauri, J., Hackstein, F., Kühl, J.-U., submitted 2025. Qualitätssteigerung oberflächennaher Geothermiesysteme - QEWSplus: Schlussbericht.

Van de Ven, A., Koenigsdorff, R., Hofmann, S., 2018. Entwicklung konsistenter Auslegungsmodelle für oberflächennahe geothermische Quellensysteme, in: BauSIM 2018. 7. Deutsch-Österreichische IBPSA-Konferenz. Tagungsband, Karlsruhe. 26. - 28. 09.2018, pp. 508–515.

Van de Ven, A., Koenigsdorff, R., Neth, F., Zorn, R., Schüppler, S., Huttenloch, P., Steger, H., Albers, A., Fuchs, H., Schilling, F., Karrer, H., Osgyan, P., Fuchs, M., Kainzlsperger, M., 2022. Advanced thermal and geophysical test methods of shallow geothermal systems, in: European Geothermal Congress 2022. Proceedings. European Geothermal Congress, Berlin. 18.10.2022 - 20.10.2022, pp. 1–9.

Van de Ven, A., Neth, F., Kainzlsperger, M., Koenigsdorff, R., 2023. Thermal Response Tests an Erdwärmekollektoren. Geothermische Energie (104), 12–15.

Van de Ven, A., Neth, F., Köhler, A., Albers, A., Schindler, L., Buchmiller, D., Denninger, M., Steger, H., Zorn, R., Koenigsdorff, R., 2025. Thermal reaction of the subsurface on the operation of a geothermal planar trench collector. Scientific Data 12 (1), 1661.

2013. VDI-Wärmeatlas: Mit 320 Tabellen, 11., bearb. und erw. Aufl. ed. VDI/-Buch]. Springer Vieweg, Berlin, Heidelberg, 1760 pp.

Verein Deutscher Ingenieure e. V., 2019. Thermische Nutzung des Untergrunds: Erdgekoppelte Wärmepumpenanlagen. Beuth Verlag GmbH, Berlin, 139 pp.

Verein Deutscher Ingenieure e. V., 2020. Thermische Nutzung des Untergrunds: Thermal Response Test (TRT). Beuth Verlag GmbH, Berlin, 64 pp.

Wagner, V., Bayer, P., Bisch, G., Kübert, M., Blum, P., 2014. Hydraulic characterization of aquifers by thermal response testing: Validation by large-scale tank and field experiments. Water Resour. Res. 50 (1), 71–85.

Wagner, V., Blum, P., Kübert, M., Bayer, P., 2013. Analytical approach to groundwater-influenced thermal response tests of grouted borehole heat exchangers. Geothermics 46 (2), 22–31.

Wang, D., Lu, L., Cui, P., 2016. A new analytical solution for horizontal geothermal heat exchangers with vertical spiral coils. International Journal of Heat and Mass Transfer 100, 111–120.

Westring, P., Gibb, D., Uguen, G., 2024. European Heat Pump Market and Statistics Report 2024: Summary for policy makers. https://www.ehpa.org/market-data/. Accessed 23 January 2025.

Witte, H.J., Heinrichs, F.A., Reichl, C., Meeng, C., Doerr, C., Steuerer, A., Kling, S., 2022. Development and validation of analytical solutions for earth basket (spiral) heat exchangers, in: European Geothermal Congress 2022. Proceedings. European Geothermal Congress, Berlin. 18.10.2022 - 20.10.2022, pp. 1–9.

Wu, Y., Gan, G., Verhoef, A., Vidale, P.L., Gonzalez, R.G., 2010. Experimental measurement and numerical simulation of horizontal-coupled slinky ground source heat exchangers. Applied Thermal Engineering 30 (16), 2574–2583.

Xiong, Z., Fisher, D.E., Spitler, J.D., 2015. Development and validation of a Slinky™ ground heat exchanger model. Applied Energy 141, 57–69.

Yang, W., Kong, L., Chen, Y., 2015. Numerical evaluation on the effects of soil freezing on underground temperature variations of soil around ground heat exchangers. Applied Thermal Engineering 75, 259–269.

Yang, W., Xu, R., Wang, F., Chen, S., 2020. Experimental and numerical investigations on the thermal performance of a horizontal spiral-coil ground heat exchanger. Renewable Energy 147, 979–995.

Yavuzturk, C., Spitler, J.D., Rees, S.J., 1999. A Transient Two-Dimensional Finite Volume Model for the Simulation of Vertical U-Tube Ground Heat Exchangers. ASHRAE Transactions (105(2)), 465–474.

Yoon, S., Lee, S.-R., Go, G.-H., 2014. A numerical and experimental approach to the estimation of borehole thermal resistance in ground heat exchangers. Energy 71, 547–555.

Young, T.R., 2004. Development, verification, and design analysis of the borehole fluid thermal mass model for approximating short term borehole thermal response. master thesis, Stillwater, USA.

Yu, X., Zhang, Y., Deng, N., Wang, J., Zhang, D., Wang, J., 2013. Thermal response test and numerical analysis based on two models for ground-source heat pump system. Energy and Buildings 66 (99), 657–666.

Zeng, H.Y., Diao, N.R., Fang, Z.H., 2002. A finite line-source model for boreholes in geothermal heat exchangers. Heat Trans. Asian Res. 31 (7), 558–567.

Zhang, L., Shi, Z., Yuan, T., 2020. Study on the Coupled Heat Transfer Model Based on Groundwater Advection and Axial Heat Conduction for the Double U-Tube Vertical Borehole Heat Exchanger. Sustainability 12 (18), 7345.

Zhou, M.M., Meschke, G., 2013. A three-phase thermo-hydro-mechanical finite element model for freezing soils. International Journal for Numerical and Analytical Methods in Geomechanics 37 (18), 3173–3193.

Zhou, Y., Bidarmaghz, A., Makasis, N., Narsilio, G., 2021. Ground-Source Heat Pump Systems: The Effects of Variable Trench Separations and Pipe Configurations in Horizontal Ground Heat Exchangers. Energies 14 (13), 3919.

Zhou, Y., Zheng, Z., Zhao, G., 2022. Analytical models for heat transfer around a single ground heat exchanger in the presence of both horizontal and vertical groundwater flow considering a convective boundary condition. Energy 245, 123159.

7 Appendix

7.1 Chapter 3 – Analytical simulation of heat conduction around planar trench collectors

Computationally optimised solution of the mean result of the FPS:

$$\bar{T}_{\mathrm{FPS}}(y,t) = \frac{\dot{q}}{4\pi\lambda L_{\mathrm{c}} H_{\mathrm{c}}} \quad (a+b+c+d+e+f+g+h+i+j+k+l+m+n+o+p+q+r) \tag{A I}$$

$$a = \frac{4}{3}\left((y^2)^{\frac{3}{2}} \operatorname{erfc}\left(\sqrt{\frac{y^2}{4\alpha t}}\right) - \sqrt{\frac{4\alpha t}{\pi}}(4\alpha t + y^2)\mathrm{e}^{\frac{-y^2}{4\alpha t}} \right)$$

$$-\left(y^2 + {H_{\mathrm{c}}}^2\right)^{\frac{3}{2}} \operatorname{erfc}\left(\sqrt{\frac{y^2 + {H_{\mathrm{c}}}^2}{4\alpha t}}\right) + \sqrt{\frac{4\alpha t}{\pi}}\left(4\alpha t + y^2 + {H_{\mathrm{c}}}^2\right)\mathrm{e}^{\frac{-y^2-{H_{\mathrm{c}}}^2}{4\alpha t}}$$

$$-\left({L_{\mathrm{c}}}^2 + y^2\right)^{\frac{3}{2}} \operatorname{erfc}\left(\sqrt{\frac{{L_{\mathrm{c}}}^2 + y^2}{4\alpha t}}\right) + \sqrt{\frac{4\alpha t}{\pi}}\left(4\alpha t + {L_{\mathrm{c}}}^2 + y^2\right)\mathrm{e}^{\frac{-{L_{\mathrm{c}}}^2-y^2}{4\alpha t}} \tag{A II}$$

$$+\left({L_{\mathrm{c}}}^2 + y^2 + {H_{\mathrm{c}}}^2\right)^{\frac{3}{2}} \operatorname{erfc}\left(\sqrt{\frac{{L_{\mathrm{c}}}^2 + y^2 + {H_{\mathrm{c}}}^2}{4\alpha t}}\right)$$

$$+\sqrt{\frac{4\alpha t}{\pi}}\left(4\alpha t + {L_{\mathrm{c}}}^2 + y^2 + {H_{\mathrm{c}}}^2\right)\mathrm{e}^{\frac{-{L_{\mathrm{c}}}^2-y^2-{H_{\mathrm{c}}}^2}{4\alpha t}}$$

$$b = \frac{2}{\sqrt{\pi}}(4\alpha t)^{\frac{3}{2}}\left(\mathrm{e}^{\frac{-y^2}{4\alpha t}} - \mathrm{e}^{\frac{-y^2-{H_{\mathrm{c}}}^2}{4\alpha t}} - \mathrm{e}^{\frac{-{L_{\mathrm{c}}}^2-y^2}{4\alpha t}} + \mathrm{e}^{\frac{-{L_{\mathrm{c}}}^2-y^2-{H_{\mathrm{c}}}^2}{4\alpha t}}\right) \tag{A III}$$

$$c = -8\alpha t L_{\mathrm{c}}\left(\mathrm{e}^{\frac{-y^2}{4\alpha t}} - \mathrm{e}^{\frac{-y^2-{H_{\mathrm{c}}}^2}{4\alpha t}}\right)\operatorname{erf}\left(\frac{L_{\mathrm{c}}}{\sqrt{4\alpha t}}\right) \tag{A IV}$$

$$d = -8\alpha t H_{\mathrm{c}}\left(\mathrm{e}^{\frac{-y^2}{4\alpha t}} - \mathrm{e}^{\frac{-{L_{\mathrm{c}}}^2-y^2}{4\alpha t}}\right)\operatorname{erf}\left(\frac{H_{\mathrm{c}}}{\sqrt{4\alpha t}}\right) \tag{A V}$$

$$e = 2\ L_c\sqrt{4\alpha t}$$

$$\int_{-L_c}^{L_c} \sqrt{\frac{\mu^2+y^2}{4\alpha t}}\ \operatorname{erfc}\left(\sqrt{\frac{\mu^2+y^2}{4\alpha t}}\right) - \sqrt{\frac{\mu^2+y^2+{H_c}^2}{4\alpha t}}\ \operatorname{erfc}\left(\sqrt{\frac{\mu^2+y^2+{H_c}^2}{4\alpha t}}\right) d\mu \tag{A VI}$$

$$f = 2H_c\sqrt{4\alpha t}$$

$$\int_{-H_c}^{H_c} \sqrt{\frac{y^2+\zeta^2}{4\alpha t}}\ \operatorname{erfc}\left(\sqrt{\frac{y^2+\zeta^2}{4\alpha t}}\right) - \sqrt{\frac{{L_c}^2+y^2+\zeta^2}{4\alpha t}}\ \operatorname{erfc}\left(\sqrt{\frac{{L_c}^2+y^2+\zeta^2}{4\alpha t}}\right) d\zeta \tag{A VII}$$

$$g = L_c\ H_c\sqrt{4\alpha t}\int_{-H_c}^{H_c}\int_{-L_c}^{L_c} \frac{\operatorname{erfc}\left(\sqrt{\frac{\mu^2+y^2+\zeta^2}{4\alpha t}}\right)}{\sqrt{\mu^2+y^2+\zeta^2}}\ d\mu\ d\zeta \tag{A VIII}$$

$$h = \frac{2}{3}\left\{ 2\left[\begin{array}{l} (y^2+(H_{\text{inst}}+H_{\text{tot}})^2)^{\frac{3}{2}}\operatorname{erfc}\left(\sqrt{\frac{y^2+(H_{\text{inst}}+H_{\text{tot}})^2}{4\alpha t}}\right) \\ -\sqrt{\frac{4\alpha t}{\pi}}(4\alpha t+y^2+(H_{\text{inst}}+H_{\text{tot}})^2)\mathrm{e}^{\frac{-y^2-(H_{\text{inst}}+H_{\text{tot}})^2}{4\alpha t}} \end{array} \right] \right. \\ -(y^2+(2H_{\text{inst}})^2)^{\frac{3}{2}}\operatorname{erfc}\left(\sqrt{\frac{y^2+(2H_{\text{inst}})^2}{4\alpha t}}\right) \\ +\sqrt{\frac{4\alpha t}{\pi}}(4\alpha t+y^2+(2H_{\text{inst}})^2)\mathrm{e}^{\frac{-y^2-(2H_{\text{inst}})^2}{4\alpha t}} \\ -(y^2+(2H_{\text{tot}})^2)^{\frac{3}{2}}\operatorname{erfc}\left(\sqrt{\frac{y^2+(2H_{\text{tot}})^2}{4\alpha t}}\right) \\ \left. +\sqrt{\frac{4\alpha t}{\pi}}(4\alpha t+y^2+(2H_{\text{tot}})^2)\mathrm{e}^{\frac{-y^2-(2H_{\text{tot}})^2}{4\alpha t}} \right\} \tag{A IX}$$

$$i = -\frac{2}{3}\left\{\begin{array}{l} 2\left[\begin{array}{l} \left(L_c{}^2 + y^2 + (H_{inst} + H_{tot})^2\right)^{\frac{3}{2}}\mathrm{erfc}\left(\sqrt{\dfrac{L_c{}^2 + y^2 + (H_{inst} + H_{tot})^2}{4\alpha t}}\right) \\ -\sqrt{\dfrac{4\alpha t}{\pi}}\left(4\alpha t + L_c{}^2 + y^2 + (H_{inst} + H_{tot})^2\right)\mathrm{e}^{\frac{-L_c{}^2 - y^2 - (H_{inst}+H_{tot})^2}{4\alpha t}} \end{array}\right] \\ -\left(L_c{}^2 + y^2 + (2H_{inst})^2\right)^{\frac{3}{2}}\mathrm{erfc}\left(\sqrt{\dfrac{L_c{}^2 + y^2 + (2H_{inst})^2}{4\alpha t}}\right) \\ +\sqrt{\dfrac{4\alpha t}{\pi}}\left(4\alpha t + L_c{}^2 + y^2 + (2H_{inst})^2\right)\mathrm{e}^{\frac{-L_c{}^2 - y^2 - (2H_{inst})^2}{4\alpha t}} \\ -\left(L_c{}^2 + y^2 + (2H_{tot})^2\right)^{\frac{3}{2}}\mathrm{erfc}\left(\sqrt{\dfrac{L_c{}^2 + y^2 + (2H_{tot})^2}{4\alpha t}}\right) \\ +\sqrt{\dfrac{4\alpha t}{\pi}}\left(4\alpha t + L_c{}^2 + y^2 + (2H_{tot})^2\right)\mathrm{e}^{\frac{-L_c{}^2 - y^2 - (2H_{tot})^2}{4\alpha t}} \end{array}\right\} \quad \text{(A X)}$$

$$j = \frac{(4\alpha t)^{\frac{3}{2}}}{\sqrt{\pi}}\left(2\mathrm{e}^{\frac{-y^2-(H_{inst}+H_{tot})^2}{4\alpha t}} - \mathrm{e}^{\frac{-y^2-(2H_{inst})^2}{4\alpha t}} - \mathrm{e}^{\frac{-y^2-(2H_{tot})^2}{4\alpha t}}\right) \quad \text{(A XI)}$$

$$k = -\frac{(4\alpha t)^{\frac{3}{2}}}{\sqrt{\pi}}\left(2\mathrm{e}^{\frac{-L_c{}^2-y^2-(H_{inst}+H_{tot})^2}{4\alpha t}} - \mathrm{e}^{\frac{-L_c{}^2-y^2-(2H_{inst})^2}{4\alpha t}} - \mathrm{e}^{\frac{-L_c{}^2-y^2-(2H_{tot})^2}{4\alpha t}}\right) \quad \text{(A XII)}$$

$$l = -4\alpha t L_c\left(2\mathrm{e}^{\frac{-y^2-(H_{inst}+H_{tot})^2}{4\alpha t}} - \mathrm{e}^{\frac{-y^2-(2H_{inst})^2}{4\alpha t}} - \mathrm{e}^{\frac{-y^2-(2H_{tot})^2}{4\alpha t}}\right)\mathrm{erf}\left(\frac{L_c}{\sqrt{4\alpha t}}\right) \quad \text{(A XIII)}$$

$$m = 2\alpha t\left(\mathrm{e}^{\frac{-y^2}{4\alpha t}} - \mathrm{e}^{\frac{-L_c-y^2}{4\alpha t}}\right)\left(\begin{array}{c} 4(H_{inst} + H_{tot})\mathrm{erf}\left(\dfrac{(H_{inst} + H_{tot})}{\sqrt{4\alpha t}}\right) \\ -4H_{inst}\ \mathrm{erf}\left(\dfrac{2H_{inst}}{\sqrt{4\alpha t}}\right) - 4H_{tot}\ \mathrm{erf}\left(\dfrac{2H_{tot}}{\sqrt{4\alpha t}}\right) \end{array}\right) \quad \text{(A XIV)}$$

$$
\begin{aligned}
&n \\
&= L_c \sqrt{4\alpha t} \int_{-L_c}^{L_c} 2 \sqrt{\frac{\mu^2 + y^2 + (H_{inst} + H_{tot})^2}{4\alpha t}} \operatorname{erfc}\left(\sqrt{\frac{\mu^2 + y^2 + (H_{inst} + H_{tot})^2}{4\alpha t}}\right) \\
&- \sqrt{\frac{\mu^2 + y^2 + (2H_{inst})^2}{4\alpha t}} \operatorname{erfc}\left(\sqrt{\frac{\mu^2 + y^2 + (2H_{inst})^2}{4\alpha t}}\right) \\
&- \sqrt{\frac{\mu^2 + y^2 + (2H_{tot})^2}{4\alpha t}} \operatorname{erfc}\left(\sqrt{\frac{\mu^2 + y^2 + (2H_{tot})^2}{4\alpha t}}\right) d\mu
\end{aligned}
\tag{A XV}
$$

$$
\begin{aligned}
&o = 4H_{inst} \sqrt{4\alpha t} \\
&\int_{2H_{inst}}^{H_{inst}+H_{tot}} \sqrt{\frac{{L_c}^2 + y^2 + \eta^2}{4\alpha t}} \operatorname{erfc}\left(\sqrt{\frac{{L_c}^2 + y^2 + \eta^2}{4\alpha t}}\right) \\
&\qquad - \sqrt{\frac{y^2 + \eta^2}{4\alpha t}} \operatorname{erfc}\left(\sqrt{\frac{y^2 + \eta^2}{4\alpha t}}\right) d\eta
\end{aligned}
\tag{A XVI}
$$

$$
\begin{aligned}
&p = 4H_{tot} \sqrt{4\alpha t} \\
&\int_{H_{inst}+H_{tot}}^{2H_{tot}} \sqrt{\frac{y^2 + \eta^2}{4\alpha t}} \operatorname{erfc}\left(\sqrt{\frac{y^2 + \eta^2}{4\alpha t}}\right) \\
&\qquad - \sqrt{\frac{{L_c}^2 + y^2 + \eta^2}{4\alpha t}} \operatorname{erfc}\left(\sqrt{\frac{{L_c}^2 + y^2 + \eta^2}{4\alpha t}}\right) d\eta
\end{aligned}
\tag{A XVII}
$$

$$
q = -2H_{inst} L_c \int_{2H_{inst}}^{H_{inst}+H_{tot}} \int_{-L_c}^{L_c} \frac{\operatorname{erfc}\left(\sqrt{\frac{\mu^2 + y^2 + \eta^2}{4\alpha t}}\right)}{\sqrt{\mu^2 + y^2 + \eta^2}} \, d\mu \, d\eta \tag{A XVIII}
$$

$$
r = 2H_{tot} L_c \int_{H_{inst}+H_{tot}}^{2H_{tot}} \int_{-L_c}^{L_c} \frac{\operatorname{erfc}\left(\sqrt{\frac{\mu^2 + y^2 + \eta^2}{4\alpha t}}\right)}{\sqrt{\mu^2 + y^2 + \eta^2}} \, d\mu \, d\eta \tag{A XIX}
$$

7.2 Chapter 4 – Analytical simulation of ground freezing and thawing around ground heat collectors

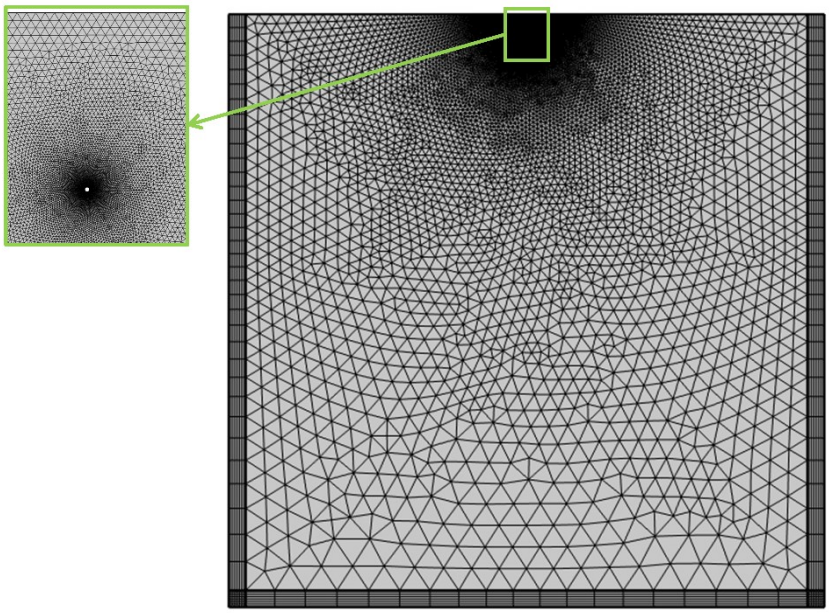

Fig. A 1: Mesh of the numerical model of the horizontal pipe with a zoom of the vicinity of the heat source. The mesh consists of 29,880 elements and is extreme fine in the vicinity of the source.

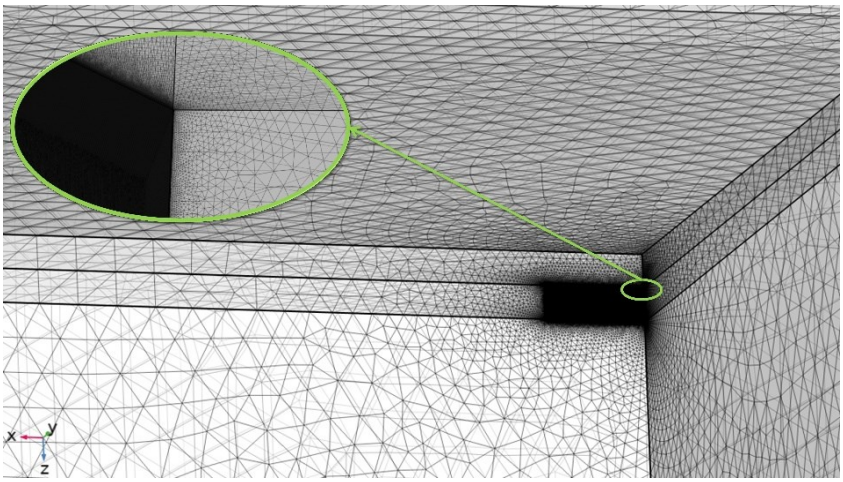

Fig. A 2: Mesh of the numerical model of the planar trench collector with a zoom of the vicinity of the heat source. As the collector is only 6 mm thick, the mesh is extremely fine at the source. The Mesh consists of 16,484,061 elements.

Curriculum vitae

Personal information

First name: Adinda

Last name: Van de Ven

Professional experience

Since 2016	Research Associate	Hochschule Biberach
2014–2016	Refrigeration Engineer	AL-KO THERM GMBH

Education

2011–2014	M. Sc. Gebäudeklimatik	Hochschule Biberach
2008–2011	B. A. Architektur	Hochschule Biberach

List of peer-reviewed publications

Van de Ven, A.; Koenigsdorff, R.; Bayer, P. (2021): Enhanced Steady-State Solution of the Infinite Moving Line Source Model for the Thermal Design of Grouted Borehole Heat Exchangers with Groundwater Advection. In: Geosciences 11 (10), S. 410. DOI: 10.3390/geosciences11100410.

Van de Ven, A.; Bayer, P.; Koenigsdorff, R. (2024): Analytical solution for the simulation of ground thermal conditions around planar trench collectors. In: Geothermics 124, S. 103123. DOI: 10.1016/j.geothermics.2024.103123.

Miocic, J. M.; Schleichert, L.; **Van de Ven, A.**; Koenigsdorff, R. (2024): Fast calculation of the technical shallow geothermal energy potential of large areas with a steady-state solution of the finite line source. In: Geothermics 116, 102851. S. 102851. DOI: 10.106/j.geothermics.2023.102851.

Van de Ven, A.; Neth, F.; Köhler, A.; Albers, A.; Schindler, L.; Buchmiller, D.; Denninger, M.; Steger, H.; Zorn, R.; Koenigsdorff, R. (2025): Behaviour of the subsurface as a reaction on an operating planar trench collector. In: Scientific Data 12, 1661. DOI: 10.1038/s41597-025-06072-8.

Van de Ven, A.; Bayer, P.; Koenigsdorff, R. (2025): Analytical Modelling Approach of Ground Freezing and Thawing Around Ground Heat Collectors. In: Geothermal Energy 13 (43). DOI: 10.1186/s40517-025-00367-0.

List of non-peer-reviewed publications and conference papers

Karrer, H.; Burkhardt, F.; Kirschbaum, A.; Koenigsdorff, R.; Makni, L.; Meier, S.; Reuß, M.; Riegger, M.; Steger, H.; **Van de Ven, A.**; Wilke, S.; Zorn, R. (2018): Das Verbundvorhaben QEWS II – Qualitätssicherung bei Erdwärmesonden II. In: Der Geothermiekongress DGK 2018. Tagungsband, Essen. 27.–29.11.2018. S.1-12.

Koenigsdorff, R.; **Van de Ven, A.** (2019): Vereinfachte Auslegung oberflächennaher Geothermiesysteme - Versionen 3 & 4 des Programms GEO-HANDlight. In: bbr 70 (12–2019), S. 72–76. ISSN: 1611-1478

Van de Ven, A.; Koenigsdorff, R.; Hofmann, S. (2018): Entwicklung konsistenter Auslegungsmodelle für oberflächennahe geothermische Quellensysteme. In: BauSIM 2018. 7. Deutsch-Österreichische IBPSA-Konferenz. Tagungsband, Karlsruhe. 26. - 28. 09.2018, S. 508–515.

Karrer, H.; Hagel, K.; Kirschbaum, A.; Kötting, I.; Kuckelkorn, J. M.; Osgyan, P.; Pendzich, L.; Pinnekamp, M.; Reuß, M.; Streib, G.; Bachseitz, M.; Koenigsdorff, R.; **Van de Ven, A.**; Meier, S.; Fuchs, H.; Koch, F.; Steger, H.; Wilke, S.; Schindler, L.; Schüppler, S.; Zorn, R.; Lutz, T.; Reduth, Y.; Riegger, M.; Rolker, J.; Burkhardt, F. (Eds.) (2020): Qualitätssicherung bei Erdwärmesonden II mit Beteiligung am IEA ECES ANNEX 27 - QEWS II : Schlussbericht : Laufzeit des Vorhabens: 01.10.2016-31.03.2020. ZAE Bayern. DOI: 10.2314/KXP:176101739X.

Van de Ven, A.; Koenigsdorff, R.; Neth, F.; Zorn, R.; Schüppler, S.; Huttenloch, P.; Steger, H.; Albers, A.; Fuchs, H.; Schilling, F.; Karrer, H.; Osgyan, P.; Fuchs, M.; Kainzlsperger, M. (2022): Advanced thermal and geophysical test methods of shallow geothermal systems. In: European Geothermal Congress 2022. Proceedings. European Geothermal Congress, Berlin. 18.10.2022 - 20.10.2022, S. 1–9.

Van de Ven, A.; Neth, F.; Kainzlsperger, M.; Koenigsdorff, R. (2023): Thermal Response Tests an Erdwärmekollektoren. In: Geothermische Energie 32 (104), S. 12–15. ISSN: 0948-6615

Koenigsdorff, R.; Schleichert, L.; **Van de Ven, A.** (2023): Fast Calculation Method for Borehole Heat Exchanger Fields in Groundwater Flow, in: GeoTHERM Journal. GeoTHERM expo & Congress, Offenburg, Offenburg, pp. 17–25.

Van de Ven, A.; Braun, S.; Denninger, M.; Koenigsdorff, R.; Neth, F.; Schleichert, L.; Kainzlsperger, M.; Karrer, H.; Kuckelkorn, J.; Nienborg, B.; Osgyan, P.; Pendzich, L.; Pinnekamp, M.; Brand, T.; Mangold, D.; Reduth, Y.; Theophil, T.; Albers, A.; Fuchs, H.; Schilling, F.; Steger, H.; Huttenloch, P.; Schindler, L.; Zorn, R.; Burkhardt, F.; Bittscheidt, M; Hauri, F.; Hauri, J.; Hackstein, F.; Kühl, J.-U. (submitted 2025). Qualitätssteigerung oberflächennaher Geothermiesysteme - QEWSplus. Schlussbericht. Submitted to Technische Informationsbibliothek in June 2025.

Declaration

Ich erkläre an Eides statt, dass ich die Arbeit selbständig und ohne fremde Hilfe verfasst, keine anderen als die von mir angegebenen Quellen und Hilfsmittel benutzt und die den benutzten Werken wörtlich oder inhaltlich entnommenen Stellen als solche kenntlich gemacht habe.

I declare under penalty of perjury that this thesis is my own work entirely and has been written without any help from other people. I used only the sources mentioned and included all the citations correctly both in word or content.

Datum / Date Unterschrift / Signature